

FAKULTÄT FÜR PHYSIK DER
TECHNISCHEN UNIVERSITÄT MÜNCHEN
LEHRSTUHL FÜR EXPERIMENTALPHYSIK E21



**Generation of a high-brightness
pulsed positron beam for the
Munich scanning positron microscope**

Dissertation

Christian Piochacz



TECHNISCHE UNIVERSITÄT MÜNCHEN

TECHNISCHE UNIVERSITÄT MÜNCHEN

Fakultät für Physik der Technischen Universität München
Lehrstuhl für Experimentalphysik E21

Generation of a high-brightness pulsed positron beam for the Munich scanning positron microscope

Dipl.-Phys. Univ. Christian Piochacz

Vollständiger Abdruck der von der Fakultät für Physik der Technischen
Universität München zur Erlangung des akademischen Grades eines

Doktors der Naturwissenschaften (Dr. rer. nat.)

genehmigten Dissertation.

Vorsitzender: Univ.-Prof. Dr. P. Vogl
Prüfer der Dissertation: 1. Univ.-Prof. Dr. K. Schreckenbach
2. Univ.-Prof. Dr. W. Petry

Die Dissertation wurde am 15.09.2009 bei der Technischen Universität
München eingereicht und durch die Fakultät für Physik am 20.11.2009
angenommen.

Contents

Zusammenfassung	v
Summary	vii
1 Introduction	1
2 Positrons in matter	3
2.1 Fundamental properties of the positron and positronium	3
2.2 Implantation and thermalization of positrons in solids	4
2.3 Experimental methods	7
2.3.1 Electron momentum measurements	7
2.3.2 Positron annihilation lifetime spectroscopy (PALS)	10
3 Positron beam techniques	13
3.1 Overview	13
3.2 Positron sources	14
3.2.1 Radioactive sources	14
3.2.2 Pair production	15
3.3 Moderation and beam formation	16
3.3.1 Moderation in gases	16
3.3.2 Moderation in solids	19
3.4 Beam transport and manipulation	25
3.4.1 Motion of charged particles in electromagnetic fields	25
3.4.2 Adiabatic, magnetic beam transport	28
3.4.3 Capture and release of charged particles in an axial symmetric magnetic field	32
3.4.4 Focusing a charged particle beam by static and rotationally sym- metric electric and magnetic lenses	34
3.5 Brightness enhancement	39
3.5.1 Beam characterizing quantities	40
3.5.2 Liouville's theorem	42
3.5.3 Re-moderation	42
3.6 Beam pulsing	43
3.6.1 Bunching techniques	44
3.6.2 Beam chopping	54

Contents

4	Positron beam preparation at NEPOMUC	57
4.1	The NEPOMUC re-moderator	57
4.1.1	The positron source NEPOMUC	57
4.1.2	The setup of the NEPOMUC re-moderator	60
4.1.3	Experimental results	72
4.2	The SPM interface	79
4.2.1	The SPM project and the design of the SPM interface	79
4.2.2	The bunching units of the SPM interface	86
4.2.3	The beam transport within the interface	99
4.2.4	Experimental results	108
5	First positron annihilation measurements at UMo	123
5.1	Overview and sample preparation	123
5.2	Positron annihilation measurements	124
5.3	Summary and outlook for the UMo examinations	130
6	Conclusion and outlook	133
	Acknowledgment	135
	List of publications	147

Zusammenfassung

Im Rahmen dieser Arbeit wurden die Voraussetzungen für den Betrieb des *Munich scanning positron microscope* (SPM) an der hoch intensiven *neutron induced positron source Munich* (NEPOMUC) geschaffen. Dies gelang in zwei Schritten: Zunächst wurde ein Positronen-Remoderator an der Positronenstrahlanlage NEPOMUC eingebaut, der die Brillanz des Positronenstrahls für alle angeschlossenen Experimente erhöht. Im zweiten Schritt erfolgte die Konstruktion, der Aufbau und die Inbetriebnahme eines SPM-Interfaces zur hocheffizienten Konvertierung des kontinuierlichen Strahls in einen gepulsten Positronenstrahl.

Die In-Pile Positronenquelle NEPOMUC erzeugt typischerweise einen Positronenstrahl mit einem Durchmesser von 7 mm und einer kinetischen Energie von 1 keV, wobei die Energieverteilung eine Breite von 50 eV aufweist. Der NEPOMUC Remoderator erzeugt aus diesem Strahl einen niederenergetischen Positronenstrahl (20 – 200 eV) mit einem Durchmesser von weniger als 2 mm und einer Energieverteilung mit einer Breite von deutlich unter 2,5 eV. Diese Brillanzerhöhung wurde mit einer exzellenten Gesamteffizienz von $6,55 \pm 0,25 \%$ erzielt. Der Remoderator war nicht nur der erste Schritt zum Aufbau des SPM an der Positronenquelle, er ermöglichte auch den Betrieb des *pulsed low energy positron beam systems* (PLEPS). Mit diesem Spektrometer wurden im Rahmen dieser Arbeit erste Positronenlebensdauermessungen durchgeführt, welche die Charakterisierung, der durch Ionenbestrahlung induzierten Defekte in einer Uran-Molybdän Probe ermöglichten. Darüber hinaus profitieren die Instrumente, welche bereits an der Positronenstrahlanlage NEPOMUC betrieben werden, erheblich von der Brillanzerhöhung.

Im neu aufgebauten SPM-Interface erhöht eine zusätzliche Remoderationsstufe die Brillanz des Strahls nochmals um Positronenlebensdauermessungen am SPM mit einer lateralen Auflösung von unter 1 μm zu ermöglichen. Die Effizienz des Remoderationsprozesses in dieser zweiten Stufe wurde zu $24,5 \pm 4,5 \%$ bestimmt. Um den kontinuierlichen Strahl mit hoher Effizienz in einen gepulsten Strahl mit einer Repetitionsrate von 50 MHz und einer Pulsdauer von weniger als 50 ps umzuwandeln, wurde ein subharmonischer Pulser mit zwei Sinuswellen-Pulser kombiniert. Zudem ermöglicht die zusätzliche Remoderationsstufe im SPM-Interface eine aberrationsfreie Pulsung, wodurch die Zeitauflösung der Positronenlebensdauermessungen letztlich nur durch das verwendete Detektorsystem begrenzt wird.

Die Kombination aus hochintensiver Positronenquelle NEPOMUC, zweifacher Remoderierung, aberrationsfreier Strahlpulsung und der Leistungsfähigkeit des SPM wird die Messung von dreidimensionalen Defektkarten mit einer lateralen Auflösung unter 1 μm innerhalb kürzester Messzeiten ermöglichen und dadurch die mikroskopische Positronenlebensdauermessung zu einer Standardmessmethode etablieren.

Summary

Within the present work the prerequisites for the operation of the Munich scanning positron microscope (SPM) at the high intense neutron induced positron source Munich (NEPOMUC) were established. This was accomplished in two steps: Firstly, a re-moderation device was installed at the positron beam facility NEPOMUC, which enhances the brightness of the positron beam for all connected experiments. The second step was the design, set up and initial operation of the SPM interface for the high efficient conversion of the continuous beam into a bunched beam.

The in-pile positron source NEPOMUC creates a positron beam with a diameter of typically 7 mm, a kinetic energy of 1 keV and an energy spread of 50 eV. The NEPOMUC re-moderator generates from this beam a low energy positron beam (20 – 200 eV) with a diameter of less than 2 mm and an energy spread well below 2.5 eV. This was achieved with an excellent total efficiency of 6.55 ± 0.25 %. The re-moderator was not only the first step to implement the SPM at NEPOMUC, it enables also the operation of the pulsed low energy positron beam system (PLEPS). Within the present work, at this spectrometer first positron lifetime measurements were performed, which revealed the defect types of an ion irradiated uranium molybdenum alloy. Moreover, the instruments which were already connected to the positron beam facility benefits considerably of the high brightness enhancement.

In the new SPM interface an additional re-moderation stage enhances the brightness of the beam even more and will enable positron lifetime measurements at the SPM with a lateral resolution below 1 μm . The efficiency of the re-moderation process in this second stage was 24.5 ± 4.5 %. In order to convert high efficiently the continuous positron beam into a pulsed beam with a repetition rate of 50 MHz and a pulse duration of less than 50 ps, a sub-harmonic pre-buncher was combined with two sine wave bunchers. Furthermore, the additional re-moderation stage of the SPM enable an aberration-free bunching and thus the timing resolution of the positron lifetime measurements is only limited by the detection system.

The combination of the high intense positron source NEPOMUC, the twofold brightness enhancement, the high efficient, aberration-free beam pulsing and the performance of the SPM will enable measurements of three dimensional defect maps with a lateral resolution below 1 μm within shortest measurement times and will hence establish the microscopic positron lifetime measurement as a standard technique.

1 Introduction

The positron is a well-established probe for defect spectroscopy for many years and offers the examination of defects in metals, semiconductors and isolators [1, 2, 3, 4, 5]. The positron as a probe scans the specimen over a wide range of up to several 100 nm depending on the material and the defect density. Many defect types, for instant open-volume like defects and negatively charged impurities, have an attractive potential for positrons and trap them very efficiently. The high trapping efficiency and the long diffusion length are responsible for the enormous defect sensitivity of the positron.

As important as the sensitivity is, that the state of the positron depends on the electronic structure of the specimen. Since the properties of the annihilation radiation vary with the state of the positron, details of the electronic structure get observable by detecting this radiation. By measuring the positron lifetime (PALS) the defect types and their concentration can be revealed. The deviation from the collinearity of the radiation and the broadness of the annihilation line provides information about the momentum distribution of the electrons in the specimen. This measurements are the scope of the angular correlation of the annihilation radiation (ACAR) measurements and the Doppler broadening spectroscopy (DBS).

These techniques have been performed successfully for decades with the help of radioactive positron emitters and provide still an important contribution to the exploration of defects and the electronic structure of various systems. But the range of applications is enlarged enormously if a monoenergetic positron beam is used for the experiments. Due to its tunable energy, depth resolved measurements can be performed what is not only interesting in layered systems. By focusing the beam three dimensionally resolved measurements are possible.

Both, a very high lateral and timing resolution is provided by the Munich scanning positron microscope (SPM) [6, 7, 8]. It allows the measurement of three dimensional positron lifetime maps, with a lateral resolution of up to 1 μm [9, 10]. This resolution allows the direct observation of small structures such as whiskers, cracks and voids. The maximum depth and the depth resolution at a non-focusing positron instruments is limited by the maximum positron energy and the broadening of the implantation profile. In the case of the SPM, both can be enhanced by scanning the microbeam over a wedge-shaped cut. This is especially interesting in the case of layered systems [11].

Up to now, the SPM is operated with positrons provided by a β^+ -emitter. Since the positron intensity of such a source is limited, SPM measurements take an accordingly

1 Introduction

long time in the range of one to two weeks. With the neutron induced positron source Munich (NEPOMUC) up to $9 \cdot 10^8$ moderated positrons per second are now available and hence about three orders of magnitude more than the strongest beam systems operated by β^+ -emitters [12]. Since the NEPOMUC source is operated as a multi purpose source, the beam properties have to be adapted for the requirements of the SPM. Within this work, the brightness of the NEPOMUC beam is enhanced and transformed from a continuous to a pulsed beam by using several advanced techniques.

Since the positron differs from the electron only in the charge the particle optics of both is equivalent. Nevertheless there are important differences in the applicable techniques. The main reason for this is that usual electron sources are not only several orders of magnitude more intense but also provide a much brighter beam than a positron source. Therefore, the low intensity of positron sources prohibits the usage of apertures, collimators, and energy filter which are in electron beam systems the basic elements to restrict the phase space volume occupied by the beam. Fortunately there is also a beam enhancement technique which is restricted to the positrons only: the re-moderation [13, 14, 15, 16]. This technique allows the reduction of the phase space volume occupied by a positron beam much more efficiently and therefore with much less positron loss than by the techniques common in electron beam systems.

Since the SPM measures the positron lifetime the beam has to be pulsed in order to gain the timing information. A common technique to achieve a pulsed beam is to exclude the parts of the beam which are not within the desired time interval at the expense of beam intensity. Since the positron is charged there is a superior technique which is often referred as bunching and which conserves the time-averaged intensity. By this technique, the energy of the positrons of the continuous beam is periodically modulated in such a way that after a certain drift a time focus appears [17, 18, 19].

The focus of this work is set on the preparation of the NEPOMUC positron beam, which was accomplished by a re-moderation stage, which enhances the beam brightness for all experiments at the NEPOMUC positron beam facility, and an beam preparation interface for the SPM. This interface converts the continuous beam into a pulsed beam and uses therefore several different bunching units and additionally the re-moderation technique, which enables aberration-free bunching and hence extremely short positron pulses of less than 50 ps. Beside this, the re-moderator at the interface is crucial to attain a lateral resolution below $1 \mu\text{m}$ for the lifetime measurements at the SPM.

Beside the successful setup and operation of these positron beam related parts, first DB and PALS measurements on an irradiated uranium molybdenum alloy were made. Aim of this explorative measurements was, to determine which information can be gained by such measurements at such a material. Moreover, it was ascertained what has to be considered for a comprehensive examination of this alloy, including both, the sample preparation and the measurement methods.

2 Positrons in matter

2.1 Fundamental properties of the positron and positronium

The positron was postulated in 1930 by Paul Dirac as the particle related to the negative energies occurring in his relativistic electron theory and only three years later Carl David Anderson discovered the antiparticle of the electron with the help of a cloud chamber [20, 21, 22]. Since it is the antiparticle of the electron the rest mass, rest energy and spin are equal, but as it is oppositely charged it has a positive magnetic moment. The lifetime in vacuum is longer than $2 \cdot 10^{21} a$ and can therefore be regarded as stable. However, in matter the positron annihilates with an electron mostly in two or three γ -quanta. Because of the spin conservation the actual decay channel depends on the spin state of the positron electron pair. If it is zero it annihilates predominantly into two quanta, and if the spin state equals one, the annihilation is dominated by the 3- γ decay.

In some cases the positron electron pair can bind to a hydrogen-like state which is called positronium. The binding energy of this system is half the ground state of the hydrogen atom, which is in the vacuum about 6.8 eV. The triplet state of the positronium is called ortho-positronium (o-Ps), and the singlet state is called para-positronium (p-Ps). Comparing the Feynman diagrams of the two and three gamma decays, in the latter one an additional vertex occurs and hence this decay is suppressed by the amount of the fine-structure constant $\alpha \approx 1/137$ ¹. This leads to an extended lifetime of the o-Ps, which is in the vacuum about 142 ns. Within matter the o-Ps lifetime is reduced mainly because of the pick-off processes. In this process the electron, which is bound to the positron is replaced by an electron of the vicinity with an opposite directed spin. Hence, the o-Ps is converted into a p-Ps which has a lifetime of 125 ps. Since this conversion lasts a certain time the reduced o-Ps lifetime is between 142 ns and 125 ps. The formation ratio of o-Ps and p-Ps is according to the spin multiplicities 3:1. However, due to the high suppression of the 3- γ decay and the high efficiency of the pick-off process in matter the annihilation into 2 γ -quanta dominates the annihilation spectra.

¹A more detailed analysis shows that the three gamma decay of a slow, free positron electron pair is reduced by a factor of 1/370 [23].

rest mass	$9.10938215(45) \cdot 10^{-31} \text{ kg}$
rest energy	$0.510998910(13) \text{ MeV}/c^2$
charge	$+1.602176487(40) \cdot 10^{-19} \text{ C}$
spin	$1/2$
magnetic moment	$1.00115965218111(74) \mu_B$

Table 2.1: Physical properties of the positron [24].

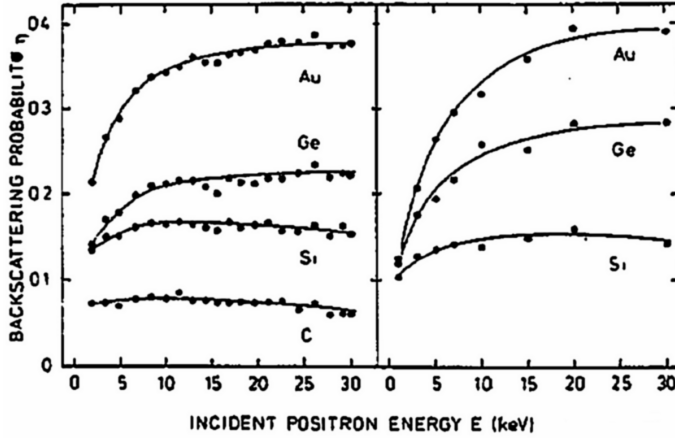


Figure 2.1: Positron backscattering probabilities. Left: experimental data. Right: results from Monte Carlo calculations (from [25]).

2.2 Implantation and thermalization of positrons in solids

Before positrons can enter a solid, they have to pass the surface at which a certain fraction is reflected. For slow² positrons this fraction can reach up to about 40 % in the case of high Z solids and high energies (see Fig. 2.1).

Inside the solid the positrons lose their energy due to inelastic scattering processes within only a few picoseconds until they are thermalized. At high energies ($E_{\text{Fermi}} < E < 100 \text{ keV}$) the inelastic scattering is dominated by the excitation of core and valence electrons or in the case of metals by the scattering at conduction-electrons. At lower energies, but still above the Fermi-energy, plasmon excitations become dominant and below the threshold for this collective mode electron-hole excitations occur. In the very low energy region the phonon scattering is the dominating process. Because of the band gap, in semiconductors and isolators the cooling process is already at higher energies only possible due to phonon scattering. Since the cross-section and energy transfer for

²In positron annihilation physics this term is not well defined, but since the beam systems which are currently used for solid state physics provide positrons with an energy below 50 keV, this might be regarded as an upper energy limit for the term slow. This term is also used to distinguish the positrons which are moderated and therefore have a relatively low and sharp energy, from those positrons emitted by a radioactive source or created by pair production.

2.2 Implantation and thermalization of positrons in solids

this scattering is much lower than at electric scattering processes, the thermalization time in materials with a wide band gap is extended. The low probability and energy deposition of phonon scattering are the reasons why in all materials most of the short thermalization time is needed at the low energies, little above the thermal equilibrium [26, 27, 28].

The implantation distribution can be described by the so called Makhovian implantation profile [29]:

$$P(z) = \frac{mz^{m-1}}{z_0^m} \exp\left(-\left(\frac{z}{z_0}\right)^m\right) \quad (2.1)$$

Where m is a dimensionless and material dependent parameter and z_0 is defined as follows:

$$z_0 = \frac{\bar{z}}{\Gamma\left(\frac{1}{m} + 1\right)} \quad (2.2)$$

The mean stopping depth \bar{z} is usually approximated by a power law:

$$\bar{z} = \frac{A}{\rho} E^n \quad (2.3)$$

A and n are again material dependent parameters which are gained semi-empirically by Monte Carlo simulations. A collection of this parameters and also of the parameter m from Eq. (2.1) can be found e.g. in [3]³. As shown in Fig. 2.2 the distribution becomes remarkable broader with increasing energy and hence the resolution of depth resolved measurements is deteriorated at high energies.

When the positrons are thermalized they are scattered quasi-elastically by phonons until they annihilate. The diffusion length L_+ is given by

$$L_+ = \sqrt{\frac{D_+}{\lambda_b + \kappa}} = \sqrt{D_+ \tau} \quad (2.4)$$

Where κ is the defect trapping rate and λ_b is the annihilation rate in the defect free lattice which is the reciprocal of the so called bulk lifetime $\tau_b = 1/\lambda_b$. The value of the positron diffusion coefficient D_+ depends on the scattering processes involved during the diffusion. In metals these are mainly longitudinal-acoustic phonons which lead to a theoretical $T^{-1/2}$ dependence of the diffusion coefficient. In the case of other materials

³Unfortunately the reference for the measurements of Soininen et al. in [3] is wrong and also parts of the values are quoted incorrectly. The right values published by Soininen et al. can be found in [30].

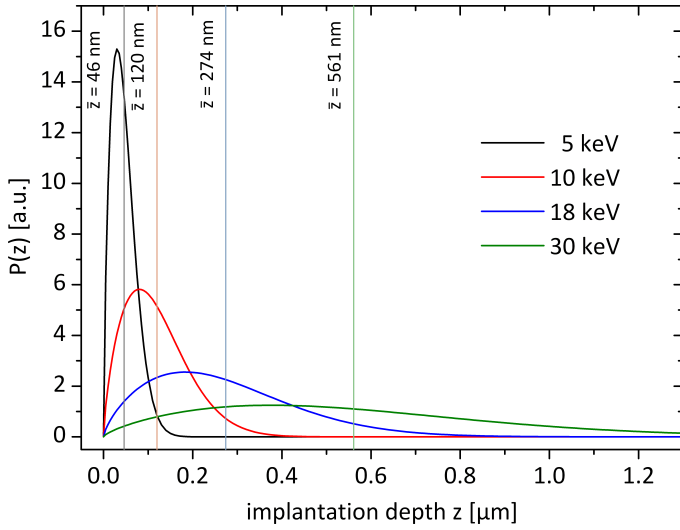


Figure 2.2: Makhovian profiles for an UMo alloy at different positron beam energies. For this alloy are no parameter (A,m,n) published, but since these parameters depend only slightly on the density, a good approximation is given by taking the (averaged) parameters of gold (see e.g. [3]) and the density of UMo.

the temperature dependence is more complicated due to remarkable contributions from e.g. optical phonons [3].

In the defect-free lattice the positrons can be described as a delocalized Bloch-state. In the presence of open-volume defects the potential for the positrons is lower due to the absence of the repulsive ion. This leads to a localization of the positrons at the defect, with the released energy being transferred to the host. This process is called defect trapping [3] and is also possible at sites which are not open-volume like as e.g. negatively charged defects. In the case of shallow traps, the reversed process—the so called detrapping—is also possible due to thermal activation of the positron.

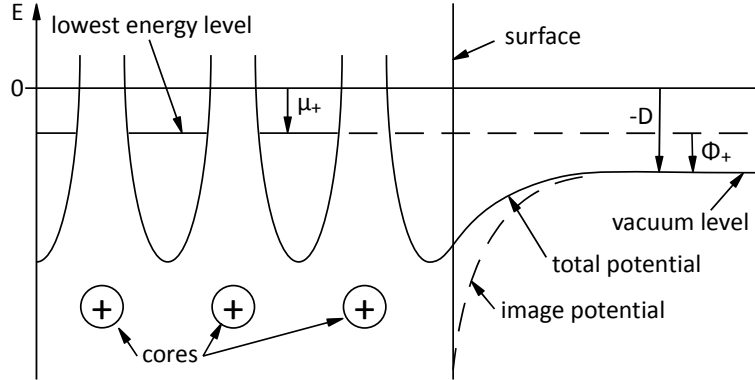
The trapping model provides basic mathematical expressions to handle the trapping process [3, 31, 32]. If there is only one defect type present in the specimen the following rate equations can be written:

$$\begin{aligned} \frac{df_b}{dt} &= -\lambda_b f_b - \kappa f_b + f_i \\ \frac{df_t}{dt} &= -\lambda_t f_t + \kappa f_b \end{aligned} \quad (2.5)$$

Where f_b and f_t are the probabilities that the positron is free in the bulk or trapped in a defect, respectively, f_i is the rate by which new positrons enter the solid, and the λ denote the annihilation rates in the corresponding state.

If the positron is implanted with a low energy or if the specimen is thin enough there is a finite probability that the positron reaches the surface of the solid during the diffusion. There are some materials which emits thermalized positrons with a sharp

Figure 2.3: The positron work function Φ_+ is the sum of the chemical potential μ_+ and the dipole barrier D . If $\Phi_+ < 0$ thermalized positrons at the surface are emitted perpendicularly into the vacuum.



energy if they reach a surface. Usually a certain energy is required to remove a positron from the bulk ad infinitum. The amount of this energy is given by the positron work function Φ_+ which consists mainly of two components: the chemical potential μ_+ of the positrons and the surface dipole barrier D . The first is the chemical potential of the positron and is the sum of a repulsive potential induced by the ion cores and an attractive contribution from the electrons. It is always positive and leads to a force directed toward the solid. The dipole barrier gives a negative contribution to the work function and hence the sum of both can lead to a negative positron work function (see Fig. 2.3). The mathematical expressions are as follows:

$$\Phi_+ = -D - \mu_+ \quad (2.6)$$

If a solid has a negative positron work function, thermalized positrons which diffuse to the surface are emitted perpendicularly into the vacuum with a kinetic energy equal to the absolute amount of the negative positron work function [2]. Materials with this feature are used to create from positrons e.g. emitted by a positron source a directed positron beam with a sharp energy. This technique is called moderation and is explained in detail in Sec. 3.3.2. They are also used for re-moderation of a positron beam, in order to enhance the brightness of the beam (see Sec. 3.5.3).

2.3 Experimental methods

2.3.1 Electron momentum measurements

As mentioned above, in metals the positron annihilates mostly by emitting 2 γ -quanta. In the center of mass system of the positron electron pair these quanta are emitted exactly collinearly and each has exactly the energy equal to one electron mass. The

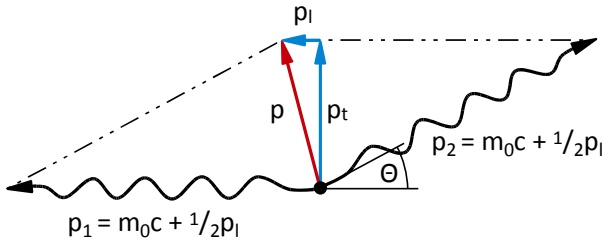


Figure 2.4: In the lab-system the conservation of the momentum of the annihilating electron leads to a deviation from the collinearity and to a Doppler shift of the annihilation quanta.

finite velocity of the positron electron pair in the lab-system leads to deviations from this exact values (see Fig. 2.4). In most cases the positron is thermalized before it annihilates, and therefore, its kinetic energy can be neglected in comparison to that of the electron. Therefore, the deviations from the exact values bear information of the momentum of the electron which was involved in the annihilation. According to the two different deviations there are also two measurement methods. Since the energy variation of the γ -quanta which is measured is caused by the Doppler effect the associated measurement method is called Doppler broadening (DB) technique. The technique which measures the deviation from the collinearity is called angular correlation of the annihilation radiation (ACAR) and is measured by means of spatial resolving detectors.

Doppler broadening (DB)

For the positron Doppler spectroscopy the transversal Doppler effect can be neglected and only the longitudinal Doppler shift, i.e. the shift which arises due to the velocity component which is directed along the annihilation quantum, has to be regarded. The frequency f_i of the Doppler shifted γ -quanta is given by the following equation:

$$f_{1,2} = f_0 \sqrt{\frac{c \pm v_1}{c \mp v_1}} \approx f_0 \left(1 \pm \frac{v_1}{c}\right) \quad (2.7)$$

The index zero denotes the frequency of the γ -quanta in the center of mass system, the index 1 the blue-shifted and the index 2 the γ -quantum shifted to a lower energy. Since the electrons are not monoenergetic and only a projection of the momenta is observed the Doppler shift varies and hence in the recorded annihilation spectra the annihilation line appears not shifted but broadened. The broadness is hence a value for the velocity distribution of the electrons at the annihilation sites. If a positron is trapped e.g. within a vacancy the positron wave function gets localized at this site and its overlap with the high momentum core electrons is lower as in the delocalized state. Therefore, the annihilation line is narrower if the positron annihilates from an open volume defect. The common quantity which emphasize the change of the shape of the annihilation line more than e.g. the FWHM is the S-parameter. As shown in

Figure 2.5: The broadened annihilation line is usually characterized by the S-parameter, which characterizes the differences in the line shape. The S-parameter is defined by the ratio of the intensities of a center area I_B and the total intensity $I_{\text{tot}} = I_A + I_B + I_C$: $S = I_B/I_{\text{tot}}$

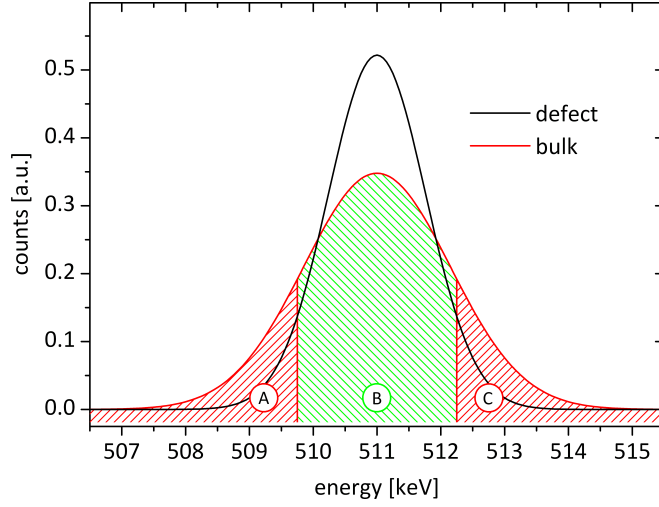


Fig. 2.5 it is defined as the ratio between an arbitrary chosen central area below the annihilation line and the total amount of counts. Since the Doppler broadening is of the order of some keV germanium detectors which provide a high energy resolution have to be used to obtain DB spectra.

The background of such measurements can be reduced enormously by using two germanium detectors in coincidence. The angular deviation of the emitted quanta is so small that the detectors have to be mounted collinearly together with the specimen. Beside this geometrical constraint the time coincidence is used. But most important is the fact that due to energy conservation the energy sum of both annihilation quanta has to have the total rest energy of the electron and the positron. Indeed there are very small deviations from the total energy of 1022 keV caused e.g. by the binding energy of the positron within the defect. But since such energies are in the range of eV they can be neglected. Due to the high background reduction, this technique, which is called coincident Doppler broadening (CDB) spectroscopy, is used to analyze the wings of the annihilation line. The signal from this high momentum areas arise by the annihilation with core electrons. Since these electrons bear the information of the element they are bound, the CDB spectroscopy enables the examination of the chemical vicinity of e.g. open volume defects [33].

Angular correlation of the annihilation radiation (ACAR) measurements

The angular deviation which arises due to the electron momentum can be derived directly from Fig. 2.4:

$$\sin \Theta = \frac{p_t}{p_2} = \frac{p_t}{m_0 c - \frac{1}{2} p_1} \approx \frac{p_t}{m_0 c} \Rightarrow \Theta \approx \frac{p_t}{m_0 c} \quad (2.8)$$

Today, ACAR measurements are made with detector systems which provide a 2D resolution of few millimeters e.g. Anger cameras. Since the angular deviations are about 10 mrad and less, the detectors have to be several meters apart from the specimen. Due to this large distance, the counting rate becomes accordingly low and the measurements get very time consuming. Nevertheless this technique was and is used successfully to measure Fermi surfaces [34, 35].

3D momentum measurements

In both approaches—DB and ACAR—only the projection of the electron momenta are measured. But if these techniques are combined all dimensions of the reciprocal space are directly accessible. For such measurements two segmented high purity germanium detectors have to be placed in an adequate distance from the specimen. Up to now this approach has not been realized.

2.3.2 Positron annihilation lifetime spectroscopy (PALS)

The lifetime of a positron depends on the electron density in its vicinity. The cross section for the annihilation of a thermal positron is in good approximation given by [1]:

$$\sigma = \pi r_0^2 c / v_{e+} \quad (2.9)$$

Where $r_0 = e^2 / (m_0 c^2)$ denotes the classical electron radius and v_{e+} is the velocity of the positron. The lifetime of the positron τ_{e+} is calculated from the cross section as follows:

$$\tau_{e+} \equiv \Gamma^{-1} = \frac{1}{\sigma v_{e+} n_{e-}} \propto \frac{1}{n_{e-}} \quad (2.10)$$

Hence, the lifetime is inversely proportional to the electron density n_{e-} . Since this density is at open volume defects lower than in the unperturbed lattice the lifetime of positrons trapped by defects is longer. Because the electron density is generally lower as the defect is larger, different defect types can be distinguished by the different positron lifetimes. For an exact calculation of the positron lifetimes the two-component density-functional theory together with the local density approximation have to be used [3].

For the lifetime measurement a start and a stop signal are needed, with one of both being provided by the annihilation radiation. In the conventional lifetime spectroscopy a ^{22}Na source, attached in an appropriate geometry to the specimen, is used. Often the so called sandwich geometry is used, where the source is in the middle of two identical specimens. This geometry has the advantage, that no annihilation in unintended

2.3 Experimental methods

material can occur and thus the background is low. A disadvantage of this geometry is that two identical specimens are needed. ^{22}Na is used because beside the positron it also emits a prompt γ -quantum with an energy of 1275 keV which can be used as stop signal⁴.

Another possibility is to use a pulsed beam and to derive the stop signal from the master clock of the pulsing system. Using a beam has the advantage, that energy and hence depth dependent measurements can be performed. Further, such systems provide higher peak to background ratio and a higher timing resolution than a conventional systems. The background corrected lifetime spectra are the convolution of the resolution function of the experimental setup and the superposition of a certain amount of exponential functions representing the lifetimes. Due to the high timing resolution of a pulsed beam system, up to three lifetimes can be separated.

⁴In order to reduce the dead time of the measurement setup, the stop and the start signal are often reversed.

3 Positron beam techniques

3.1 Overview

Many of the experimental techniques, mentioned above could be performed by using positrons emitted from a β^+ emitter. For this purpose, the radioactive positron source is positioned in an appropriate geometry near the specimen and the detectors are arranged around this setup. Depending on the measurement method there are different arrangements of specimen and detector, which ensure low background, high energy and/or time resolution, and nevertheless high statistics within a reasonable measurement time. Because of the continuous β^+ spectrum and the endpoint energy, only bulk information can be obtained and moreover, there are only limited options for lateral resolved measurements. But despite this restrictions a large amount of the positron experiments in solid state physics are performed with β^+ sources.

The driving force for the development of slow positron beams was not given by solid state physics but by atomic and later on by surface physics. In the field of atomic scattering and surface analyzing techniques, which have an electron counterpart like low energy positron diffraction (LEPD), the desirable level was always set by the capability of commercial available electron guns. But not only regarding the intensities, but also in the context of *brightness*, the positron sources have always been far behind their electron counterparts.

Due to the improvements in creating intense slow monoenergetic positron beams this beam technique became also in solid state physics more and more important. Because of the adjustable beam energy, depth resolved positron annihilation spectroscopy (PAS) became feasible. With the positron specific technique for the *brightness* enhancement, the *re-moderation*, and with the experience of electron microscopy, the idea of a positron microscope was born [13].

In this chapter the components and techniques, which are necessary to create, guide, focus, enhance and pulse a positron beam, are shown. Moreover, the quantities, which can be used to characterize a beam of charged particles are presented.

	$T_{1/2}$	Intensity [%]	E_{end} [keV]	E_{average} [keV]
^{22}Na	2.60 y	89.84	545.5	215.5
^{58}Co	70.82 d	14.96	475.2	201.3
^{64}Cu	12.70 h	17.86	652.5	278.1

Table 3.1: Data of radioactive positron sources, which are commonly used for positron beams (from *NuDat* database [41]).

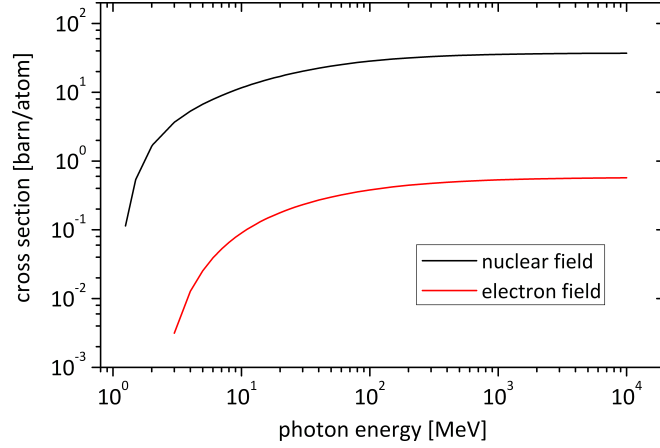
3.2 Positron sources

3.2.1 Radioactive sources

The first part of every positron beam is the source, which emits positrons. In small laboratory beam systems this is usually a radioactive isotope. From the various existent β^+ -sources mainly ^{22}Na , ^{58}Co and ^{64}Cu are used for the beam production (see Tab. 3.1). ^{64}Cu has a half-life of 12.7 h and is produced at research reactors by the nuclear reaction $^{63}\text{Cu}(n,\gamma)^{64}\text{Cu}$ [36, 37]. Lynn et al. described a system, where the irradiation and the following installation of the source into a positron beam setup is done remotely controlled and therefore the radiation exposure to the involved staff could be kept low. At this beam system an intensity of $\approx 10^7$ e^+ /s was reached [38]. The ^{58}Co isotope has a longer half-life, whereby the activity and therefore the beam intensity can be regarded almost constant during the measurements. ^{58}Co is produced by irradiating ^{58}Ni with fast neutrons and thus it is possible to produce carrier-free ^{58}Co by chemical separation [39, 40]. Nevertheless the most common nuclide, which is used for beam creation, is ^{22}Na . Not only because of its long half-life, but also because it is commercially available as NaCl solution and also as sealed *ready for use* sources on acceptable costs [36].

There are many designs for simple slow positron beams documented, which use small self-made or bought β^+ emitters (see e.g. [36, 42, 37, 43] and references therein). With a typical setup, like the slow positron laboratory beam at the Technical University in Munich [37], and using a ^{22}Na source of 6 mCi, it is possible to create a beam with up to 2×10^4 $\frac{e^+}{\text{s}}$. At the same laboratory beam a positron intensity of 2×10^5 $\frac{e^+}{\text{s}}$ was attained by using a self made ^{64}Cu source. If instead of a tungsten moderator a solid rare gas moderator and a stronger source (e.g. ^{58}Co) is used, even higher intensities are possible. Intensities of up to 10^6 $\frac{e^+}{\text{s}}$ have been reported [36]. In order to create beams with even higher intensities, another *kind* of source has to be utilized. Those sources are based on the mechanism of pair production.

Figure 3.1: Cross sections for the pair production in the electric field of nuclei and electrons of platinum. Data taken from [45].



3.2.2 Pair production

When a γ -quantum with an energy E_γ enters a solid with an atomic number Z it loses energy mainly due to three processes: the photoelectric effect (ph), the Compton scattering (cs), and the pair production (pp) process. The cross sections are as follows [44]:

$$\sigma_{\text{ph}} \propto Z^n/E_\gamma^m \quad n, m \text{ within 3 and 5} \quad (3.1)$$

$$\sigma_{\text{cs}} \propto 1/E_\gamma \quad (3.2)$$

$$\sigma_{\text{pp}} \propto Z^2 f(E_\gamma, Z) \quad \text{the } Z \text{ dependence is dominated by the } Z^2 \text{ term and } f(E_\gamma, Z) \text{ increases continuously with energy.} \quad (3.3)$$

The pair production in a solid occurs in the electric field of a nucleus or electron, with a much lower probability in the latter case (see Fig. 3.1). Due to the conservation of energy, there is a threshold for pair production, which equals the rest masses of the electron and the positron as well as a certain amount which is transferred by the recoil to the field generating nucleus or electron. For the pair production in the vicinity of a nucleus this amount is negligible but in the case of an electron the threshold is doubled to four electron rest masses.

There are basically three concepts of positron sources, utilizing pair production, which differ only in the method, how the high energy γ -quantum is produced. The first concept uses high energy electrons created by a LINAC, which are dumped onto a high- Z target in order to create high energy bremsstrahlung [46, 47, 48]. The second, which is implemented at the research reactor in Delft, Netherlands, uses the high flux of γ radiation which originates from the fission process at the core of a nuclear reactor [49]. The third is also a reactor based concept, but in contrast to the concept of Delft, the high flux of thermal neutrons is used to generate high energy γ -quanta by the nuclear

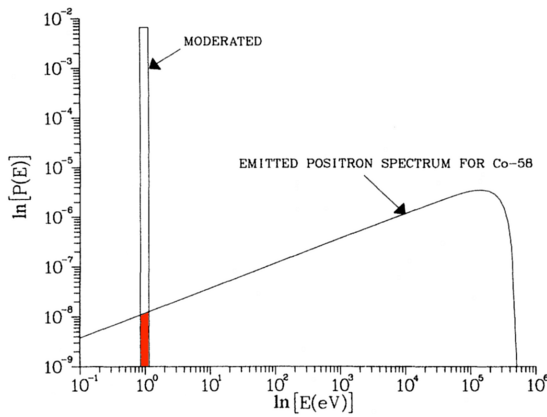


Figure 3.2: The efficiency to obtain a monoenergetic slow positron beam from a source with a continuous positron spectrum is up to 5 magnitudes higher by using the moderation technique, than by selecting only these positrons of the spectrum, which are within the desired energy range (from [2]).

reaction $^{113}\text{Cd}(n,\gamma)^{114}\text{Cd}$ [50]. The worlds strongest positron source NEPOMUC at the Heinz Maier-Leibnitz (FRM II) research reactor near Munich, Germany, uses this method and generates up to $9 \cdot 10^8$ moderated positrons per second [12]. This source will be explained in particular in section 4.1.1.

3.3 Moderation and beam formation

All sources mentioned above emit initially positrons with a continuous energy spectrum and from sufficient small sources the positrons are emitted approximately isotropic. Deviations are only due to source geometry and self absorption. In order to create a monoenergetic positron beam, there are at least two possibilities. The first is to select only those positrons within a sharp energy interval and a small solid angle, e.g. by using a β -ray spectrometer, but this would lead to a high loss in intensity. The other possibility is to cool as many positrons as possible within a small area and form from these positrons a beam by applying appropriate electric fields. The cooling process is usually performed in solids or gases and is called moderation. Although the moderation process has only an efficiency of typically 5×10^{-4} , by using a W(100) moderator crystal, it is much more efficient than using a β spectrometer as illustrated in Fig. 3.2.

3.3.1 Moderation in gases

When a positron enters a volume filled with gas it undergoes very similar processes as in the case of entering a solid. Most important in the context of moderation are the elastic and inelastic scattering processes, the annihilation and the formation of positronium. Differences to the moderation in solids are due to the lack of long range

correlation in gases and hence there is no possibility to excite collective modes like plasmons or phonons. On the other hand, there are – at least for molecular gases – the rotational and vibrational excitation, by which the positron can loose its energy in the lower energy range.

Positron moderation in gases is based on the following principles: First, there are energy ranges, where the cross sections, which would lead to positron loss, are low. Second the energy ranges, where such cross sections are high could be passed *fast*, due to a high probability for appropriate inelastic scattering process. The energy dependence of the cross sections and how they are used for efficient moderation is explained exemplarily on N_2 as a moderating gas. In general, there are two processes for positron loss: the direct annihilation and the formation of positronium. The probability for the first is very small in gases, and as shown in Fig. 3.3 the threshold for the positronium formation in N_2 is at 8.78 eV. This means the loss of positrons, which have an energy below 8.78 eV, is considerable reduced. The threshold for positronium formation arises from the lower limit for single ionization of N_2 , which is at 15.58 eV and the binding energy of positronium of 6.8 eV. The range between the two thresholds of positronium formation at 8.78 eV and the direct ionization at 15.58 eV is called Ore gap. This area, where the loss of positrons is high due to positronium formation, can be passed only due to electronic, vibrational and rotational excitations. By using only the two latter, the transition over the Ore gap would need roughly 70 scattering processes and therefore it would be very likely that the positrons form positronium. But, in contrast to other gases, the cross section for electronic excitations in N_2 is across the whole Ore gap reasonable high (see Fig. 3.4) and each excitation leads to a high energy loss between 8.5 and 10 eV. Due to this, the gap can be passed by only very few scattering processes. Below the threshold for electronic excitations at 8.55 eV, the positrons are only cooled by vibrational and rotational excitations. Due to the high cross sections for such excitations in gases like SF_6 , CF_4 and CO_2 , mixtures from these with N_2 are used [51].

By applying appropriate magnetic and electric fields the thermalized positrons can be guided, trapped and extracted from the moderation setup. This is be done either continuously or pulsed. A system of the latter type, a so called positron trap, which also allows quasi dc modes, was built up by the Surko group (see Fig. 3.5) and various systems based on this type have been built up over the last years (see e.g. [53]). With one of the first versions, it was possible to store up to 1.6×10^7 positrons within a relatively large volume with a radius of about 2 cm and length of about 5 cm. Later versions used rotating electric fields to compress the positron plasma and used space charge effects combined with a slow dumping of the trap to decrease the diameter of the released beam. Therefore, the created positron beam has not only a very low longitudinal energy¹ spread of 18 meV [54], but also a small diameter of less than 3 mm

¹The terms longitudinal and transversal energy are used as common in particle beam physics. E.g. the longitudinal energy is the amount of the kinetic energy of a particle which is related to its lon-

3 Positron beam techniques

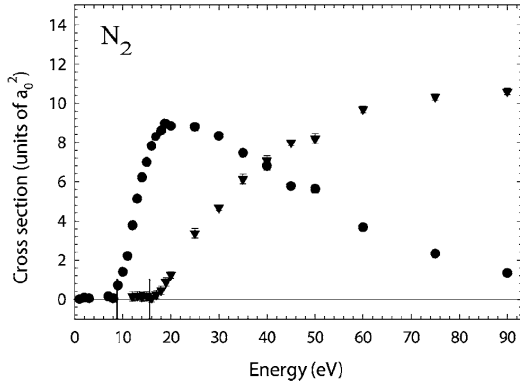


Figure 3.3: Cross sections of the direct ionization (\blacktriangledown) and the positronium formation (\bullet) in N_2 . Below the threshold of positronium formation at 8.78 eV the only process for losing positrons is the direct annihilation, which is negligibly small (from [52]).

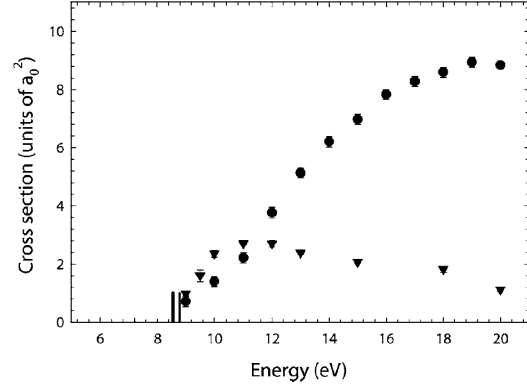


Figure 3.4: Cross sections for electronic excitations (\blacktriangledown) and positronium formation (\bullet) in N_2 . The Ore gap can be passed very fast during the thermalization process by only a few electronic excitations (from [52]).

[51]. The efficiency of trapping positrons from a slow monoenergetic beam has been reported to be up to 40% [55], and releasing from the trap was accomplished with an efficiency of 90% [51]. A good review of the interactions and trapping of positrons in gases as well as a short introduction to trap-based beams is given in [56].

gitudinal motion. The terms longitudinal and transversal are given with respect to the propagation direction of the beam.

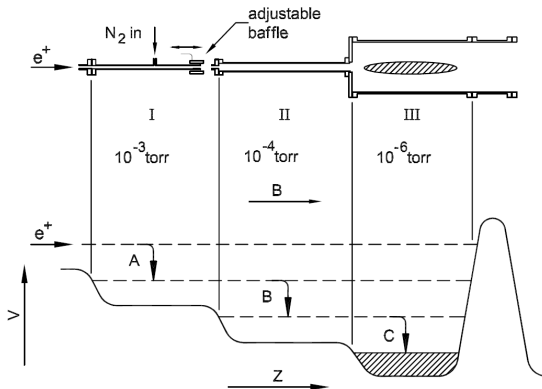


Figure 3.5: Upside: schematic of the electrodes of a positron gas moderator and trap. Below: the electric potential profile created by this electrodes. The positrons are moderated in three stages at different pressures of N_2 . In the last stage the positrons are accumulated and released from there by slowly reducing the potential barrier at the right side and/or raising the potential in front of the barrier (from [56]; for details see [55, 54]).

3.3.2 Moderation in solids

The concept of moderating positrons in gases is relatively new compared to the idea of using solids for creating thermal positrons, which goes back to Madansky et al. in 1950 [57]. Though they had the right idea, they failed to observe unambiguously moderated positrons. It took eight years more until Cherry [58] detected thermal positrons emitted from a mica foil coated with a thin layer of chromium. There were a few more experiments using coated foils [59, 60] (see also Fig. 3.11 on page 28) and also other materials and geometries were examined [61, 62, 63] until the standard moderator materials of today have been found.

The moderation in most solids is based on the following processes: High energetic positrons, which enter the solid lose energy by inelastic scattering processes until they are thermalized. When thermalized, they can diffuse through the lattice as a free particle and there is a finite probability, that they diffuse to the surface of the solid. When the solid has a negative work function for positrons, these positrons can leave the solid perpendicularly to the surface with a sharp energy corresponding to the magnitude of the negative positron work function ϕ^+ .

There are however also processes, which lead to positron loss. A certain fraction of the positrons, hitting the moderator, is backscattered and takes not part on the moderation. The amount of this fraction depends on the energy of the positrons and the atomic number of the moderating material. The next dominant process for positron loss is the annihilation with an electron. This could happen during and after the thermalization. I.e. during the elastic or inelastic scattering processes, as free particle during the diffusion, captured in a defect or a surface state, or after the formation of positronium.²

There are also effects, which do not lead to positron loss but perturb the monoenergetic spectrum of the elastic³ re-emitted positrons (see Fig. 3.6). Positrons with a higher energy than expected due to the negative work function, arise from positrons, which were implanted near the surface and therefore have not been completely thermalized before they reach the surface and are re-emitted as so called epithermal positrons. Positrons with less energy than the absolute value of the work function result from energy loss at the surface. E.g. due to vibrational excitations of molecules absorbed at the surface or creation of electron-hole pairs and phonons at the surface [64].

The energy and angular spread of the elastic peak of re-emitted positrons, is caused only by the thermal energy distribution of the positrons. Therefore, the number of thermalized positrons, which are re-emitted per unit time $F(E)$, with an energy be-

²The annihilation, the diffusion, the trapping in defects and in the surface potential have been already described in chapter 2.

³In this case elastic refers only on the re-emission process not on the complete moderation.

3 Positron beam techniques

tween E and $E + dE$ and into a solid angle $d\Omega$, is as follows [64]:

$$F(E)dE \propto Ee^{-E/kT}dEd\Omega \quad (3.4)$$

It has to be mentioned that e.g. the elastic peaks in [64] and [65] were found to be slightly broader and had to be described by using a higher *effective* temperature.

Because the value of the negative work function of the common moderating materials is in the electron volt range, the positron emission of this materials is concentrated strongly into the normal direction with respect to the crystal surface and is described by an angular distribution as follows [64]:

$$\Theta_{1/2} \simeq \left[\frac{kT}{\phi^+} \right]^{1/2} \quad (3.5)$$

Measured angular distributions for two different sample temperatures are shown in Fig. 3.7. For a more detailed explanation of the energy spectrum of re-emitted positrons and energy loss effects at the surface see e.g. [64, 66] and references therein.

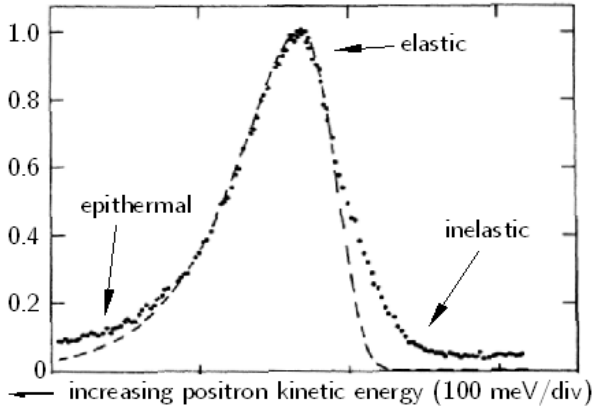


Figure 3.6: The energy spectrum of re-emitted positrons from a clean Ni(100) surface (dots) and the beam Maxwell-Boltzmann energy distribution convoluted with the energy resolution function of the analyzer (dashed curve). For the elastic peak an effective temperature of $1.2T$ had to be used. The tails on the left and right side of the elastic peak are caused by the epithermally and inelastically emitted positrons (from [64]).

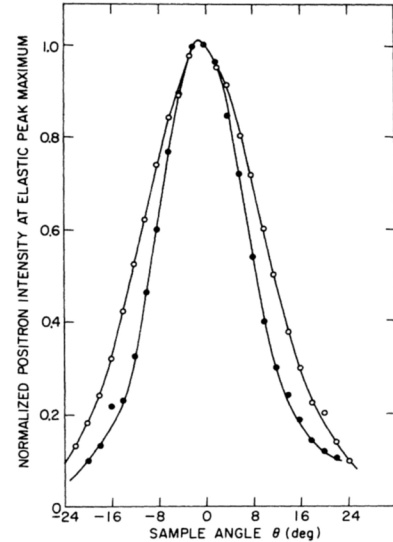


Figure 3.7: Angular distributions of moderated and elastically re-emitted positrons from a Cu(111) sample at temperatures of 23 K (\bullet) and 300 K (\circ). By reducing the temperature the angular spread decreases from $\Delta\Theta_{FWHM} = 24^\circ$ to $\Delta\Theta_{FWHM} = 18^\circ$ (from [64]).

Besides a low energy and angular spread of the re-emitted positrons, the efficiency is an important figure of merit of a moderator material. In the literature and depending

3.3 Moderation and beam formation

on the application, there are different definitions of the efficiency. In the case of a typical slow positron beam in a laboratory, when positrons of a radioactive nuclide are used and the moderator is located close to the source, the efficiency usually defines the ratio of slow positrons in the beam to the positrons emitted by the source. Therefore, not only the physical effects mentioned above but also the geometric arrangement of source and moderator, their geometry, the beam formation mechanism and additional precautions, like a high Z backing of the source, are taken into account. In another definition only the positrons, which actually hit the moderator are set into relation with the moderated positrons in the beam afterwards. In this work the first definition is denoted as *total* moderation efficiency ϵ_{tot} and the second one as moderation efficiency ϵ . ϵ_{tot} will be also used in the case of the repeated moderation of a beam, the so called re-moderation, as the efficiency of the whole setup. Hence, in this case ϵ_{tot} is the ratio of the beam intensity after and before the re-moderator setup.

Considering the processes, which leads to moderation and those, which leads to positron loss, some basic demands on a *good* moderating material can be derived: First of all the moderator needs to have a negative positron work function in order that the thermalized positrons can leave the solid. This is true for nearly all materials except for solid rare gases, which will be discussed later. Measurements of Gullikson et al. in [67] showed that the positron re-emission increases as the magnitude of the work function increases and thus a material with a high work function would be advantageous. A small Z would be favorable in order to keep the amount of backscattered positrons small. This and additionally a low density are especially in the case of re-moderation desirable, because then the injection energy of the primary beam can be kept small, without a reduction of the penetration depth and therefore no increase of epithermal positrons. Especially in the case of re-moderation, a small injection energy is desired, because then the overall energy loss at the re-moderation stage is small. The probability, that the thermalized positrons reach the surface again is enhanced by increasing the diffusion length and reducing the amount of positron trapping sites. Both can be achieved by using single crystals and moreover, the amount of trapping sites is reduced by annealing. To minimize the losses at the surface due to positronium formation, positron trapping and scattering, the surface should be as clean as possible. Therefore, besides good vacuum conditions in the lower UHV range, materials with small sticking coefficients for residual gas molecules are useful.

In this work, tungsten single crystals are used for re-moderating the NEPOMUC beam twice, in order to enhance the *brightness* of the beam. Tungsten has mainly three advantages compared to other common moderating materials. Firstly, the re-emitted positrons have a small energy spread compared to those emitted by solid rare gases. Secondly, the efficiency is in general high (see table 3.2) and depends not as critical on the vacuum conditions as the efficiency of other metallic or solid rare gas moderators. Thirdly, it can be annealed and surface cleaned simply by resistive heating. Nevertheless, there are some aspects which demand attention in order to use the full

3 Positron beam techniques

capability of tungsten as a positron moderator. In the case of tungsten carbon impurities in the bulk and at the surface as well as defects are the main reasons for reduced efficiency. Each factor is reduced by heating the crystal to temperatures of at least 2000°C [68, 69, 70, 71] at good vacuum conditions ($< 10^{-8}$ mbar) either once over a longer time of 10 to 20 minutes or by several shorter *flashes* which last 1 to 2 minutes [69]. Since the long time heating is mainly necessary to reduce the carbon and defect concentration inside the bulk, this can be also performed ex-situ and only the last 1 or 2 short flashes have to be accomplished in-situ, in order to clean the surface. But even without this in-situ cleaning a high moderation efficiency can be attained. It is to mention, that the reduction of carbon could be enhanced, if the heating is done in $\lesssim 10^{-7}$ mbar oxygen [71] and subsequent surface cleaning under lower pressure. The last step is unavoidable, because the oxygen contamination of the surface leads to a wide inelastic tail in the energy spectrum of the re-emitted positrons or even inhibits the re-emission entirely. But also under good vacuum conditions, the surface will be contaminated slightly by carbon and oxygen. As shown in Fig. 3.8 this leads to an efficiency decrease, and moreover, the contamination is responsible for inelastic tails in the energy spectrum of the re-emitted positrons (see Fig. 3.9).

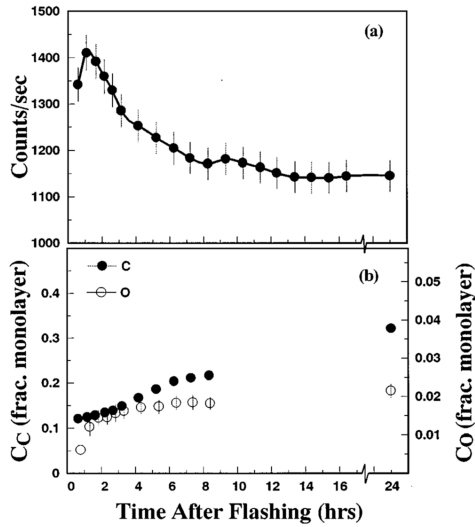


Figure 3.8: Decline of the positron re-emission from a W(100) crystal due to surface contamination with carbon (●) and oxygen (○). The intensity increase within the first hour is attributed to a very low oxygen surface contamination (from [68]).

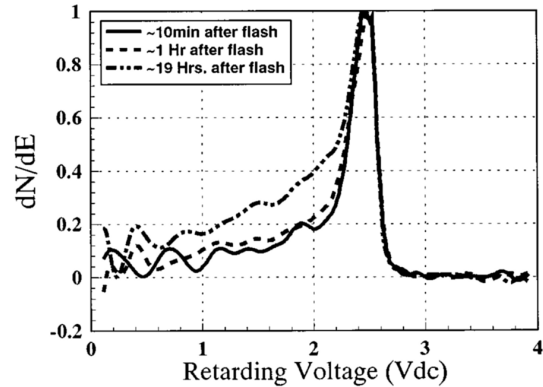


Figure 3.9: Differential energy spectra of the re-emitted positrons at different times after heat treatment of the moderator. The amount of inelastic scattered re-emitted positrons grows as the surface contamination of the moderator increases (from [68]).

Element	Orient.	Geometry	Φ_+ [eV]	ϵ	E_i [keV]	Ref.
W	(100)	T	-2.8	0.38	4.0	[72]
	(110)	R	-2.96(20)	0.33	2.0	[73]
	(111)	R	-2.59(10)	0.41	1.0	[71]
Ni	(100)	R	-1.4	0.20	2.7	[67]
	(100)	T	-1.12	0.19	5.0	[74]

Table 3.2: Positron work functions Φ^+ and achieved efficiencies ϵ of different nickel and tungsten crystals in reflexion (R) and transmission (T) geometry. The efficiency was measured for the case of re-moderation, with an energy of E_i of the primary beam.

Moderation geometries

The moderation geometry describes the geometrical alignment of the surface, from which the positrons are re-emitted to that surface, from which the positrons have entered the solid. In principle, there are four possible geometries for the moderation: reflexion, transmission, quasi-transmission and combinations of these (see Fig. 3.10). There are several criteria, that make the one or the other geometry more suitable. One aspect is, whether the primary positrons, which should be moderated, stem directly from the source and have therefore a continuous energy distribution or they have been already moderated and form a monoenergetic beam, which should be re-moderated. The dimension of the primary beam or the source is also relevant as well as the demands on the secondary beam.

In the case of moderating positrons from a β^+ -source with a high efficiency and thereby creating a beam with a sharp energy distribution, the most common way is the transmission geometry and using a single crystal tungsten foil with a thickness of about 1 μm [37, 18, 75]. If a sharp energy distribution is not as important as a high intensity, solid rare gases (see below) are interesting, because they have a higher efficiency and they can be frozen directly onto the source, whereby a large solid angle is covered and therefore the total efficiency is increased (see Fig. 3.10e). Combinations of reflexion and transmission geometry as shown in Fig. 3.10d raise the total efficiency but also the energy spread of the created beam. Other possibilities to enlarge the intensity are shown in Fig. 3.10e and Fig. 3.10f where high Z materials are used to backscatter fast positrons from the positron source to the moderation foil.

In the case of re-moderation, the reflexion geometry is more common. The main reason for this is, that the primary beam has already a low energy of a few keV. Therefore, a foil which is used in transmission geometry should have a thickness in the range of 100 to 200 nm [76, 77] and is hence much thinner than in the case of moderating high energetic positrons e.g. from a β^+ -source. Such thin foils are challenging to fabricate, difficult to handle, and they tend to be not entirely plain. In reflexion

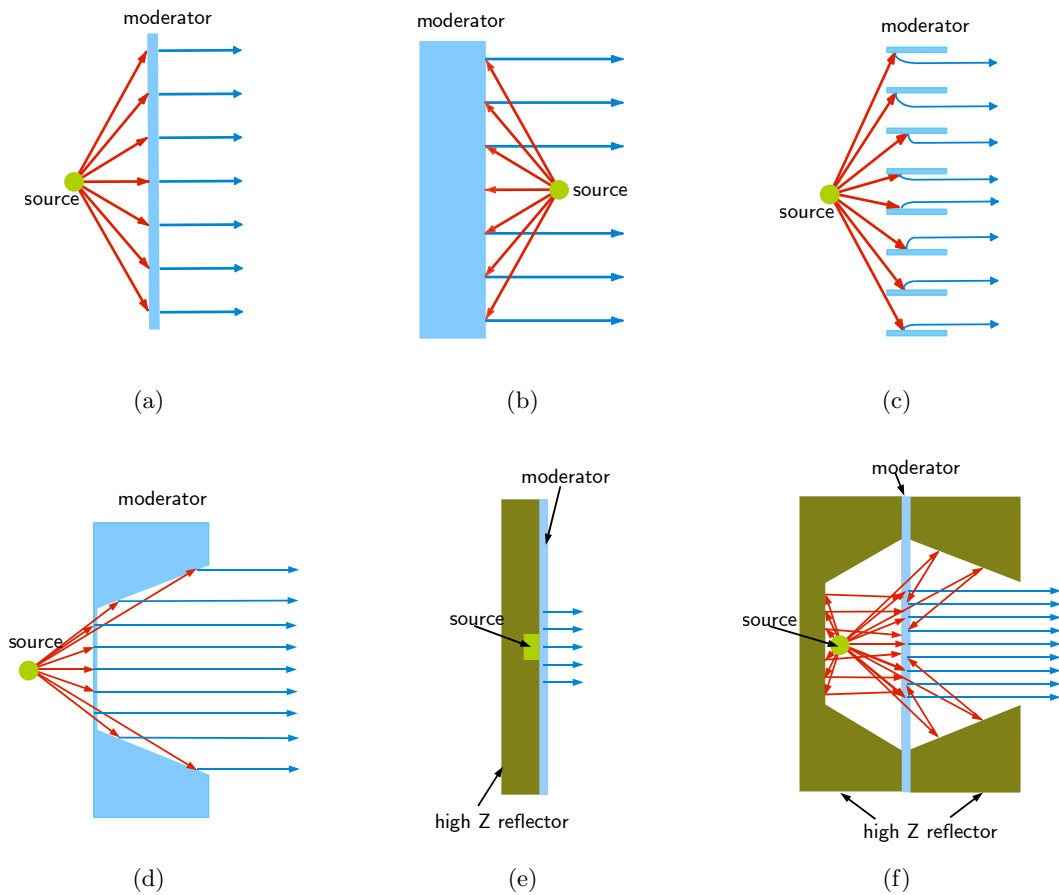


Figure 3.10: Different moderation geometries. In the case of the re-moderation, the primary positrons do not stem from the source but another (re-)moderator. For the re-moderation, so far only (a) and (b) have been realized [36, 79].

geometry, on the other hand, the single crystal can be much thicker, what avoids the mentioned drawbacks of thin foils. For the technical task of separating the incident and re-moderated beam two different solutions have been realized. In this work a magnetic dipol field is used in two different setups. In other systems special electric field arrangements have been used successfully [14, 78].

Solid rare gases

Solid rare gases are not true *moderating* materials in the narrower sense, because the positrons leave the solid with energies in the eV range but these have not been thermalized inside the rare gas solid. Gullikson and Mills showed in [80] that due to the wide band gap, the inelastic threshold is given by the threshold of positronium

3.4 Beam transport and manipulation

formation. Positrons having an energy below this threshold are very likely to leave the solid, because the only noteworthy branch for further energy loss is phonon scattering with a very small cross section. Therefore, the *hot* positrons can leave the solid despite a positive positron work function. The same authors studied the efficiency of some solid rare gases and the energy width of the re-emitted positrons (see Tab. 3.3) [81]. The high efficiencies reported are also caused by unconventional moderating geometries, which could be manufactured easily by freezing out the rare gas at e.g. suitable formed high Z substrates. Today, mostly neon is used, which is frozen directly onto the source, resulting in a large solid angle and therefore a high total efficiency. The method of freezing the rare gas in-situ also allows an easy *reconditioning* of the moderator. When the efficiency or the energy spread gets worse due to surface contamination, the old moderator can be simply evaporated and a new one can be frozen out. One drawback of such moderator materials is the energy spread of 0.58 eV, even by using neon. This is more than one order of magnitude larger than the thermally induced energy spread in the case of other moderating materials.

In principle, it would also be possible to use solid rare gases for re-moderation, but due to the high technical efforts and the broad energy distribution of the re-emitted positrons, this was performed only once [82].

	Ne	Ar	Kr	Xe
ϵ	0.70(2)	0.13(2)	0.14(2)	0.13(2)
$\Delta E[eV]$	0.58(5)	1.7(2)	1.8(2)	3.2(4)

Table 3.3: Moderation efficiencies of different solid rare gases and energy spread of the emitted positrons [81].

3.4 Beam transport and manipulation

The positron as a charged particle responds to the application of electromagnetic fields. This can be used to guide a positron beam over large distances, to focus the beam onto a small spot, and to pulse it in order to provide timing information. In this section, the basic physical principles, equations and techniques for these tasks are gathered and explained.

3.4.1 Motion of charged particles in electromagnetic fields

Since Hans Busch calculated the trajectory of cathode rays in axially symmetric electromagnetic fields [83] in 1926 the dynamic of electrons and other charged particles in electromagnetic fields has been studied extensively and the results of this wide field

3 Positron beam techniques

can be read in many textbooks [84, 85, 86, 87]. Therefore, in this section only the most important equations and conservation laws, which are relevant for this work, are collected without the demand on comprehensive derivations. The basis for the motion of a charged particle in an electromagnetic field is the Lorentz force:

$$\vec{F} = q \left(\vec{E} + \vec{v} \times \vec{B} \right). \quad (3.6)$$

Where \vec{E} is the electric field and \vec{B} is the magnetic induction as used in the Maxwell equations, q and \vec{v} are the charge and the velocity of the particle, respectively. This formula holds for static as well as for time depending fields and also for relativistic energies. By using the relativistic physical momentum

$$\vec{P} = \gamma m \vec{v}, \quad (3.7)$$

with the Lorentz factor $\gamma = (1 - \beta^2)^{-1/2}$ and the particle mass m the equation of motion can be written:

$$\frac{d\vec{P}}{dt} = \dot{\gamma} m \dot{\vec{x}} + \gamma m \ddot{\vec{x}} = q \left(\vec{E} + \dot{\vec{x}} \times \vec{B} \right) \quad (3.8)$$

In rotational symmetric systems the usage of cylindrical coordinates with the components r , φ and z is convenient. Hence, the components of the equation of motion can be written as follows:

$$\frac{d}{dt} (\gamma m \dot{r}) - \gamma m r \dot{\varphi}^2 = q (E_r + r \dot{\varphi} B_z - \dot{z} B_\varphi) \quad (3.9a)$$

$$\frac{1}{r} \frac{d}{dt} (\gamma m r^2 \dot{\varphi}) = q (E_\varphi + \dot{z} B_r - \dot{r} B_z) \quad (3.9b)$$

$$\frac{d}{dt} (\gamma m \dot{z}) = q (E_z + \dot{r} B_\varphi - r \dot{\varphi} B_r) \quad (3.9c)$$

The Newtonian form of the equations of motion are used in their non-relativistic form for the computational simulations, which are described later. As shown, the form of the equations depends on the choice of the coordinate system and therefore they are inappropriate to derive general principles. For this purpose the Lagrange equations of motion are more useful:

$$\frac{d}{dt} \frac{\partial L}{\partial \dot{q}_i} - \frac{\partial L}{\partial q_i} = 0 \quad (i = 1, 2, 3) \quad (3.10)$$

There are different possibilities to obtain a relativistic Lagrangian⁴ L (see e.g. [84, 87]):

$$L = -\frac{1}{\gamma} m c^2 - q \Phi + q \vec{v} \cdot \vec{A} \quad (3.11)$$

⁴In the literature also other definitions of the Lagrangian can be found. Often, they are similar to the definition given here but extended by an additive constant. Since the Lagrangian is no measurable quantity and only the time derivations of L appear in the equations of motion, both definitions lead to the same physical results.

3.4 Beam transport and manipulation

With the electric scalar potential Φ and the vector potential \vec{A} , these are equivalent to the Newtonian form. From the Lagrangian the canonical or conjugated momenta p_i , can be easily derived in cartesian as well as in cylindrical coordinates:

$$p_x = \frac{\partial L}{\partial \dot{x}} = \gamma m \dot{x} + qA_x \quad (3.12a) \quad p_r = \frac{\partial L}{\partial \dot{r}} = \gamma m \dot{r} + qA_r \quad (3.13a)$$

$$p_y = \frac{\partial L}{\partial \dot{y}} = \gamma m \dot{y} + qA_y \quad (3.12b) \quad p_\varphi = \frac{\partial L}{\partial \dot{\varphi}} = \gamma m r^2 \dot{\varphi} + qrA_\varphi \quad (3.13b)$$

$$p_z = \frac{\partial L}{\partial \dot{z}} = \gamma m \dot{z} + qA_z \quad (3.12c) \quad p_z = \frac{\partial L}{\partial \dot{z}} = \gamma m \dot{z} + qA_z \quad (3.13c)$$

In conservative systems the total energy, given by the Hamiltonian, and the canonical momentum are conserved. Conservative are in particular those systems, where the electromagnetic field and hence Φ , \vec{A} , L and the Hamiltonian are not explicitly dependent on time.

In conservative systems with higher symmetries additional conserved quantities can be found. For this work cylinder symmetric systems are especially important, which are independent from the azimuthal coordinate φ . By inserting the Lagrangian Eq. (3.11) in Eq. (3.10) and inserting \vec{v} in cylinder coordinates one gets for the azimuthal component:

$$\frac{d}{dt} \frac{\partial L}{\partial \dot{\varphi}} - \frac{\partial L}{\partial \varphi} = \frac{d}{dt} (\gamma m r^2 \dot{\varphi} + qrA_\varphi) - 0 = \frac{d}{dt} (rP_\varphi + qrA_\varphi) = \frac{dp_\varphi}{dt} = 0 \quad (3.14)$$

This means, that in conservative cylinder symmetric systems the canonical angular momentum is conserved. In general, all conjugated momenta of space coordinates, from which the system is independent, are conserved. This follows directly from the Hamilton equations:

$$0 = -\frac{\partial H}{\partial q_j} = \frac{\partial p_j}{\partial t} \quad \text{or} \quad p_j = \text{const.} \quad (3.15)$$

A powerful tool for analyzing the dynamics of charged particles in electromagnetic fields are the adiabatic invariants. Whenever a generalized canonical coordinate is periodic, these invariants can be derived from the action integrals J_i of the examined system:

$$J_i = \oint p_i dq_i \quad (3.16)$$

q_i and p_i denote the periodic generalized canonical coordinates and canonical momenta, respectively. The action integrals are constant, even when the system is varied slowly with respect to the period of the motion. Such a slow variation is called adiabatic variation. As shown in the next section, especially in the case when a positron is guided by a longitudinal magnetic field, this concept provides powerful conservation laws.

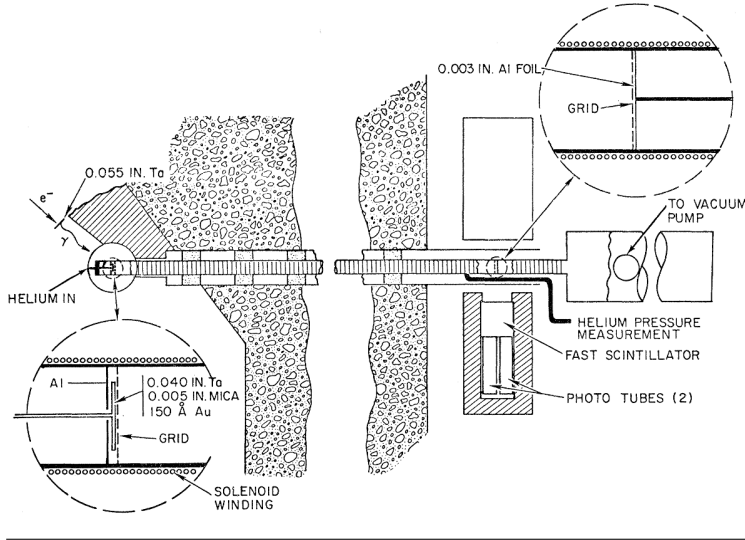


Figure 3.11: The design of the first LINAC based slow positron beam. The technique of guiding positrons by longitudinal magnetic fields is especially at large scale facilities common, where a long distance from the source to the experimental chamber has to be covered (from [60]).

3.4.2 Adiabatic, magnetic beam transport

Already the first setup, which was used for the attempt to detect thermalized positrons, used a solenoidal axial magnetic field to guide the slow positrons from the moderation site to the annihilation target [57]. In the design of the first LINAC based slow positron beam (see Fig. 3.11) the coils for the axial magnetic field were directly wound on the vacuum beam tube [88, 60]. This technique was also used for smaller sized laboratory positron beams utilizing β^+ emitters [59] as well as in recent developments [12, 37]. The physical principles of this beam transport technique and the resulting consequences are presented here.

In a static and solely magnetic field, v^2 and therefore also the Lorentz factor is constant. By using this, the Lorentz force Eq. (3.8) simplifies as follows:

$$\frac{d(\gamma m \vec{v})}{dt} = \gamma m \dot{\vec{v}} = q \vec{v} \times \vec{B} \quad (3.17)$$

$$\Leftrightarrow \dot{\vec{v}} = \vec{v} \times \vec{B} \frac{q}{\gamma m} = \vec{v} \times \vec{\omega}_g \quad (3.18)$$

This describes a circular motion with the cyclotron or gyration frequency ω_g perpendicular to \vec{B} and an uniform motion with the velocity v_{\parallel} along \vec{B} . When \vec{B} is, without loss of generality, along the unit vector \vec{e}_3 and \vec{e}_i ($i = 1, 2, 3$) represents a set of orthogonal basis vectors, the solution of Eq. (3.18) is:

$$\vec{v}(t) = v_{\parallel} \vec{e}_3 + \omega_g r_g (\vec{e}_1 - i \vec{e}_2) e^{i \omega_g t}, \quad (3.19)$$

3.4 Beam transport and manipulation

which leads, by integrating one time, to the path of the particle:

$$\vec{x}(t) = x_0 + v_{\parallel} t \vec{e}_3 + i r_g (\vec{e}_1 - i \vec{e}_2) e^{i \omega_g t}, \quad (3.20)$$

The resulting trajectory is a helix with the radius r_g and the pitch l_g :

$$r_g = \frac{\gamma m v_{\perp}}{e B} = \gamma \frac{v_{\perp}}{\omega_g} \quad (3.21)$$

$$l_g = 2\pi \frac{\gamma m v_{\parallel}}{e B} = 2\pi \gamma \frac{v_{\parallel}}{\omega_g} \quad (3.22)$$

The radius is called gyration radius and the pitch is called gyration length. Both values are useful to estimate the conditions for adiabatic motion and plotted for this purpose for typical positron energies and magnetic field strengths in Figs. 3.12 and 3.13. In the case of the magnetic transport of positrons this slow change is not restricted to a temporal change but includes also the variation of the magnetic field strength and direction along the flight path. The scales within such variations are adiabatic, are set by the gyration radius and length and can be expressed in the following forms:

$$\frac{\vec{r}_g \cdot \nabla \vec{B}}{B} \ll 1 \quad \text{and} \quad l_g \cdot \frac{|\nabla \vec{B}|}{B} \ll 1 \quad (3.23)$$

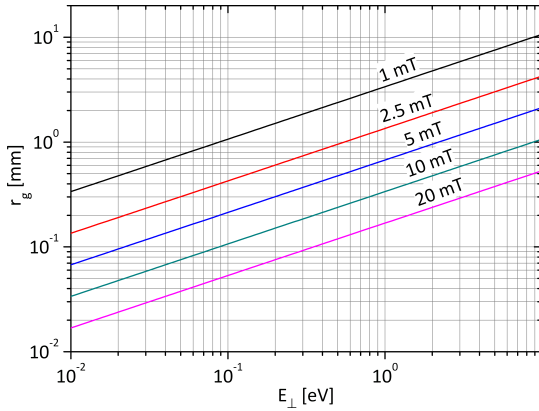


Figure 3.12: The gyration radius r_g plotted against the transverse energy at different strengths of the magnetic induction.

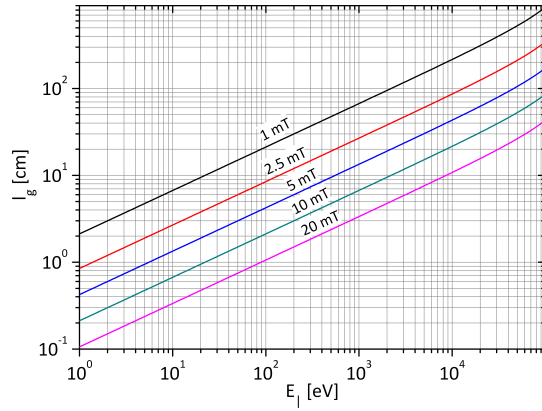


Figure 3.13: The gyration length l_g plotted against the longitudinal energy at different strengths of the magnetic induction.

Consequently, a solenoidal magnetic field can be used for adiabatic beam transport even if the field has small perturbations or even if the solenoid is bent with a sufficient large radius R . In the latter case, however, an additional drift appears, which has two reasons: First, the different densities of windings on the inner and the outer side of the

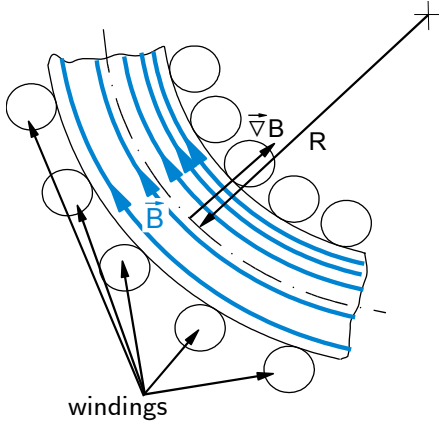


Figure 3.14: Due to the geometry of a bend the winding density and hence the current density at the outer side of the bend is lower than on the inner side. This leads to a gradient of the magnetic induction, which points towards the center of the bend. This gradient leads to the so called gradient drift. The curvature of the induction leads to the centrifugal drift.

bend, lead to a magnetic field gradient, pointing anti-parallel to the radius vector from the outer side to the inner side of the bend (see Fig. 3.14). Therefore, this component of the drift leads to the so called gradient drift. As shown in Fig. 3.15 the field gradient leads to a space dependence of the gyration radius. Since the gyration radius is not only dependent on the magnetic field but also on the transversal velocity $v_{\perp} = r_g \omega_g$, the drift depends on both, the magnetic gradient and on the transversal velocity of the particle. The second reason for a drift motion is the curvature of the magnetic induction. The charged particle gyrate around the field lines and hence they are forced to follow the bend. This means that a centrifugal acceleration⁵ acts on the particle. As shown in Fig. 3.16 this acceleration leads also to a drift perpendicular to the curvature R and the magnetic induction B . In contrast to the gradient drift, this drift, which is called centrifugal or curvature drift, depends on v_{\parallel} . For the sum of the two drift velocities the following expression can be found [87, 89]:

$$\vec{v}_D = \frac{1}{\omega_g R} \left(\underbrace{v_{\parallel}^2}_{\text{curv.}} + \underbrace{\frac{1}{2}v_{\perp}^2}_{\text{grad.}} \right) \left(\frac{\vec{R} \times \vec{B}}{RB} \right) \quad (3.24)$$

In practice the longitudinal velocity is in the energy range from some eV to a few keV and is therefore much larger than the transversal velocity, which is usually in the range from 0.1 eV to few eV. Hence the gradient drift can be neglected in most cases.

In order to guide the positrons without any displacement caused by the drift or by perturbation through a bend, correction coils are necessary which allows to create

⁵In [87, 89] this problem is solved by introducing a force (e.g. caused by an electric field) in addition to a straight solenoidal magnetic induction. Therefore, the corresponding equations could be used to derive an expression for the drift.

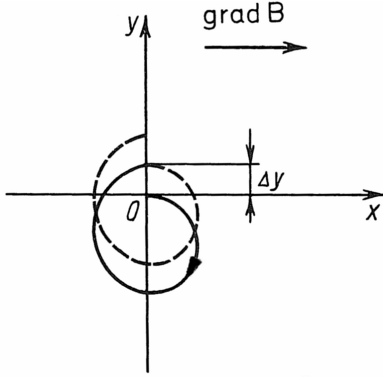


Figure 3.15: Illustration of the gradient drift. The gyration radius depends on the magnetic induction and hence the radius varies if there is a gradient in the induction. On the left side of the gyrations the radius is larger than on the right side. This leads to a drift perpendicular to the gradient of the magnetic induction and the direction of the induction itself (from [89]).

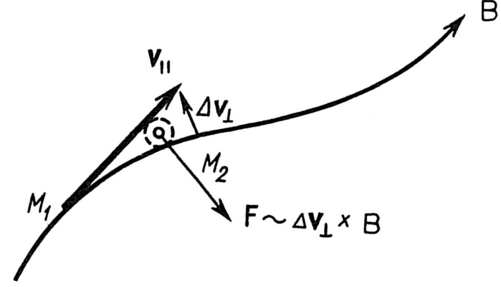


Figure 3.16: Illustration of the centrifugal drift. Because the magnetic induction lines bent away a velocity component arises, which is perpendicular to the induction. This leads to a force and therefore to a drift perpendicular to the curvature of the induction. For a positive charged particle the drift points into the drawing plane (from [89]).

a magnetic field perpendicular to the beam direction. Because of the perturbations which have to be corrected, such coils are also common on the straight beam lines.

The positron is gyrating along the magnetic induction and hence the azimuthal coordinate φ is periodic. The action integral for φ and its conjugated momentum $p_\varphi = \gamma m r_g^2 \omega_g + q r A_\varphi$ is as follows:

$$J = \oint p_\varphi d\varphi = 2\pi \gamma m \omega_g r_g^2 + q \oint A_\varphi r d\varphi \quad (3.25)$$

By choosing for the integration of the second summand a path along one gyration cycle, it can be written as:

$$\begin{aligned} q \oint_{2\pi} A_\varphi r_g d\varphi &= q \oint_{2\pi r_g} A_\varphi dl = q \int_{\pi r_g^2} (\nabla \times \vec{A}) d\vec{S} = q \int_{\pi r_g^2} \vec{B} d\vec{S} \\ &= -q\pi r_g^2 B = -\pi \gamma m \omega_g r_g^2 \end{aligned} \quad (3.26)$$

Inserting this in Eq. (3.25) one gets expressions, which are constant even under adiabatic variation of the magnetic induction:

$$J = \pi \gamma m \omega_g r_g^2 = \pi e B r_g^2 = \frac{\pi}{e} \frac{P_\perp^2}{B} = \text{const.} \quad (3.27)$$

3 Positron beam techniques

Thus $B r_g^2$ and P_\perp^2 / B are adiabatic invariants, where P_\perp denote the mechanical momentum in direction of φ .

In summary, the (adiabatic) motion of a charged particle in an inhomogeneous magnetic field can be decomposed into three motions:

1. A gyration motion with the radius $r_g \propto 1/\sqrt{B}$ and a velocity $v_\perp \propto \sqrt{B}$, with the orbit enclosing a constant magnetic flux.
2. A longitudinal motion of the gyration center along the magnetic field lines with the velocity v_\parallel , for which holds $v_\parallel^2 + v_\perp^2 = \text{const.}$
3. A drift of the gyration center with the velocity v_D perpendicular to v_\parallel as described by Eq. (3.24).

It is important, that the description of the motions and the derived conservative laws are also true, when the gyration center of the particle lies not on the rotation axis of the system. This is especially then of interest, when the dynamic of a beam is examined. A beam consists of an ensemble of particles with different initial conditions including different starting points which are off axis. Due to this different starting points, each particle is gyrating around a center, which has certain distance r from the axis of the system. Hence, the total radius of the beam is determined by the maximum of this distance and the gyration radius (see Fig. 3.17). In practice, however, this is not as relevant, because on the one hand the distance of the gyration center to the axis is usually much bigger than the gyration radius ($r \gg r_g$), and hence the beam diameter is dominated by r . On the other hand, a definition of the beam diameter which uses a certain intensity level like the FWHM of the cross section through the beam profile is more appropriate (see e.g. Fig. 4.14).

Nevertheless this picture is helpful to illustrate a further adiabatic invariant, which is similar to the first in Eq. (3.27) and actually has the same origin. When the magnetic induction is increased adiabatically the field lines get closer. As the flux through the orbit of one particle has to be invariant, the gyration centers are also forced to get closer (see Fig. 3.18). This means that the beam radius r can be varied by an adiabatic change of the magnetic induction over the beam path. By simple geometric considerations it is clear that the radius r depends on the magnetic induction B as $r \propto 1/\sqrt{B}$ or:

$$r^2 B = \text{const.} \quad (3.28)$$

3.4.3 Capture and release of charged particles in an axial symmetric magnetic field

In the last section the adiabatic transport of positrons by a magnetic field was described. In that case the gyration radius and the beam radius change, when the

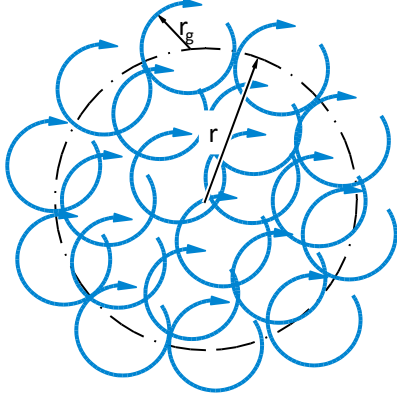


Figure 3.17: A beam consists of many positrons, each gyrating around its own center. Hence, the theoretical total beam radius is the sum of the distance r from the beam center to the radially outermost gyration center and its gyration radius r_g .

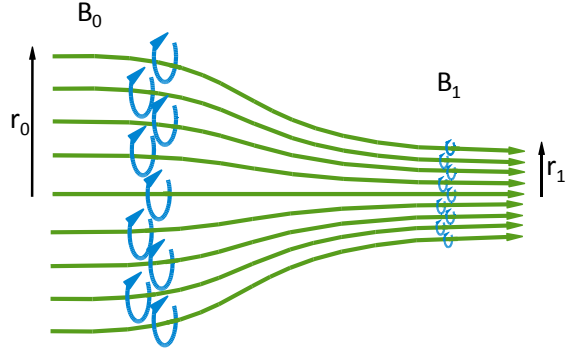


Figure 3.18: By increasing the magnetic induction from B_0 to B_1 , the beam radius is reduced from r_0 to r_1 . This is caused by the fact, that the positrons are guided by the field lines, which get closer by rising the magnetic induction.

positrons move from an area with a higher magnetic field to an area with a lower field and vice versa. When on the other hand the variation is over a short distance, the positrons depart from the field lines and the beam radius does not change. This *adiabatic* transition is especially interesting, when a positron beam should be released from or injected into a magnetic transport field. Although the beam radius can be kept constant, a perturbation of the beam is unavoidable.

Consider the following situation: A positron moves from an area I, with a magnetic induction of B_z^I and a distance from the center r to an area II, with the magnetic induction of B_z^{II} . Since the transition should be adiabatic, the radius in area I and II are the same and due to the conservation law also the canonical angular momentums p_φ^I and p_φ^{II} are equal. Supposing constant solenoidal fields in each area, the vector potential can be written as $A_\varphi = r/2B_z$ and it follows with Eq. (3.13c):

$$p_\varphi^I = p_\varphi^{II}$$

$$\gamma m r^2 \dot{\varphi}^I + \frac{1}{2} e r^2 B_z^I = \gamma m r^2 \dot{\varphi}^{II} + \frac{1}{2} e r^2 B_z^{II}$$

After further rearranging:

$$\Delta P_\varphi = \gamma m (r \dot{\varphi}^{II} - r \dot{\varphi}^I) = \frac{1}{2} e r \Delta B_z \quad (3.29)$$

3 Positron beam techniques

And hence:

$$\begin{aligned}\Delta E_{\perp}[eV] &= \frac{\Delta P_{\varphi}^2}{2m} = \frac{1}{8} \frac{e^2}{m} r^2 \Delta B_z^2 \\ &\approx 2.2 \cdot 10^{-2} \cdot r^2[\text{mm}] \cdot \Delta B_z^2[\text{mT}]\end{aligned}\tag{3.30}$$

Therefore, the positrons get an additional angular momentum in φ direction, during the transition between two areas with different field strengths. This could be understood, by accounting that in the transition area the magnetic field must have a radial component and since the positrons are not guided adiabatically they have to cross this field lines (see Fig. 3.19a). By this illustrative picture it becomes clear, that the direction of the additional momentum depends whether the field lines converge or diverge. Moreover the dependence from r becomes explainable, since the number of field lines which are crossed and therewith the amount of transferred momentum depends on the distance from the center axis. It is noteworthy, that this additional angular momentum could be eliminated again, when the positrons get in a subsequent region, with an equal field strength as in the first region.

Since the amount of ΔP_{φ} depends on the amount of field lines which are crossed during the transition, the transferred momentum can be reduced by guiding the magnetic field lines within an appropriate formed, magnetic material in such a way that they can not be crossed by the positron trajectories. The principle and an possible geometry is shown in Fig. 3.19b. This method do not break the law of conservation of the angular momentum, because the rotational symmetry is broken by introducing the appropriate formed magnetic material. In this work a simple and efficient venetian blind geometry is used but also other, more complex geometries were used in other systems [90, 91].

3.4.4 Focusing a charged particle beam by static and rotationally symmetric electric and magnetic lenses

Adequate but relatively simple producible field arrangements behave like optical lenses. In this work, both, electric and magnetic fields are used for imaging and focusing the positron beam. The electric lenses are mainly used for transporting purposes whereas magnetic lenses focus the beam to a small spot. The theoretically depiction of electron (and therefore positron) optics is far behind the scope of this work and hence the author refers to the textbooks [85, 84, 86]. But nevertheless a brief summary of the methods and ideas involved in the theoretically handling of electric and magnetic lenses will be given.

Gaussian optics

The most important idea in electron optics is to regard only those particle trajectories which are close to the optical axis of the system. More precisely this means, that the

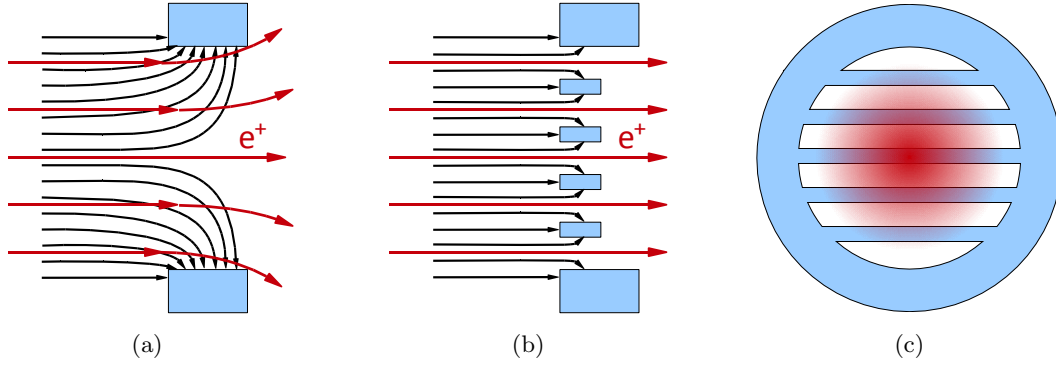


Figure 3.19: (a) When a beam crosses the area, where the magnetic transport field ends, it gets due to the conservation of the angular momentum a *kick* in the φ direction. This can be understood by regarding that in this area the magnetic field must have a radial component B_r , which leads together with the velocity component v_{\parallel} to an acceleration in the φ direction. Since ΔP_{φ} depends on the amount of magnetic flux which is crossed, it can be reduced by leading the flux inside a material with a high permeability outwards as shown in (b). Fig. (c) shows Fig. (b) in beam direction.

distance r of the particle from the center axis of the system has to be much smaller than the radii of the field generating elements e.g. the electrodes, coils or the pole pieces of a magnetic lens. A second constrain is, that the angles between the particle trajectories and the center axis—the slopes—have to be small. This approximations leads to the paraxial equations of motions. There are several ways to derive this equations, but only the most common and intuitive one should be described here briefly.

Because of the rotational symmetry the magnetic field can be derived from a magnetic scalar potential in the same way as the electric field can be derived from the electric scalar potential:

$$\begin{aligned}\vec{B}(r, z) &= -\nabla\Phi_m(r, z) \\ \vec{E}(r, z) &= -\nabla\Phi(r, z)\end{aligned}$$

The components of the magnetic induction and of the electric field can be written as

3 Positron beam techniques

follows:

$$B_z(r, z) = B - \frac{r^2}{4} \frac{\partial^2 B}{\partial z^2} + \frac{r^4}{64} \frac{\partial^4 B}{\partial z^4} - \dots \quad (3.31a)$$

$$B_r(r, z) = -\frac{r}{2} \frac{\partial B}{\partial z} + \frac{r^3}{16} \frac{\partial^3 B}{\partial z^3} - \dots \quad (3.31b)$$

$$E_z(r, z) = -\frac{\partial V}{\partial z} + \frac{r^2}{4} \frac{\partial^3 V}{\partial z^3} + \frac{r^4}{64} \frac{\partial^5 V}{\partial z^5} - \dots \quad (3.31c)$$

$$E_r(r, z) = -\frac{r}{2} \frac{\partial^2 V}{\partial z^2} + \frac{r^3}{16} \frac{\partial^4 V}{\partial z^4} - \dots \quad (3.31d)$$

In the paraxial approximation, only terms up to first order in r and dr/dz are considered, and that is the reason, why the approximation holds only if r and the slope of the particle trajectories are small. If lens aberrations are in the scope of interest, the higher order contributions have to be taken into account.

As far as rotationally symmetric electron lenses are investigated, the radius r and the slope dr/dz are the most interesting values, because with them a geometrical treatment of lenses becomes possible. Therefore, it is reasonable to derive from the general equations of motion a paraxial ray equation that describes the radial motion. This is achieved by inserting the power series of the fields Eq. (3.31) up to the first order terms into the equations of motion (3.9a to 3.9c on page 26). After using the implications of the paraxial approximation and separating the azimuthal parts the following expression for the radial motion can be found [84]:

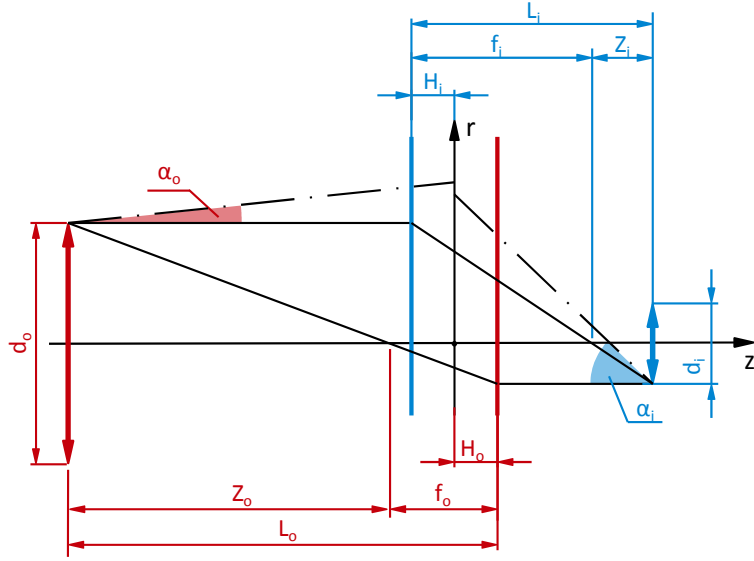
$$r'' + \frac{V'}{2V} r' + \frac{V''}{4V} r + \frac{q^2 B^2}{8mqV} r - \frac{p_\varphi^2}{2mqV} \frac{1}{r^3} = 0 \quad (3.32)$$

V and qV are positive quantities, which represent the voltage equivalent of the kinetic energy of the particle. This equation holds only for the nonrelativistic case, however it is more instructive than the relativistic counterpart. The first term is just the change of the slope of the particle trace. Each other term can be assigned to a certain field or field component and its effect onto the particle: The second term changes the velocity of the particle and arises from the axial electric field. The third and the fourth term describes the focusing focusing due to the radial electric field and the magnetic field, respectively.

The last terms describes the implications of the conservation of canonical angular momentum. This term ensures, that any particle that has an initial canonical momentum can never cross the optical axis. Since the magnetic field can not change the absolute value of the particle velocity, as it is possible for the electric field, the magnetic analogon of the second term is missing.

By further simplification and rearranging of Eq. (3.32) the important equations of

Figure 3.20: The cardinal elements and the denomination of commonly used lengths of a Gaussian optical system. $d_{o/i}$ are the diameters of the object and image, respectively. $\alpha_{o/i}$ denote the object and image side opening angle and $f_{o/i}$ the according focal lengths.



Gaussian optics of rotationally symmetric systems can be derived. Most important for this work, are the lens equations and the equations for the different magnifications:

$$\frac{f_o}{L_o} + \frac{f_i}{L_i} = 1 \quad \text{lens equation} \quad (3.33)$$

$$Z_i Z_o = f_i f_o \quad \text{Newton's lens equation} \quad (3.34)$$

$$M = \frac{d_i}{d_o} = \frac{f_o}{f_i} \frac{L_i}{L_o} \quad \text{Magnification} \quad (3.35)$$

$$M_\alpha = \frac{\alpha_i}{\alpha_o} = \frac{1}{M} \frac{f_i}{f_o} \quad \text{Angular Magnification} \quad (3.36)$$

The meaning of the different quantities, as far as they are not defined by the equations themselves, are shown in Fig. 3.20.

Optical aberrations

Within the paraxial equations a point in the object space is imaged by a lens to a sharp point at an image plain perpendicular to the optical axis. In real systems there are aberrations, which are grouped according to their origin.

Geometrical aberrations are due to the terms of higher order, which are neglected in the first order approximation. To this group belong e.g. the spherical aberration, coma, and astigmatism.

Chromatic aberrations are induced by the energy spread of the beam.

3 Positron beam techniques

Space-charge effects have to be considered in positron beam physics so far only in the case of positron traps and not in terms of imaging aberrations.

Imperfections e.g. mechanical misalignment of the optical elements.

Most significant for this work are the spherical and chromatic aberrations. They limit, beneath other things, the minimal spot size, which can be produced by the probe forming lenses in the re-moderation stages and later on in the specimen chamber. The spherical aberration is caused from the third order terms. These terms are responsible, that particles which pass the lens in a large distance from the optical axis are refracted too strong, so that they intersect the optical axis in front of the Gaussian image plain. Hence, in the image plain, not a sharp point but a disk with the radius r_b appears:

$$r_b \approx C'_s \alpha_i^3$$

C'_s is the spherical aberration coefficient, which is not solely a lens property but also depends on the object distance and the aperture. More important than the radius r_b is, that there is a plane in front of the Gaussian image plane, where the blur is minimal. The disk, which appears in this plane is called disk of least confusion. It can be shown, that the radius r_s of this disk is approximately given by:

$$r_s \approx \frac{1}{4} C_s \alpha_i^3 \quad (3.37)$$

The spherical aberration coefficient C_s or related quantities can be found in tabulations [92] or can be calculated with the help of computer programs⁶.

Because the focal length depends on the beam energy, rays that origin from one point in the object plane but have different energies, end in different points in the image plane. Hence this aberration leads also to a blur, whose radius is as follows:

$$r_c = \alpha_i C_c \frac{\Delta E_{\parallel}}{E} \quad (3.38)$$

Where α_i is the angle of convergence (see Fig. 3.20), ΔE_{\parallel} the longitudinal energy spread and $E \approx E_{\parallel}$ the kinetic energy of the reference particle. The chromatic aberration coefficient C_c is usually obtained from the same sources as C_s [92].

Beam transport by thin lenses

Not only in the case of high (de-) magnifying probe forming lenses one has to take care about the aberrations. There are in principle two possibilities to transport a positron beam over a certain distance. The first is the adiabatic beam transport and the second is to use several (thin) lenses, which are placed in an appropriate distance to each other. In the latter case, the aberration, induced by each lens, accumulate and it is necessary, to keep the aberrations of each lens as low as possible. Electric lenses usually have

⁶e.g. Magnetic Lens Design (MLD) by Lencova

smaller aberrations than magnetic lenses, and additionally, the aberrations at each lens can be kept low by using long focal length and hence avoid large α_i . Moreover, by using lenses with long focal lengths the amount of lenses can be kept low, what leads again to smaller total aberrations.

Minimal spot size of probe forming lenses

The minimal spot size, which can be attained by a probe forming lens can be calculated with the Eq. (3.35 – 3.38). For thin lenses the object side and image side focal lengths are equal and hence it follows from Eq. (3.35) together with Eq. (3.36):

$$r_i = \frac{\alpha_o}{\alpha_i} r_o = \sqrt{\frac{\Delta E_{\perp}^{(o)}}{E_{\parallel}^{(o)}} \frac{r_o}{\alpha_i}} \quad (3.39)$$

Because it is for this work more convenient, the object side opening angle is expressed in terms of $E_{\parallel}^{(o)}$ and $\Delta E_{\perp}^{(o)}$, which are the longitudinal energy and the transversal energy spread of the beam in front of the lens, respectively. Further, the minimal spot size is limited by the angle of convergence at the image plane, which is determined by the focal length of the lens. Since it is much easier to gain short focal lengths with magnetic lenses they are usually preferred for the usage of high de-magnifying lenses, although the aberrations of electric lenses are usually smaller.

To estimate the real spot size r_{rm} the aberrations have to be taken into account. As the regarded aberrations are independent from each other and from the radius given by the Gaussian optic, they must be added quadratically to the radius of Eq. (3.39):

$$r_{\text{rm}}^2 = r_i^2 + r_s^2 + r_c^2 = \frac{\Delta E_{\perp}^{(o)}}{E_{\parallel}^{(o)}} \left(\frac{r_o}{\alpha_i} \right)^2 + \frac{1}{16} C_s^2 \alpha_i^6 + C_c^2 \alpha_i^2 \left(\frac{\Delta E_{\parallel}}{E} \right)^2 \quad (3.40)$$

This equation is used to estimate the attainable spot sizes at the re-moderation stages (see Sec. 4.1 and 4.2).

3.5 Brightness enhancement

The brightness is a figure of merit of a charged particle beam and especially in the case of positrons there are possibilities to enhance this value. But before the enhancement of the brightness is explained, some common and useful quantities, which characterize a beam of charged particle are defined, as the occupied phase space volume, the emittance and the brightness itself.

3.5.1 Beam characterizing quantities

It depends on the context which quantities are most suitable to characterize a beam of charged particles. The most basic quantities are the space coordinates (x_1, x_2, x_3) and the conjugated momenta (p_1, p_2, p_3) of each particle at each time. Because of the large number of particles, these values are in this form not very useful. It is more helpful to look at the volume, which is occupied by the ensemble of beam particles in the six-dimensional phase space⁷. The phase space is spanned by the three spatial and three conjugated momentum dimensions and each point in this space represents a certain state of one particle of the beam.

In rotational symmetric systems cylinder coordinates are preferable, with the azimuthal angle being irrelevant for optical considerations. Hence the dimensions of the phase space can be reduced to the two generalized space coordinates (r, z) and the conjugated momenta (p_r, p_z) . The z-components are usually only necessary, when a bunched beam is regarded. In this case, it is preferable to use instead of the pair z, p_z , the pair Δt and ΔE , which are the time interval and energy difference to a reference particle. Regardless, whether a beam is bunched or not, the longitudinal energy spread can also be of interest e.g. for considering chromatic aberrations. However, it is uncommon to include the longitudinal energy spread without the timing information into a phase space volume quantity. In some cases, it is useful to split the four-dimensional phase space into a longitudinal and a transversal subspace. This is only reasonable, if there is no intermixing of the two associated volumes or if this intermixing can be neglected.

In Figs. 3.21a – (c) an example for a phase space volume which represent the transversal properties of a beam and the perturbing influence of lens aberrations is shown. Although the occupied volume keeps constant it is evident, that a beam occupying a well formed phase space volume as shown in Fig. 3.21a has better optical properties and is therefore more desirable than a beam with a phase space volume as shown in Fig. 3.21c. Hence, it is reasonable to regard an effective phase space volume, which is defined by the borders of the phase space volume. This effective phase space volume is not constant but expands with each passed lens.

In accelerator physics the emittance is another common quantity which describes the quality of a beam. Unfortunately there are several different definitions common in the literature. The most common depend on the longitudinal momentum and are therefore not comparable for different beam energies. The most elemental definition is closely related to the transversal phase space volume but instead of the transversal momentum, the slope $r' = dr/dz$ is taken into account. This volume is also called *trace*

⁷This definition of phase space volume actually differs from the definition, which is common in Hamilton mechanics. There, each particle has its *own* phase space of $2M$ dimensions. Where M is the number of generalized coordinates and momenta, respectively. Hence the dynamic of a beam with N particles is described by a trace within a space with $N 2M$ dimensions and each point in this space represents the state of the *whole* beam at a certain moment.

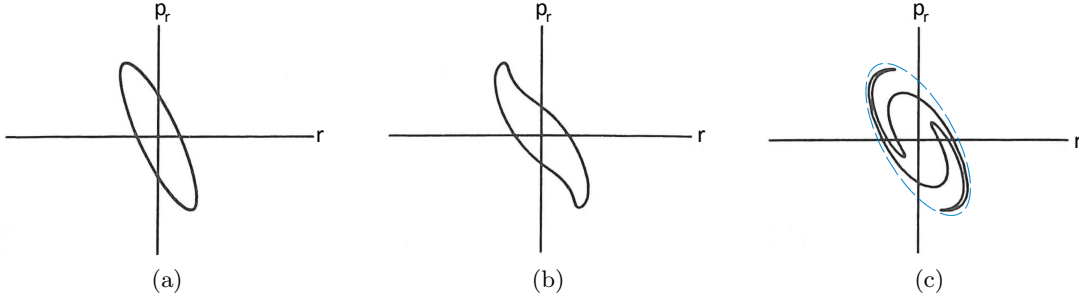


Figure 3.21: Transversal phase space volume and the increasing disorder due to lens aberrations. Because the lens aberrations accumulate, the initial phase space volume of (a) gets more disordered with each subsequent lens (b–c). After several lenses the volume in (a) and (c) is equal, but the *effective* volume of (c) enclosed by the dashed line became larger than in (a) (Illustrations from [84], edited).

space volume. The more sophisticated emittance definitions⁸ account for the grade of perturbation of the beam and/or the particle distribution within the beam.

Both, the phase space volume and the emittance do not consider the beam intensity. This means that both can be reduced to any amount by using appropriate apertures and/or an energy filter. This is not reasonable and therefore quantities considering the phase space volume or any related quantity and the beam intensity are defined. The most important quantity in positron beam physics is the *brightness per electron volt*, which is also just called *brightness*. There are basically two different definitions in literature, which differ, however, only by a factor of $4/\pi^2$:

$$B = \frac{I}{d^2\Theta^2 E_{\parallel}} = \frac{I}{d^2 P_{\perp}^2 / 2m_e} \quad (3.41)$$

$$R_v = \frac{I(4/\pi)^2}{4d^2\Theta^2 E_{\parallel}} = \frac{4}{\pi^2} B \quad (3.42)$$

The first definition is given by Mills in [13] and the second by Canter in [93]. In order to emphasize the quality of a positron beam setup, the brightness is sometimes reported *normalized* to source intensity [94].

These definitions of brightness are based only on the transversal phase space volume. Up to now, there is no definition in the field of positron physics, which accounts for the longitudinal phase space volume. There are two reasonable possibilities to extend the existing brightness definitions in this sense. The most *natural* way would be to multiply

⁸For details of such advanced definitions the reader has to be advised to the already mentioned text books [84, 85].

3 Positron beam techniques

the denominators with the term $\Delta t \Delta E_{\parallel}$, but this would impede the comparison of the brightness of bunched and un-bunched beams. The second possibility is to extend the denominator only by ΔE_{\parallel} , what would keep up the mentioned comparability and would also lead to meaningful expressions in the case of brightness enhancement of a pulsed beam due to re-moderation. Hence, in this work as a further figure of merit, the following definition of brightness is used:

$$B^* = \frac{I}{d^2 P_{\perp}^2 / 2m_e \Delta E_{\parallel}} = \frac{I}{d^2 E_{\perp} \Delta E_{\parallel}} \quad (3.43)$$

3.5.2 Liouville's theorem

The phase space volume and the brightness as used here, obeys Liouville's theorem which states, that the phase space volume occupied of an ensemble of non-interacting particles keeps constant under the influence of conservative forces. An alternative formulation states that under the mentioned conditions, the phase space *density* keeps constant. This theorem is of great importance. It implies, that the minimal diameter, which can be obtained by focusing a beam, is determined already by the properties of the source, because there the inherent size of the phase space volume is defined. The usage of apertures and energy filters reduces the phase space volume but does not violate Liouville's theorem, because with them non-conservative forces are introduced into the system.

3.5.3 Re-moderation

Apertures and collimators are common tools in e.g. electron microscopy to reduce the phase space. Unfortunately positron sources provide much less intensity than the electron counterparts, and hence the usage of such tools is not practicable. However, for positrons there is a superior method to overcome the restrictions, arising by Liouville's theorem, the so called re-moderation. It uses the dissipative forces during the moderation process to enhance the phase space density, and therefore the brightness of a positron beam. This approach was first suggested by Mills in [13] and the principle is as follows (see Fig. 3.22): A beam occupying a certain phase space volume is focused onto a moderator. Due to Liouville's theorem, the transversal momentum must grow, in order to compensate the reduction in the real space. The focused positrons enter the solid and loose their energy by inelastic scattering until they reach the thermal equilibrium, and therefore, they also loose most of their transversal momentum. Since the diffusion length is of the order of 100 nm, and hence usually much smaller than the attainable diameter according to Eq. (3.40), the latitude in real space can be treated as constant. Both, the loss of energy and the reduction of the diameter mean, that the phase space volume gets smaller. Of course this method leads only to the desired

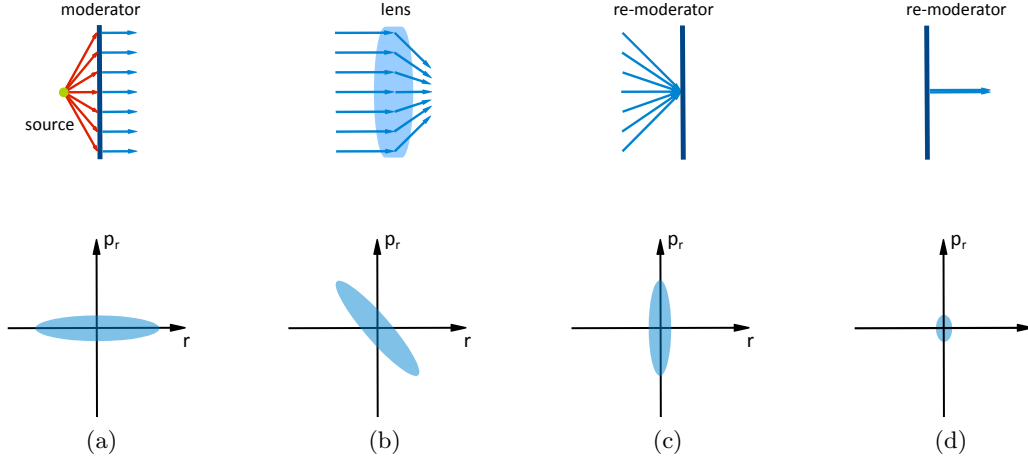


Figure 3.22: Above: Principle of re-moderation. (a) beam creation by source and moderator, (b) the influence of a lens, (c) the re-moderator at the focal plain and (d) the re-moderated beam.

Below: The transversal phase space at each state.

After the first moderation the beam has a certain extension in real and momentum space. The phase space ellipse is tilted by the lens and due to the different momenta at different radii, the ellipse shears to the upright position in the focus. The transversal momentum, which has been introduced by the lens, vanishes by the re-moderation. The result is a small sized beam, with a small transversal momentum. The same behavior can be observed for the longitudinal phase space, where the lens is replaced by a buncher (see below).

enhancement in brightness when the positron losses are sufficiently small.

The following estimation shows, that with this technique e.g. a typical laboratory beam can gain in brightness. In the regarded case the primary and the secondary beam stems both from a moderation process and hence the transversal energy can be considered as equal. The brightness enhancement is therefore determined by the reduction in diameter and by the efficiency. As already written in section 3.3 the efficiency for re-moderation is up to 40 % and a de-magnification factor of about 50 can be reached. With these numbers brightness enhancement can be calculated:

$$\frac{B_2}{B_1} = \frac{I_2}{I_1} \left(\frac{d_1}{d_2} \right)^2 = \epsilon (1/M)^2 \approx 1000 \quad (3.44)$$

3.6 Beam pulsing

The usage of a pulsed beam is not restricted to positron lifetime spectroscopy. It provides also the basic prerequisite e.g. for rising the beam energy with the help of an

3 Positron beam techniques

rf-accelerator.

In principle there are two possibilities to generate a time structured positron beam. The first is to chop the beam, and hence to remove all particles, which are not within the desired short time intervals of the final pulses. It is obvious, that this leads to a high intensity loss, especially when the pulses should be as short as possible. On the other hand the energy spread, most notably the longitudinal energy spread, keeps constant, under ideal conditions. A contrary method is the beam bunching, where the longitudinal energy of a beam is periodically modulated to gain a temporal focus. In the following sections both techniques are presented in detail⁹.

3.6.1 Bunching techniques

The bunching technique is based on the periodically modulation of the longitudinal energy of the particles of a beam (see also Fig. 3.23). The modulation is done in such a way, that particles which are behind a reference particle are accelerated and such which are in front are decelerated. By choosing the right modulation function, the particles will converge to small bunches. After a certain drift, the temporal extension of this bunches become minimal and a temporal focus appears. This technique causes, in the ideal case, no intensity loss.

There are different methods to accomplish the time dependent energy modulation of the positron beam. All have in common, that the energy is changed by an electric field gradient within a gap between two electrodes. The differences are in the function, which is used for the modulation and how the field creation is realized. For estimations a simple expression can be derived, which gives the dependence of the modulation function from time, drift energy and distance to the point, where the time focus appears. Let t_2 be the time, when an arbitrary particle reaches the point L where the time focus should appear:

$$t_2 = t_1 + \frac{L}{v_m} \quad (3.45)$$

Where t_1 is the moment, when a particle is at the buncher gap, and v_m the velocity of the positron immediately after this gap. In this simple approach an instantaneous velocity change at the center of the gap is assumed and hence the extension of the field within the gap and into the tubes is neglected. This approximation holds only, when the extension of the electric field and therefore the gap itself as well as the diameter of the tubes are small. Let the first tube be on a dc potential of U_0 and the second one to the same dc level and an additional time dependent potential $U_m(t)$, which is responsible for the energy modulation. If the positron energy is given with respect to the source potential, the energy of them is in front of the gap eU_0 and within the drift

⁹It is noteworthy, that sometimes, e.g. in ion beam physics, the technique, which is in this work called chopping, is also called bunching. In positron beam physics the nomenclature as used in this work is common and helps to distinguish the two very different techniques of bunching and chopping.

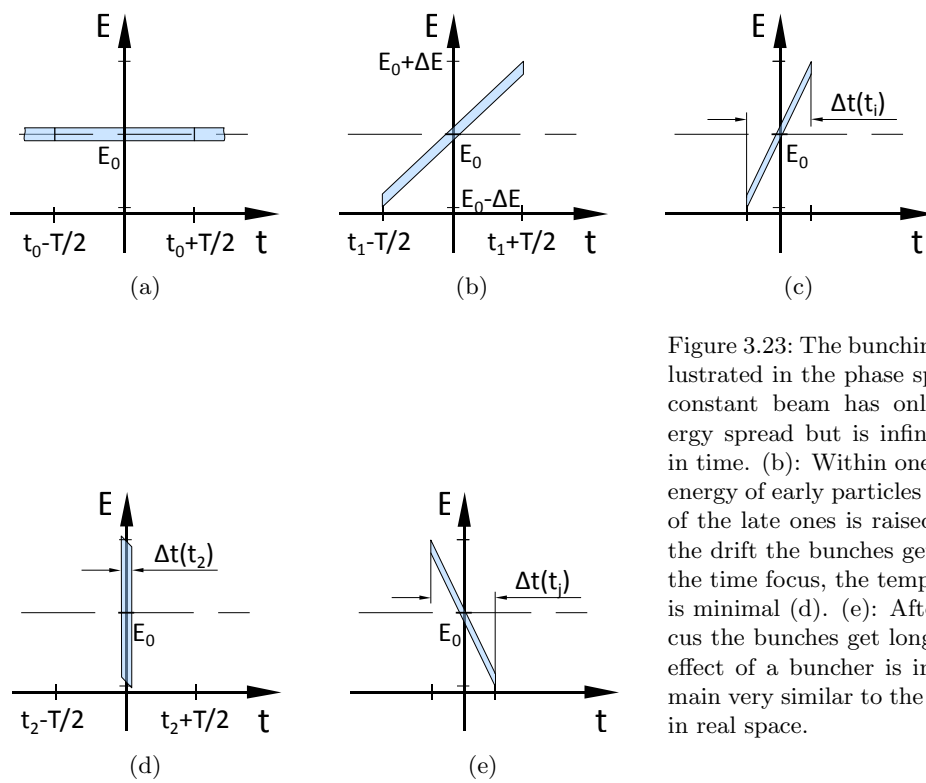


Figure 3.23: The bunching technique illustrated in the phase space. (a): The constant beam has only a small energy spread but is infinitely extended in time. (b): Within one period T , the energy of early particles is reduced and of the late ones is raised. (c): During the drift the bunches get closer and at the time focus, the temporal extension is minimal (d). (e): After the time focus the bunches get longer again. The effect of a buncher is in the time domain very similar to the effect of a lens in real space.

3 Positron beam techniques

tube $e(U_0 + U_m(t))$. The velocity after the gap is hence:

$$v_m = \sqrt{2e/m(U_0 + U_m)} \quad (3.46)$$

Inserting this into Eq. (3.45) leads to:

$$t_2 = t_1 + \frac{L}{\sqrt{2e/m(U_0 + U_m)}} \quad (3.47)$$

$U_m(t)$ is a periodic function and should have no additional offset. Therefore, there are moments, when the first and the second tube are on the same potential. The energy of positrons crossing the gap at this time keeps constant. Such particles are called reference particles and for them Eq. (3.47) simplifies to:

$$t_2^0 = t_1^0 + \frac{L}{\sqrt{2e/mU_0}} \quad (3.48)$$

Where t^0 are the moments when the reference particle crosses the gap and the point L , respectively. If a time focus appears, the particles which have passed the buncher gap at different moments t_1 reach the point L at the same time t_2 . Without loss of generality this is also true for the reference particle and any other:

$$\begin{aligned} t_2^0 &= t_2 \\ t_1^0 + \frac{L}{\sqrt{2e/mU_0}} &= t_1 + \frac{L}{\sqrt{2e/m(U_0 + U_m)}} \\ t_0 &= t_1 - t_1^0 + \frac{L}{\sqrt{2e/m(U_0 + U_m)}} \\ t_0 &= \Delta t + \frac{L}{\sqrt{2e/m(U_0 + U_m)}} \end{aligned} \quad (3.49)$$

By rearranging this equation one gets the following expression for the modulation voltage:

$$U_m = \frac{1}{2} \frac{m}{e} \left(\frac{L}{t_0 - \Delta t} \right)^2 - U_0 \quad (3.50)$$

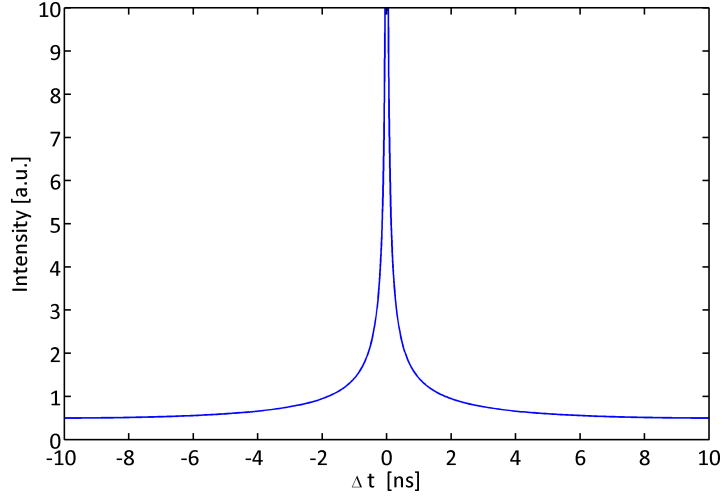
$$= \frac{1}{2} \frac{m}{e} \left(\frac{L}{t_0} \right)^2 \left(\frac{1}{1 - \Delta t/t_0} \right)^2 - U_0 \quad (3.51)$$

$$= U_0 \left(\left(\frac{1}{1 - \Delta t/t_0} \right)^2 - 1 \right) \quad (3.52)$$

When the time $t_0 = L/v_0$, which the reference particle needs for the distance L , is sufficiently large, this function can be approximated by a linear relation between the arrival time Δt of a positron at the buncher gap and the modulation function:

$$U_m \approx 2U_0 \frac{\Delta t}{t_0} = \sqrt{8e/m} U_0^{3/2} \frac{\Delta t}{L} \quad (3.53)$$

Figure 3.24: Time spectrum generated by a sine wave buncher according to Eq. (3.55). Due to the deviation of the sine wave from the ideal modulation function, a background remains over the whole spectrum. For the plot the following values have been used: $\omega = 50$ MHz, $L = 0.5$ m, $U_0 = 409$ V and $\hat{U} = \sqrt{8e/m} U_0^{3/2} (L\omega)^{-1} \approx 60.4$ V.



Therefore, with a sawtooth like modulation function a continuous beam can be converted into a pulsed beam, if the drift length and velocity of the bunching system is chosen accordingly.

Sine wave bunching

Sine functions are often used for the energy modulation, because they are easy to create and to amplify, even though the region, which approximates the linear modulation function sufficiently is only about 25%. By following the derivation, which is given in [95] a parametric expression for the time spectrum at the time focus, which is generated by a sinusoidal energy modulation, can be obtained:

$$\Delta t|_L = t_2 - \frac{L}{v_0} = t_1 - \frac{1}{2} \frac{L}{v_0} \frac{\hat{U}}{U_0} \sin(\omega t_1) \quad (3.54)$$

$$I = 1 - \frac{1}{2} \omega \frac{L}{v_0} \frac{\hat{U}}{U_0} \cos(\omega t_1) \quad (3.55)$$

$\Delta t|_L$ denotes the time difference of an arbitrary particle, that reached the buncher gap at the time t_1 and the reference particle, which crosses the gap at $t_1 = 0$. The time difference is measured, when the reference particle is at the point L , where the time focus appears. Hence, the curve $(x(t_1), I(t_1))$ gives the time spectrum at this point. In the derivation of the expression, transit effects are not regarded and the variables are used as in the derivation of Eq. (3.53). By plotting this distribution one observes beside the main peak a remaining background (see Fig. 3.24).

The situation can be improved by imposing a reasonable number of harmonics in order

3 Positron beam techniques

to gain a more precise approximation of the ideal modulation function. But in this case the coupling of the signal to the electrode gets much more demanding, as the frequency is typically in the order of some 10 MHz. The rf-signal can be transmitted by shielded cables, and if these cables are terminated correctly, all frequencies and therefore the whole signal is transmitted without perturbations. But in the case of bunching at the end of the rf-cable the electrode has to be connected, which acts as a part of the wire and hence makes a frequency independent termination very difficult. Thus, the time dependence of the electric field, which appears at the gap can differ considerably from the intended form. Thereby, the negative influence of the electrode grows with its size.

To avoid such coupling problems, so called double-drift systems were invented, which actually consist of two bunchers, where the second buncher is operated at the first harmonic of the first buncher [96]. By using appropriately dimensioned drift tubes and bunching amplitudes, the two bunchers act like one buncher, which imposes both frequencies. Hence the demanding coupling of a broadband signal to one bunching electrode is avoided. Due to the separation each buncher can be implemented as a $\lambda/4$ -resonator, which enables high bunching amplitudes and avoids the distortion of the sine wave due to imperfect coupling.

This technique was originally developed for pulsing heavy ion beams but the benefits of $\lambda/4$ -resonators were also employed in the first pulsed positron beam system, which provided a high time resolution [17]. Due to other design considerations, this system used for both bunchers, the same frequency, in contrast to the double-drift buncher described above. Therefore, the system converted only a small amount of the dc beam to sharp pulses and the remaining background had to be suppressed by an additional chopper system. Another problem at this system arose due to the low mass of the positrons compared to that of the ions. On the one hand, the lower mass allows lower bunching amplitudes, but on the other hand, it makes the positrons more sensitive on little deviations of the correct bunching amplitude. Hence, the $\lambda/4$ -resonators had to work much more stable, than in the case of ions. Another drawback of the $\lambda/4$ -resonators was, that reasonable dimensions of the resonator necessitated a repetition rate of 200 MHz. This high rate restricted the time spectra to 5 ns, what was especially for the investigation of polymers and other materials, where long lifetimes could appear, too short. This were, among other things, the reasons why this kind of resonators were replaced by the solution described in the following [97, 98].

The three electrode buncher

The approach was to build a RLC circuit, where one buncher electrode is used as capacitance (Ⓔ in Fig. 3.25). Besides the advantage that no complicate coupling has to be accomplished, the dimension of this setup is independent on the frequency and the amplification and hence the energy modulation is not as sensitive to e.g. temperature fluctuations. Further, there is a second gap (Ⓔ), where the modulating electric field appears for a second time. By adjusting the energy and therefore the transit time

of the positrons through the center electrode of the buncher, both gaps can be used for the energy modulation. A correct energy modulation at both gaps occurs, if early positrons are decelerated and late positrons are accelerated at each gap. This means e.g. for early positrons, the center electrode must be on a repulsive potential, when they reach the first gap and on an attractive potential, when they reach the second gap. For late positrons the potential conditions have to be the other way around. Hence there is a phase relation between the first and the second gap of π and the transit time of the un-modulated reference particle must therefore be half the period T of the sine wave¹⁰. Therewith it follows for the velocity v_0 of the reference particle through a center electrode with the length b :

$$v_0 = \frac{2b}{T} \quad (3.56)$$

For this double gap buncher it is also possible to derive a basic equation, which provides similar information as Eq. (3.53) [97]. The following situation shall be considered (see also Fig. 3.25): The energy of the positrons is modulated at both gaps so that early positrons are slowed down and late positrons are accelerated. This means, that the reference particle must have an energy U_0 according to Eq. (3.56) between the two gaps. The energy of the reference particle after the second gap shall be U_1 . It is taken into account, that the temporal extension of the bunches at the first gap Δt_1 get smaller during the transit through the buncher tube and that therefore the energy transfer at the second gap is accordingly smaller although the amplitude \hat{U} is the same of course. The temporal extension at the second gap Δt_2 can be calculated by simple geometric considerations (see lower part of Fig. 3.25):

$$\Delta t_2 = \Delta t_1 \frac{D}{L} = \Delta t_1 \frac{L-b}{L} = \Delta t_1 \left(1 - \frac{b}{L}\right) \quad (3.57)$$

The total potential difference U_s , which a positron undergoes during the transit through the buncher, is the sum of the potential differences at each gap. By using Eq. (3.53), which gives the potential difference at a single gap in dependence of the arrival time, and Eq. (3.57) the following expression for U_s can be derived:

$$\Delta U_s = \Delta U_1 + \Delta U_2 = \hat{U} \Delta t_1 + \hat{U} \Delta t_2 = \Delta U_1 \left(2 - \frac{b}{L}\right) \quad (3.58)$$

Eq. (3.53) can also be used to gain the following relation:

¹⁰In principle the phase relation can be any odd multiple of π ($(2n-1)\pi$, $(n \in \mathbb{N})$) but this would lead to unnecessary long buncher electrodes and/or drift tubes.

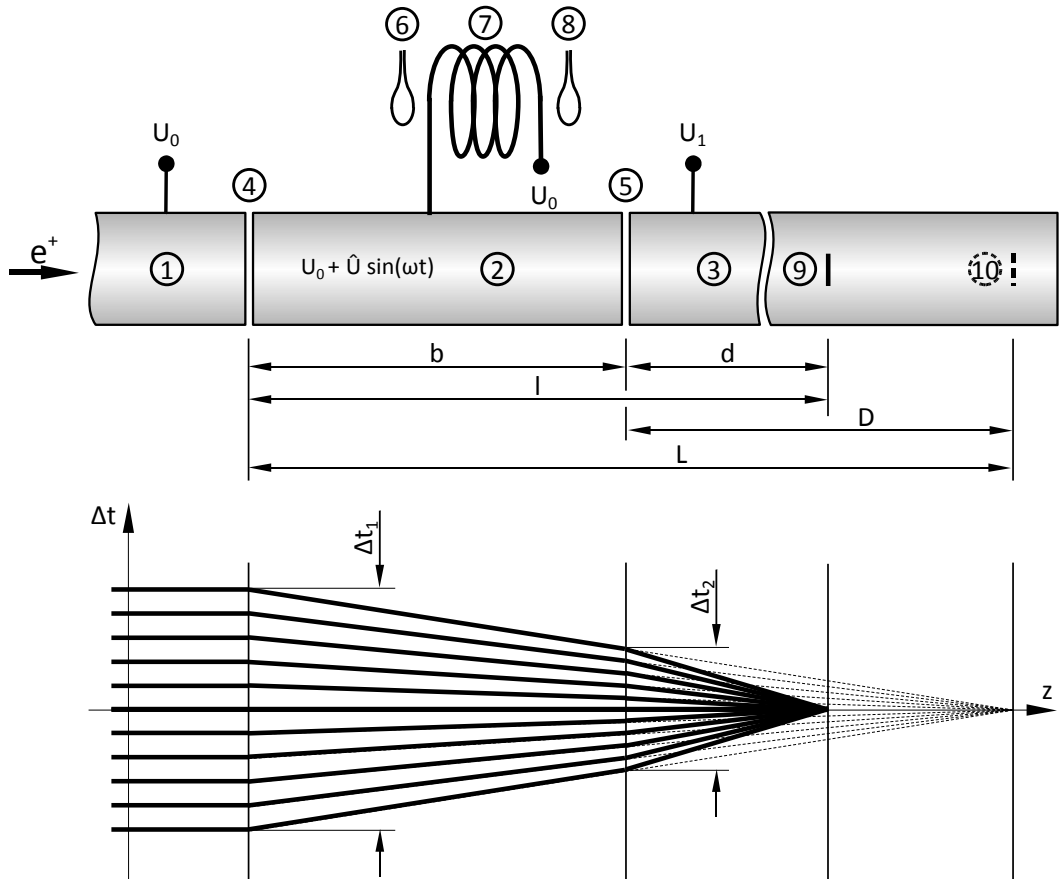


Figure 3.25: Schematic of a three electrode buncher.

Above: The entrance ① and exit ③ electrode are set on the constant potentials U_0 and U_1 , respectively. The center electrode ② acts as the main capacitance in a RLC circuit, which is built up together with the coil ⑦. Therefore, it oscillates around a constant potential U_0 with the frequency ω and the amplitude \hat{U} . Thus, at the gaps ④ and ⑤ an electric field appears which has components in or contrary to the beam direction depending on the phase of the oscillator. By choosing an appropriate transit time through the buncher electrode, the electric field at both gaps, modulate the positron energy in such a way, that they form bunches. The temporal extension gets minimal after the drift d at the point ⑨. If only the first gap had an effect to the particles, the time focus would be at the point ⑩. ⑥ and ⑧ are the coupling and pickup coils which are used to couple the signal to the resonator and to monitor the resonant amplitude.

Below: The time difference of the positrons with respect to the reference particle. Before the first gap all positrons have the same energy and hence the temporal distance remain constant. At the gaps, the energy is modulated in dependence of the arrival time. Due to this the temporal distance becomes smaller with increasing distance from the gap.

$$d = \sqrt{8 \frac{e}{m} \frac{U_1^{3/2}}{\Delta U_s}} \Delta t_s \quad (3.59)$$

Inserting Δt_2 and ΔU_s and rearranging leads to the following quadratic expression:

$$\left[\frac{2db}{\sqrt{8 \frac{e}{m} U_0^{3/2} \Delta t_1}} \right] \Delta U_1^2 - \left[b \left(\frac{U_1}{U_0} \right)^{3/2} + 2d \right] \Delta U_1 + \left[\sqrt{8 \frac{e}{m} U_1^{3/2} \Delta t_1} \right] = 0 \quad (3.60)$$

With this equation, a relation between the modulation energy $e\Delta U_1$ and the drift energy eU_1 as well as the point of the time focus $l = b + d$ is given. This equation will be used in the following chapter to proof the bunching concept of the SPM interface.

Sawtooth bunching

The second gap of the three electrode buncher allows smaller bunching amplitudes or shorter distances to the point where the time focus appears. But because on both gaps the time dependence of the electric fields is given by a sine wave with the same frequency, the background between the positron pulses is still relatively high. As already stated, a lower background can only be attained by approximating the time dependence described by Eq. (3.52) more closely e.g. by a sawtooth function. But this leads not only to the serious coupling problems described above. Because such a signal is broadband, resonant amplification is not possible. This has two implications: First, it is much more challenging to create a signal with a high amplitude, especially, if the signal is used to excite an electrode with a high capacitance. Second, there is no possibility for a setup with only one working gap like in the case of a $\lambda/4$ -resonator. Because the preferable sawtooth function has, unlike a sine wave, only a falling *or* rising edge, at one of the two gaps a wrong energy modulation occurs.

To overcome the second problem the conditions have to be chosen in such a way, that the time focus appears in front of the second gap. I.e. the bunching amplitude has to be high, and because the bunching electrode now acts also as drift tube it has to be sufficiently long. If the positrons are now accelerated at the second gap by a voltage much larger than the bunching amplitude, the energy modulation at the second gap gets negligible and the time focus is *conserved*. However, the longer the bunching electrode the higher is the capacitance of it and hence high bunching amplitudes gets more difficult to achieve. Nevertheless, this approach is realized in the beam preparation section at the existing SPM [99].

Another possibility to avoid a wrong energy modulation at the second gap is to use transit time effects at the second gap. Because of the finite diameter of the electrodes, the electric field penetrates into the inner of them. In theory this field would extend infinitely into the tubes but already after a distance equal to the diameter d of the tube,

3 Positron beam techniques

the field strength is beneath 5% of the maximum (see Fig. 3.26). Hence, during the time the positrons travel the distance of about $2d$ the accelerating or decelerating forces change and lead to an *effective* energy modulation. Usually, this effect is unwanted because it leads to a lower energy modulation which has to be adjusted by a higher buncher amplitude. To avoid this, the diameter of the buncher tubes are chosen as small as possible. On the other hand, the energy modulation can be averaged to zero by extending the area of electric field and matching the positron transit time. This is only true for modulation functions, which are anti-symmetric in time as the sine wave or a sawtooth. For a sine wave function the average voltage in the buncher gap, during the time difference $t_b - t_a$ is as follows [100]:

$$\begin{aligned}\langle U_s \rangle &= \frac{1}{\tau} \int_{t_a}^{t_b} \hat{U} f(t) dt = -\frac{\hat{U}}{\omega\tau} [\cos(\omega t_b) - \cos(\omega t_a)] \\ &= \frac{\hat{U}}{\omega\tau} \left[\cos(\omega t_a) - \cos\left(\omega\left(t_a + \frac{g}{v_0}\right)\right) \right]\end{aligned}\quad (3.61)$$

Hence, the average voltage vanishes, if the so called transit angle $\omega\tau = \omega g/v_0$ is a multiple of 2π . By using the Fourier expansion, this can be also proofed for the sawtooth function:

$$\begin{aligned}\langle U_s \rangle &= \frac{1}{\tau} \int_{t_a}^{t_b} \hat{U} 2 \sum_{n=1}^{\infty} (-1)^n \frac{\sin(n\omega t)}{n} dt \\ &= \frac{2\hat{U}}{\tau} \sum_{n=1}^{\infty} \frac{(-1)^n}{n} \int_{t_a}^{t_b} \sin(n\omega t) dt \\ &= \frac{2\hat{U}}{\tau} \sum_{n=1}^{\infty} \frac{(-1)^n}{n} \left[\cos(\omega t_a) - \cos\left(\omega\left(t_a + \frac{g}{v_0}\right)\right) \right]\end{aligned}\quad (3.62)$$

Under the same conditions as above, each summand vanishes and therefore the average voltage becomes zero. Therefore, the energy modulation at the second gap can be avoided by spreading the area, where the modulation voltage acts onto the positron over a certain distance and adapting the transit velocity. In difference to the first approach this method needs no long bunching electrodes and is therefore implemented in this work. The details are explained in the following chapter.

Aberrations

There are mainly two kinds of aberrations, which lead to a finite spread of the time focus [101]. Because a buncher can be understood as a lens in the time domain (cp. lower part of Fig. 3.25) and the reasons for the spread are similar, they are called spherical and chromatic aberrations following the notation in optics. The spherical aberrations $\Delta\tau_s$ arise from an energy modulation, which differs from the ideal form,

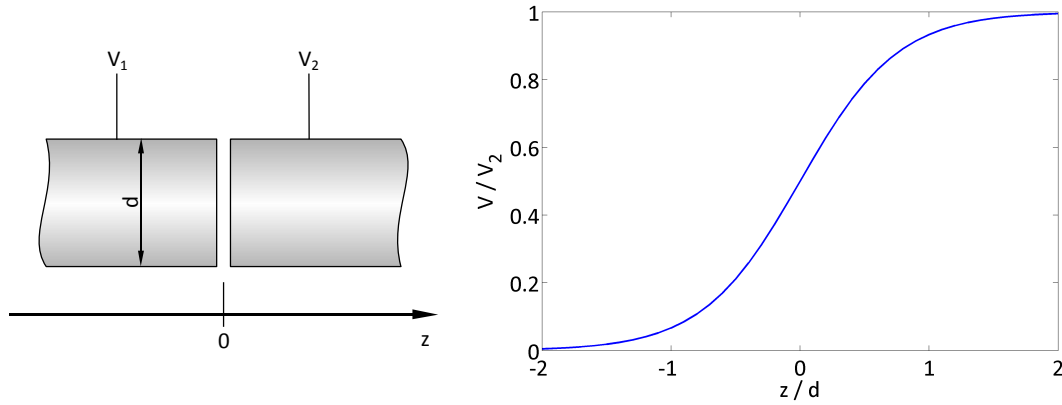


Figure 3.26: Illustration of two coaxial cylinders and the approximation of axial potential according to $V = \frac{V_1+V_2}{2} \left[1 + \frac{1-\gamma}{1+\gamma} \tanh(\omega z) \right]$ with $\gamma = V_1/V_2$ and $\omega = 1.318$. For the plot the potential V_1 was set to zero [86].

given by Eq. (3.52). For the case of a sine wave buncher, the following approximation can be derived [101]:

$$\Delta\tau_s \approx \frac{\pi^3 p^3}{3 \omega} \approx 10.3 \frac{p^3}{\omega} \quad (3.63)$$

With $p := \frac{\Delta t_{\max}}{T} = \frac{\omega \Delta t}{2\pi}$ defining the time interval of one period, which is converted to the final pulse. This value of $\Delta\tau_s$ is achieved by using the modulation amplitude given by Eq. (3.53). Similar as in the optic case, where at a certain place the disk of least confusion can be found, the temporal spread can be reduced to

$$\Delta\tau_s \approx \frac{2\pi^3 p^3}{9\sqrt{3} \omega} \approx 4 \frac{p^3}{\omega} \quad (3.64)$$

by applying a higher bunching amplitude [101]. The amplitude is to be chosen in such a way, that the positrons, which are at the moments $\pm\Delta t_{\max}/2$ with respect to the reference particle at the buncher gap, reach the time focus at the same time. In practice this value differs not much from the *ideal* value and could be found empirically. This technique is called *overbunching* and leads theoretically to a microstructure of the peak, which is usually not observable e.g. due to the time resolution of the detector system.

The chromatic aberrations are – as in the optic case – due to the finite energy spread of the primary beam. This energy spread leads to different drift times after the energy modulation. The value of the chromatic aberration is given by rearranging Eq. (3.52):

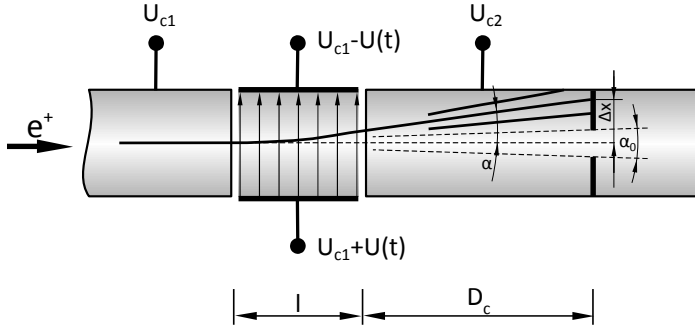


Figure 3.27: Scheme of a simple chopper. By applying a square wave voltage to the chopper plates, the electric field between them deflects the beam. If the voltage as well as the drift are appropriately chosen, the deflection angle is larger than the beam divergence and the beam is stopped at an aperture.

$$\Delta\tau_c = (8e/m)^{-1/2} \frac{L}{U_0^{3/2}} \Delta E/e \quad (3.65)$$

Hence, the chromatic aberration can be reduced if the distance L is decreased or the drift energy is raised. However, each of the two changes necessitates an increased amplitude for the energy modulation.

3.6.2 Beam chopping

As already stated, chopping leads to a high intensity loss if it is used as a single device to create a pulsed beam. But if a chopper is applied onto an already bunched beam, it reduces only the background between the pulses. However, if the chopper is used for heavy particles like ions or if there is a magnetic transport field, the design of a chopper can be at least as demanding as a buncher system [102, 17, 103, 6]. Fortunately, the positron is a light particle and the chopper can be located in an area without a magnetic transport field. These two factors make the construction much easier than other systems and hence the most obvious approach for such a system can be used (see Fig. 3.27): The beam passes a pair of capacitor plates, on which—in the ideal case—a square wave voltage is applied. When the voltage is on the high level the beam is deflected by the electric field and stopped at an aperture in a certain distance. When the voltage is zero, the beam passes the plates and the aperture unperturbed.

The deflection can easily be calculated, if transits and fringe effects are neglected. The force which acts on a positron within the capacitor plates is perpendicular to the center line and could be written as follows:

$$ma_{\perp} = e \frac{\Delta U_c}{d_c} \quad (3.66)$$

Where U_c is the voltage between the capacitor plates, d_c their distance and l their

3.6 Beam pulsing

length (see Fig. 3.27). By integrating once, one gets the transversal velocity, the positron gains over the transit time through the capacitor:

$$v_{\perp} = \int_{t_c} \frac{e}{m} \frac{\Delta U_c}{d_c} dt = \frac{e}{m} \frac{\Delta U_c}{d_c} \frac{l}{v_{c_1}} \quad (3.67)$$

The velocity of the positron shall be v_{c_1} within the chopper and v_{c_2} during the drift. The deflection Δx after the drift D_c is than given by:

$$\Delta x = \frac{v_{\perp}}{v_{c_2}} D_c = \frac{e}{m} \frac{\Delta U_c}{d_c} \frac{l}{v_{c_1}} \frac{D_c}{v_{c_2}} \quad (3.68)$$

In order to blank the beam entirely, it is important, that the deflection angle α is larger than the inherent divergence of the beam α_0 :

$$\alpha = \frac{v_{\perp}}{v_{c_2}} > \sqrt{\frac{E_{\perp}}{E_{\parallel}}} = \alpha_0 \quad (3.69)$$

4 Positron beam preparation at NEPOMUC

The main aim of this work was to create the first preconditions for the implementation of the SPM at the positron facility NEPOMUC at the FRM II. This task was fulfilled in two steps: First, a re-moderator was built up, connected and set into operation near the first accessible position of the NEPOMUC beam line (see Fig. 4.1), which enhances the beam brightness. The second step was to build up an interface for the last optical column of the SPM, which enhances the brightness further and converts the continuous re-moderated NEPOMUC beam to a pulsed positron beam. This interface will replace the source section and the beam preparation column of the SPM which are used in the laboratory.

In order to understand the design of the NEPOMUC re-moderator, it is necessary, to know the properties of the NEPOMUC source and of the beam it provides. Hence, these properties are depicted briefly before the design and the experimental results of the re-moderator are presented. Similar is the structure in the case of the interface. Since the interface provides the beam for the last optical column of the SPM the demands of this are essentially. Further, many of the design principles of the interface have there origin in the concept of the SPM, which is therefore explained in brief.

4.1 The NEPOMUC re-moderator

4.1.1 The positron source NEPOMUC

The positrons at NEPOMUC are created by pair production, with the γ -radiation being created by the reaction $^{113}\text{Cd}(n,\gamma)^{114}\text{Cd}$ (cp. Sec. 3.2.2). In order to gain a high gamma flux and therefore a high positron production rate, the cadmium is located in the tip of a beam tube, near the core of the FRM II (see Fig. 4.2). Inside the tube a platinum structure is located which serves two different purposes. Firstly, platinum is used as converter of the high energetic gamma radiation into fast positrons. Because this conversion is done by pair production a material with a high atomic number as platinum is preferable. Secondly, it is used as moderating material not only due its negative work function of about -2 eV but also because the radiation induced defects are annealed in-situ due to the high temperature caused by the gamma radiation [105].

4 Positron beam preparation at NEPOMUC

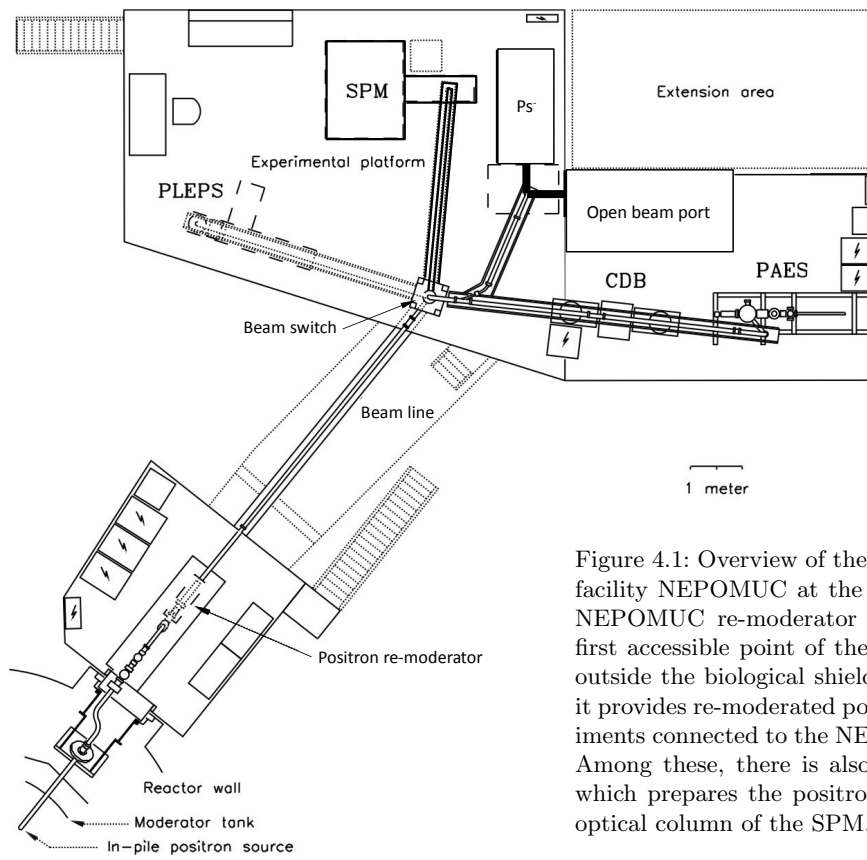
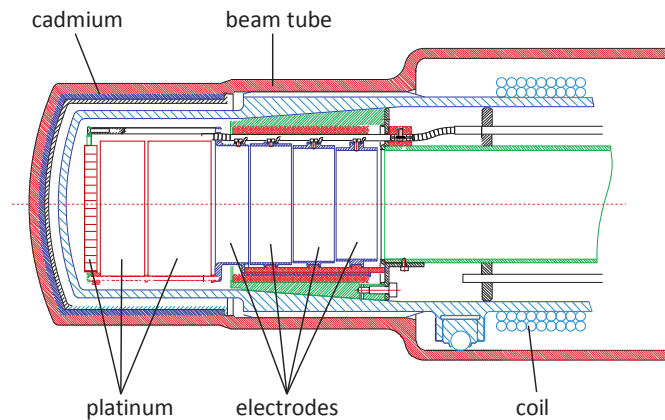


Figure 4.1: Overview of the slow positron beam facility NEPOMUC at the FRM II [104]. The NEPOMUC re-moderator is located near the first accessible point of the positron beam line outside the biological shield of the reactor and it provides re-moderated positrons for all experiments connected to the NEPOMUC beam line. Among these, there is also the SPM interface which prepares the positron beam for the last optical column of the SPM.

Figure 4.2: The NEPOMUC source section is located in the tip of a beam tube which reaches near the reactor core. Thermal neutrons are captured by a cap of ^{113}Cd , whereby inside this cap a strong field of γ -radiation arises. The γ -radiation is used to create positrons by pair production in the platinum structure. This structure is also used for the moderation of the fast positrons. The diameter of the platinum structure and the following electrical lenses, which are also made of platinum, is about 70 mm (from [106]).



The platinum foil section is divided in three parts¹: In order to provide a large volume and therefore a high conversion rate from the γ -radiation to moderated positrons, the first part is realized as a honeycomb structure, where one side is closed by a planar foil. The two further parts are intended for positron production and as electrical lenses and are therefore implemented as cylinder like elements. This section is followed by further electrical lenses which enable together with the beginning magnetic transport field the formation of a beam of moderated positrons. This beam is guided by the magnetic field through three bends, outside of the biological shield of the reactor. At this point the beam can be analyzed firstly.

The most important differences in the designs of the NEPOMUC source and of the source section of a typical laboratory beam are the dimensions and the orientation of the moderator surfaces. In laboratory beam designs, a tungsten foil is used in transmission geometry. The diameter of the *active* area, which actually emits moderated positrons, is usually between 1 and 5 mm. Due its orientation, the longitudinal and transversal energy spread of such a laboratory beam is given by the thermal broadening of the peak of the elastically re-emitted positrons. Hence the FWTM of both energy spreads is roughly 0.1 eV. It is supposed, that most of the moderated positrons which contribute to the beam intensity are emitted from the honeycomb structure, where the larger part of them is emitted from the planar front plate. Hence, the active diameter of the NEPOMUC source is given by the diameter of the honeycomb structure which is 70 mm. Since the magnetic transport field, which is converging at the place of the honeycomb structure, is not perpendicular to the emitting surfaces the

¹The design described here depict the situation before January 2008. At that time the platinum structure and electrical lenses were renewed and minor changes to the former design where made. However this modifications are not important for the estimations of the transversal and longitudinal energy spread.

4 Positron beam preparation at NEPOMUC

maximum energy spread is not given by the thermal spread of the emitted positrons. Instead, the absolute amount of the work function (2 eV) can be regarded as an upper limit for the transversal and longitudinal energy spread. Together with the positron intensities of the NEPOMUC beam² and of a typical laboratory³ beam which are $9 \cdot 10^8 \frac{e^+}{s}$ and $2 \cdot 10^5 \frac{e^+}{s}$, respectively, the brightnesses can be calculated according to the Eqs. (3.41) and (3.43):

$$\begin{aligned}
 B_{\text{NEP}} &= \frac{9 \cdot 10^8 \frac{e^+}{s}}{(70 \text{ mm})^2 \cdot 2m_e \cdot 2 \text{ eV}} \approx 9.0 \times 10^4 \left(\frac{\text{c}}{\text{eV m}} \right)^2 \frac{1}{\text{s}} \\
 B_{\text{lab}} &= \frac{2 \cdot 10^5 \frac{e^+}{s}}{(3 \text{ mm})^2 \cdot 2m_e \cdot 0.1 \text{ eV}} \approx 2.2 \times 10^5 \left(\frac{\text{c}}{\text{eV m}} \right)^2 \frac{1}{\text{s}} \\
 B_{\text{NEP}}^* &= \frac{9 \cdot 10^8 \frac{e^+}{s}}{(70 \text{ mm})^2 \cdot 2m_e (2 \text{ eV})^2} \approx 4.5 \times 10^4 \left(\frac{\text{c}}{\text{eV m}} \right)^2 \frac{1}{\text{seV}} \\
 B_{\text{lab}}^* &= \frac{2 \cdot 10^5 \frac{e^+}{s}}{(3 \text{ mm})^2 \cdot 2m_e (0.1 \text{ eV})^2} \approx 2.2 \times 10^6 \left(\frac{\text{c}}{\text{eV m}} \right)^2 \frac{1}{\text{seV}}
 \end{aligned} \tag{4.1}$$

According to these values, the brightness of a well designed laboratory beam is more than two times higher than that of the beam created by the NEPOMUC source. The difference extends to a factor of almost 50, if the longitudinal energy is also taken into account. The withdraw of the NEPOMUC source is the large phase space volume. But this can be reduced by the re-moderation technique and because of the high intensity of the source even a re-moderated NEPOMUC beam can provide much more positrons as a typical laboratory beam. E.g. with a re-moderator, which has a total efficiency of 10 % and which creates a beam with a diameter of of about 2 mm and a longitudinal as well as transversal energy spread of about 0.5 eV a brightness of about $B = 4.4 \times 10^7 \left(\frac{\text{c}}{\text{eV m}} \right)^2 \frac{1}{\text{s}}$ and $B^* = 8.8 \times 10^7 \left(\frac{\text{c}}{\text{eV m}} \right)^2 \frac{1}{\text{seV}}$ can be achieved, respectively. The relatively high energy spreads are assumed, because not only the thermal spread should be regarded but also effects which increase the energy spreads during the extraction of the re-moderated positrons from the re-moderation setup. Of course, also the brightness of the laboratory beam could be enhanced by re-moderation, but in that case the intensity of the beam might get below a reasonable value.

4.1.2 The setup of the NEPOMUC re-moderator

Already for the former designs for a neutron induced positron source at the FRM, a re-moderator was intended [107, 108] and two attempts were started to develop such a device [109, 110]. The NEPOMUC re-moderator is based on the design ideas of these developments and some parts as the vacuum chamber and the magnetic lens

²Intensity after the renewal of the source section in January 2008 [12].

³E.g. the slow positron laboratory beam at the Technical University in Munich [37].

were used again. However, several improvements have extended the former designs. E.g. an advanced extraction from the magnetic transport field and imaging of the primary beam was implemented, two crucial correction coils enable the adjustment of the magnetic field at the re-moderation crystal, and the beam extraction was optimized by additional electric lenses at the exit. Before the components of the re-moderator are explained in detail a short overview of the setup is given.

The re-moderator works in reflexion geometry and the beam transport is accomplished electrostatically. Only the focusing onto the re-moderation crystal and the separation of the primary and the re-moderated beam is done magnetically (see Fig. 4.3). To ensure an unperturbed electrostatic beam guidance the whole re-moderator is shielded by mu-metal and the magnetic guiding field of NEPOMUC is terminated at the entrance of the re-moderator. The diverging beam is focused by a special electric lens toward the operative range of a short-focal magnetic lens. This combination of lenses ensures a small spot size at the W(100) crystal and a large aperture of the optics. The three electrodes in front of the crystal and the crystal itself can be set on different potentials. This allows to form a re-moderated positron beam at different energies. The re-moderated beam is separated from the primary beam by a dipole field, which bends the slow positrons by 30° toward the exit of the system. Because of the much higher energy of the primary beam, its deflection is only 6° . The different deflection angles were also considered in the y-form of the construction. Before the positrons beam re-enter the magnetic transport field the ratio of its diameter and transversal momentum can be adjusted by further electrical lenses. In order to gain a high moderation efficiency and an unperturbed energy spectrum of the re-emitted positrons, the W(100) crystal can be annealed and its surface can be cleaned by resistive heating.

Adiabatic decompression line and magnetic field termination device

Before the positrons enter the re-moderator, they pass an adiabatic decompression line. This line is 60 cm long and is equipped with coils in different increments (see Fig. 4.4). With these coils the magnetic flux in front of the magnetic field termination can be reduced or raised smoothly to any value between 15 mT and zero. By tuning the field strength, the correlation between the beam diameter and the transversal momentum can be matched according to the demands of the subsequent particle optics (cp. Sec. 3.4.2). It has turned out experimentally, that a value between 1 and 2 mT in front of the field termination gives the highest total efficiency of the re-moderation setup.

The magnetic field termination device is placed subsequent to the adiabatic decompression line. It consists of 30 metallic glass stripes of 25 μm thickness which are mounted on a double sided CF 100 mu-metal flange with a distance of 2 mm to each other (see Fig. 4.5). In order to avoid magnetic saturation and to keep geometrical shadowing as small as possible, the width of the stripes is about 2 mm at the center and rises to 4 mm at the borders. Outside the coil the magnetic circuit is closed by cylindrically shaped mu-metal sheets.

4 Positron beam preparation at NEPOMUC

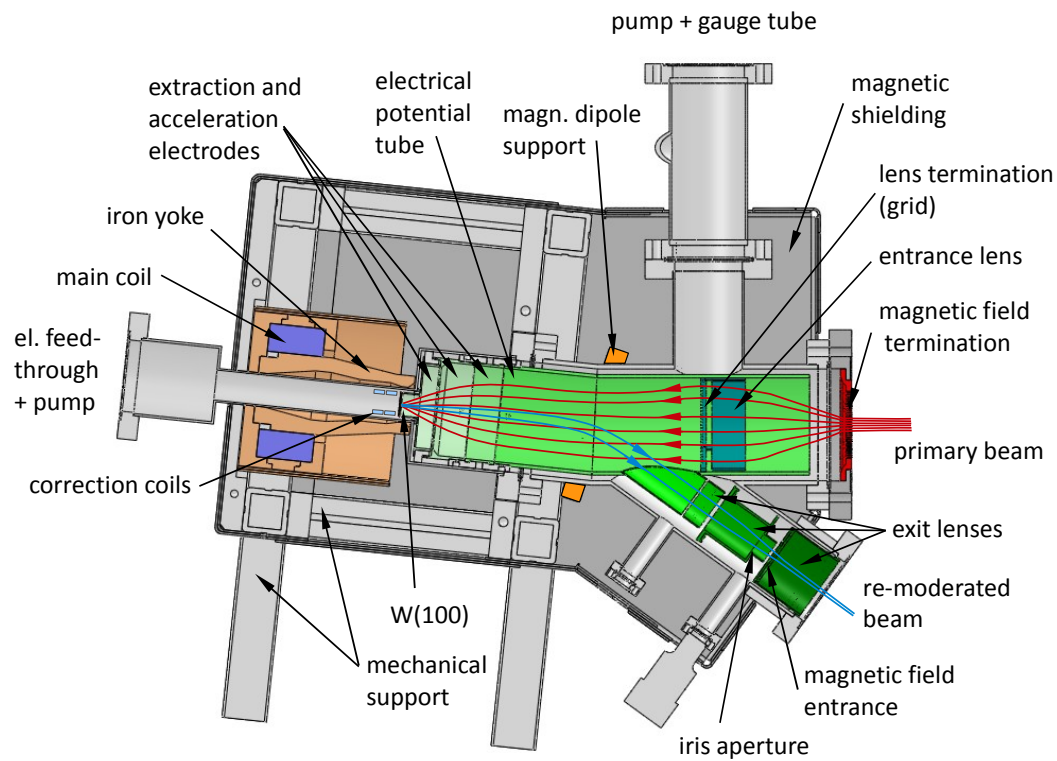


Figure 4.3: Cross sectional view of the NEPOMUC re-moderator. The primary NEPOMUC beam enters the re-moderator from the right side and is extracted from the magnetic transport field with the help of a field termination device. The free diverging beam is imaged by the entrance lens toward the operational field of the magnetic single pole lens, which focuses the beam onto a W(100) single crystal. The re-moderated positrons are accelerated and formed to a beam by three electrical lenses. A magnetic dipole field bent the re-moderated beam toward the exit, where it can be formed again by electrical lenses, before it re-enters a magnetic transport field.

Figure 4.4: Scheme of the adiabatic decompression line. Over a distance of 60 cm the magnetic flux density can be reduced smoothly, in order to adjust the ratio of beam diameter and transversal momentum in front of the magnetic field termination.

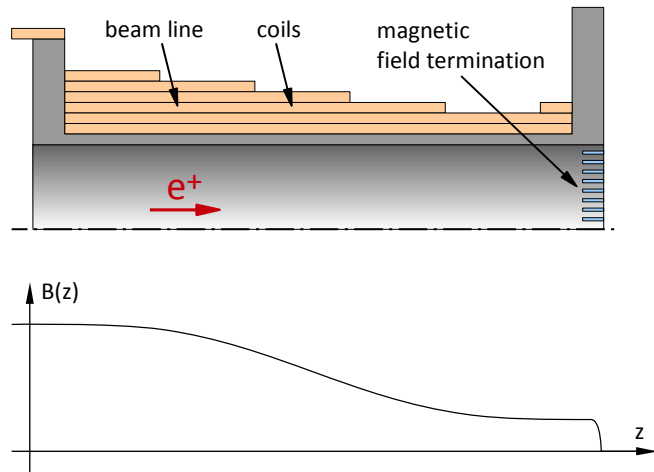
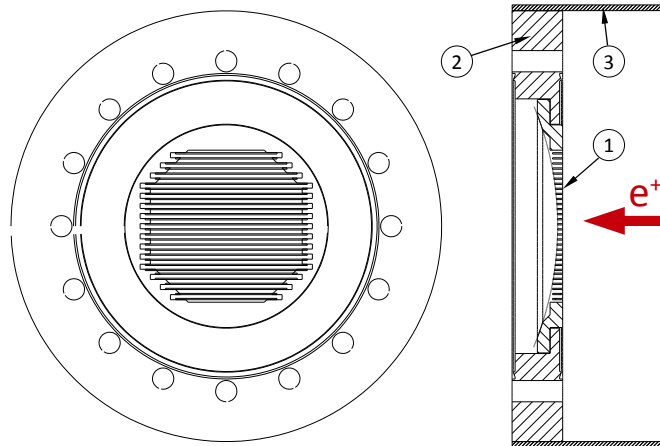


Figure 4.5: The magnetic field termination device, which is used to extract the primary NEPOMUC beam from the magnetic guiding field. It consists of metallic glass stripes ①, which are mounted on a CF 100 flange ②. By this construction, the magnetic flux is guided in the stripes outwards. The cylindrically shaped mu-metal sheets ③ are used to guide the magnetic field to the beginning of the coil and therefore to close the magnetic circuit.



4 Positron beam preparation at NEPOMUC

As written in Sec. 3.4.3, the positrons get an additional mechanical momentum in the azimuthal direction, when they transit from a region with a magnetic (transport) field into a field free region. Since the magnetic flux is guided in the metallic glass stripes, the maximum momentum, which is transferred to the positrons, is not given by the beam radius, but by half the distance between the stripes (see also Fig. 3.19). In the case of a magnetic field strength of 2 mT in front of the field termination, the maximal transversal energy, which is transferred to the positrons is given by Eq. (3.30):

$$\Delta E_{\perp} \approx 2.2 \cdot 10^{-2} \cdot \left(\frac{d}{2}\right)^2 [\text{mm}] \cdot \Delta B_z^2 [\text{mT}] \approx 20 - 90 \text{ meV} \quad (4.2)$$

Hence, the momentum which is transferred to the positron during the transition from the magnetic transport field into the re-moderator is reduced to a value which is much smaller than the approximated transversal energy of the primary beam.

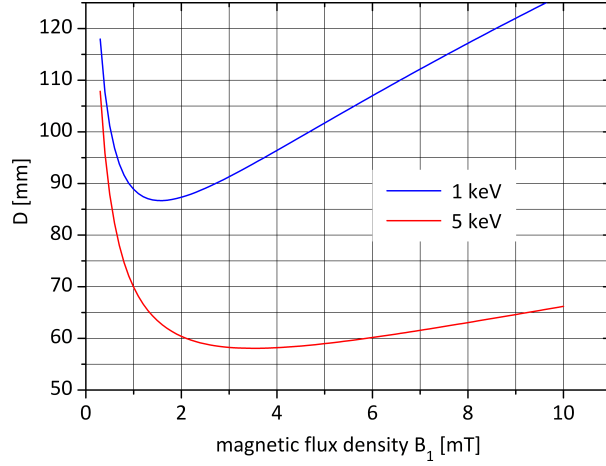
Transport and focusing of the primary beam

The construction of the NEPOMUC re-moderator started before the FRM II and NEPOMUC were set into operation. The design of the re-moderator was originally based on the assumption, that the kinetic energy of the primary beam is 5 keV with respect to ground potential, that the maximum transversal energy is given approximately by the positron work function of the moderator ($E_{\perp 0} \approx 2 \text{ eV}$), and that the positrons stem from an area with the diameter of the platinum structure ($D_0 \approx 70 \text{ mm}$). After the adiabatic decompression, these initial values are transformed to $D_1 = D_0 \sqrt{\frac{B_0}{B_1}}$, $E_{\perp 1} = E_{\perp 0} \frac{B_1}{B_0}$, with B_0 being the average field strength of the magnetic flux at the source and B_1 the field strength at the end of the adiabatic decompression line.

Since after the magnetic field termination the beam diverges in all directions within a certain opening angle, the beam profile immediately after the field termination can be regarded as a real object of the size D_1 which can be imaged by appropriate lenses. The opening angle is defined by $E_{\perp 1}$ and if this is small enough it can be ensured that all positrons are accepted by the optics of the re-moderator which transports and focuses the primary beam.

In the case of this re-moderator setup, the acceptance of the primary positron beam is restricted mainly by the inner diameter of the electrodes in front of the re-moderation crystal. Hence, the diameter of the diverging beam must be smaller than the diameter of these electrodes. The diameter D of the beam at the beginning of the operational field of the magnetic lens depends on the diameter and transversal momentum at the field termination and is calculated as follows:

Figure 4.6: The beam diameter at the beginning operational field of the magnetic lens as function of the field strength at the end of the decompression line according to Eq. (4.3).



$$\begin{aligned}
 D &= 2 \left(\frac{D_1}{2} + z_0 \sqrt{\frac{E_{\perp 1}}{E_{\parallel}}} \right) \\
 &= 2 \left(\frac{D_0}{2} \sqrt{\frac{B_0}{B_1}} + z_0 \sqrt{\frac{E_{\perp 0} B_1}{E_{\parallel} B_0}} \right)
 \end{aligned} \tag{4.3}$$

Where z_0 is the distance from the field termination to the beginning of the operational field of the magnetic lens⁴. To achieve a minimal beam diameter at the beginning of the field of the magnetic single pole lens, the optimal ratio of beam diameter and transversal momentum has to be adjusted within the adiabatic decompression line (see Fig. 4.6). For the primary beam with an energy of 5 keV the minimal attainable diameter at the beginning of the magnetic lens field is about 58 mm. This is much less than the inner diameter of the re-moderation body used in [109, 110].

During the time when NEPOMUC was set into operation it turned out, that due to the strong radiation field of the reactor core the electric insulation is affected more than assumed. Hence, it was decided to limit the maximum energy of the primary beam to 1 keV during routine operation. The lower longitudinal energy enlarges the diameter of the beam in front of the magnetic lens in the re-moderator to about 87 mm, what is slightly more than the inner diameter of the re-moderation body which is 84 mm. Hence, the positrons occupying the outermost regions of the phase space volume and having therefore both, a high transversal momentum and a large distance to the center axis, might get lost. But since these regions of the phase space volume are occupied only sparsely, the positron loss was expected to be small. Moreover, in the improved

⁴The momentum, which is transferred to the positrons during the transition into the field free area was neglected since it is much smaller than the inherent momentum (see above).

4 Positron beam preparation at NEPOMUC

version of the NEPOMUC re-moderator the additional electrical lens at the entrance is used to transport more positrons of the incoming beam toward the magnetic lens.

Since the beam profile at the field termination acts like a real object, the minimal spot size at the re-moderator can be calculated⁵ by using Eq. (3.40). The object radius r_o is given by the beam radius $D_1/2$ and the transversal energy is given by E_1 at the field termination device. As the image distance is only little larger than the focal length f , the angle of convergence α_i can be approximated as follows:

$$\alpha_i \approx \frac{D}{2f} \quad (4.4)$$

Since the maximal longitudinal energy spread of the primary NEPOMUC beam is roughly 4 eV and therefore 250 times smaller than the longitudinal energy, the chromatic aberration is negligible. Thus the minimal spot size is given by the following expression:

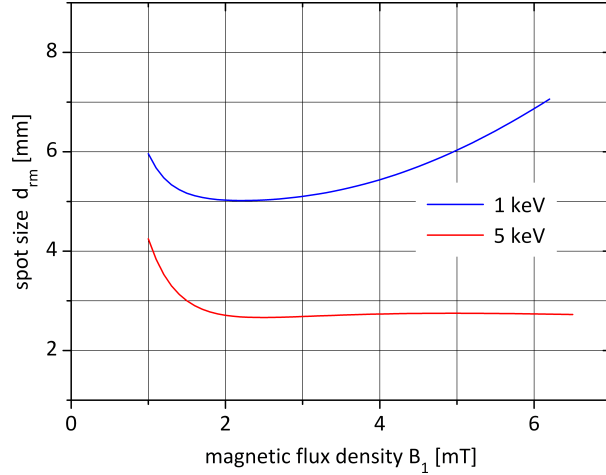
$$\begin{aligned} r_{\text{rm}}^2 &= \frac{\Delta E_{\perp}^{(o)}}{E_{\parallel}^{(o)}} \left(\frac{r_o}{\alpha_i} \right)^2 + \frac{1}{16} C_s^2 \alpha_i^6 \\ &\approx \frac{E_{\perp 1}}{E_{\parallel}} \left(\frac{D_1}{D} f \right)^2 + \frac{1}{16} C_s^2 \left(\frac{D}{2f} \right)^6 \end{aligned} \quad (4.5)$$

The properties of the lens can be estimated from general rules for magnetic lenses. The minimal focal length is roughly determined by the inner diameter of the pole yoke and hence $f_{\text{min}} \approx 30$ mm. The spherical aberration is usually between $1f$ and $0.5f$. For the estimation of the minimal spot size it is assumed to be about $0.75f$. Assuming a little lower focal length of about $f \approx 45$ mm results in a minimal diameter of about 5 mm if the primary beam has an energy of 1 keV, and below 2.7 mm in the case of a 5 keV beam (see Fig. 4.7).

Measurements at the primary NEPOMUC beam, which were made after the design and construction of the first version of the re-moderator, stated a longitudinal energy spread of about 50 eV (FWHM), what is much more than originally estimated. It is assumed, that this high energy spread is the sum of several smaller perturbations occurring in front of the first accessible position. Due to reasons of conservation of energy, it is assumable, that the transversal energy spread is of the same order. This result and the fact that the efficiency of the first re-moderator version was lower than expected, lead to the second version of the re-moderator setup, including the electric lens at the entrance.

⁵For the sake of completeness and to document the original design, both, a primary beam energy of 1 keV and 5 keV will be regarded, in the following.

Figure 4.7: The diameter of the spot is plotted in dependence of the field strength at the end of the decompression line according to Eq. (4.5).



The lens is similar to a common Einzellens, with the important difference that the second gap is terminated by a grid. This is necessary, to avoid perturbations of the re-moderated beam. The grid is made of thin wires, which are spaced with a distance of 2 mm, and has therefore a optical transmission of about 99 %. Because there are no tabularized data for such special lenses, it is difficult to estimate the minimal spot size in a similar way as above. Hence, the electric and magnetic fields were calculated numerically and the particle traces were simulated by the commercially available software package COMSOL Multiphysics. In order to use the rotational symmetric application modes, the influence of the magnetic dipole, which separates the primary and the re-moderated beam, was disregarded and hence a rectified model was simulated. A selection of the trajectory calculations for a 1 keV beam is shown in Fig. 4.8. For these simulations different starting points as well as different maximum, radially directed initial velocities were chosen. One set of trajectories represents a beam with a maximal transversal energy spread of 30 eV and a maximal diameter of 10 mm. The other set represents a beam with an energy spread of 20 eV and a diameter of 20 mm. To reduce the spot size at the re-moderation crystal for the high momentum trajectories, the magnetic field strength of the single pole lens was reduced at the expense of the spot size of the low momentum trajectories. The minimal diameter attained by this was below 10 mm. By rising the excitation of the magnetic lens and matching the excitation of the electric lens accordingly only positrons from the center of the phase space volume are guided to the crystal but a much smaller spot can be attained.

The simulations showed, that substantial modifications of the re-moderation setup had to be done, in order to extend the acceptance of the re-moderator for a beam with a larger phase space volume. For example, this would necessitate a new lens design with a larger inner diameter but this would extend inevitably the focal length and hence the minimal spot size. Moreover, a beam with larger phase space volume would lead

to a larger spot size. However, a small spot size is desirable, because by this size the phase space volume of the re-moderated beam is determined. This phase space volume should be as small as possible not only because of the experiments, which use the re-moderated beam, but also because a sufficient small phase space volume is necessary to ensure a lossless transport of the re-moderated beam to the exit of the re-moderator setup.

Transport of the re-moderated beam

Depending on the ratio of the magnetic field strengths at the re-moderation crystal and at the point where the re-moderated positrons escape from the field lines of the magnetic lens, the shape of the phase space volume can be controlled. E.g. it is possible to decide, whether the beam should have a particularly small diameter or a particularly small transversal momentum. If the re-moderation takes place within a strong magnetic field, the re-emitted positrons can be de-compressed adiabatically, whereby the transversal momentum is reduced and the diameter gets larger. If the re-moderation takes place in a low magnetic field the diameter and transversal momentum can be kept on the values set by the re-moderation. In this case, however, the re-moderation has to take place behind the high field of the magnetic lens which is used to focus the beam onto the re-moderation crystal (see Fig. 4.9). Therefore, the re-moderated beam has to surmount the high magnetic field adiabatically. The first approach enables a lens design with a short focal length and low aberration coefficients and therefore, a smaller spot size than in the second approach. Nevertheless, for the NEPOMUC re-moderator, the second approach is used for the following reason: The re-moderated positrons leave the magnetic field of the lens and there is a point, where the field strength gets below a certain value and the positrons break away from the field lines. As pointed out in Sec. 3.4.3 during the transition into the magnetic field-free area an azimuthal momentum is transferred to the positrons. The amount of this additional momentum depends on the diameter of the beam at the breakaway point. This diameter and therefore the transferred momentum can be kept lower with the second approach.

To realize a low magnetic field at the site of the crystal, two correction coils are placed shortly behind the crystal. The combination of two coils enables not only to adjust the field strength but also the field gradient at the crystal surface. Hence, the field can be adjusted in such a way that the field lines are perpendicular to the crystal surface and the electric and magnetic field lines are as congruent as possible (see Fig. 4.11). This ensures that the perpendicular emitted positrons are guided adiabatically. Consequently the positrons gain no transversal momentum due to an acceleration which is not directed along the magnetic field lines.

In the field free area, the beam diverges due to the inherent transversal energy spread and due to the momentum which is transferred at break away from the magnetic field lines. This diverging beam is bent by the magnetic dipole toward the exit, where

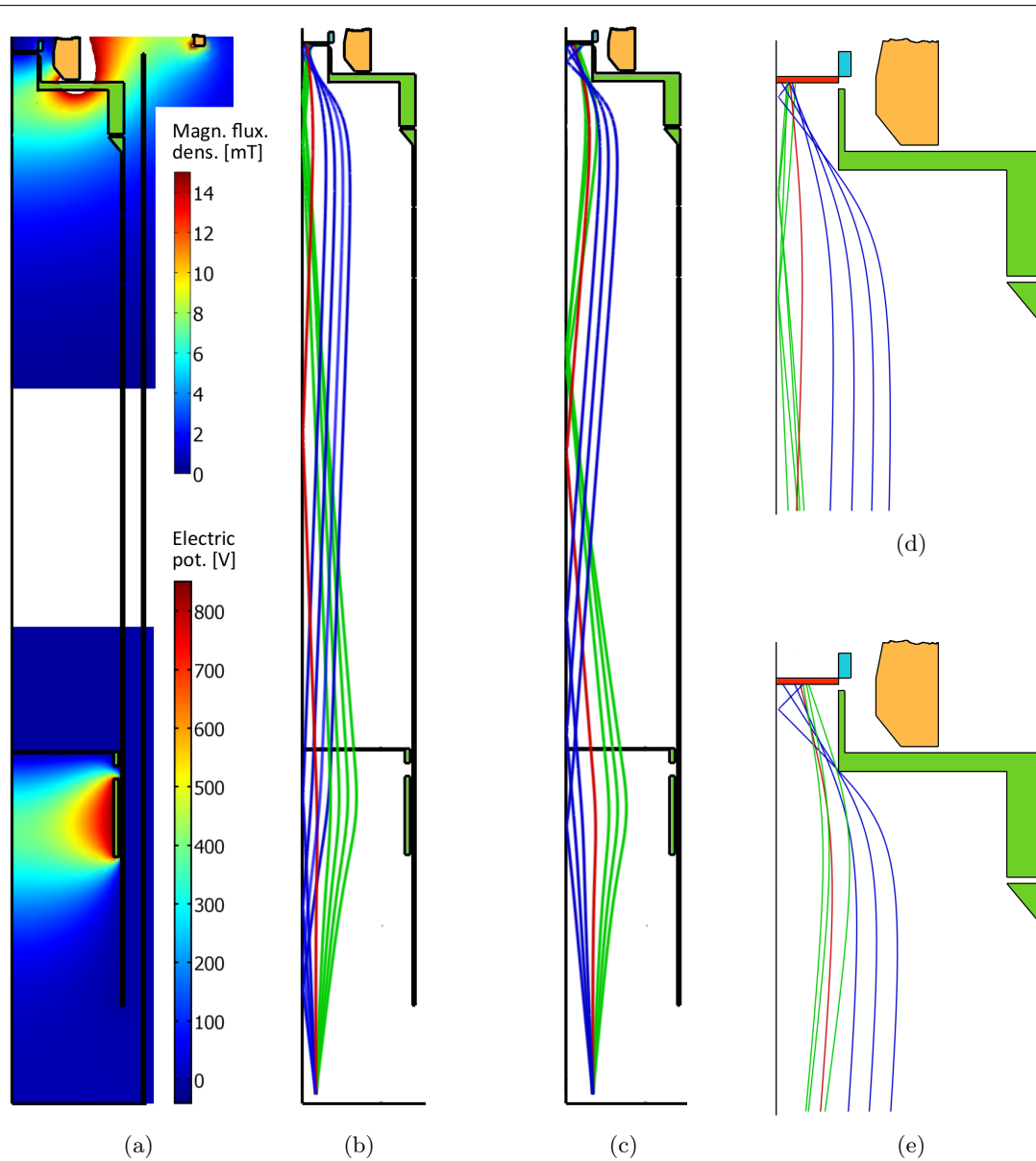


Figure 4.8: Simulation of the rotational symmetric re-moderator setup with the re-moderation crystal above. (a): Electric potential and absolute value of the magnetic flux density.

(b), (d): Positron trajectories with initial diameter $D = 10$ mm and initial transversal energies $E_{\perp} = 0, \pm 2, \pm 5, \pm 10, \pm 15$ eV.

(c), (e): Positron trajectories with initial diameter $D = 20$ mm and initial transversal energies $E_{\perp} = 0, \pm 2, \pm 5, \pm 10$ eV.

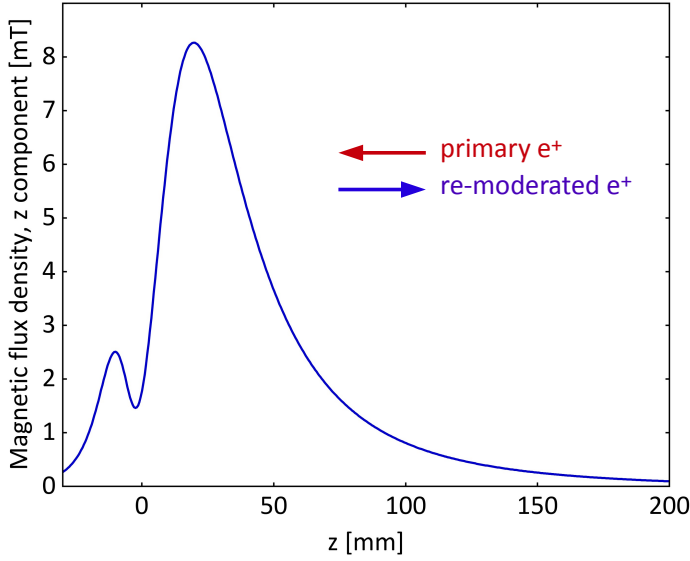


Figure 4.9: Magnetic flux density created by the single pole lens. The re-moderation crystal is located at the origin. A low magnetic flux density at the site of the re-moderation crystal leads to a smaller diameter of the re-moderated beam during the transition into the magnetic field-free area and hence the transferred azimuthal momentum can be kept low.

it is focused by electric lenses into the converging magnetic guiding field (see Fig. 4.3). Since the exact determination of the points where the positrons break away from the field lines of the magnetic lens and where they are re-captured by the field lines of the magnetic transport field is difficult, an analytic description and analysis of the re-moderated beam is very challenging. Therefore, numerical simulations were accomplished to examine the transport of the re-moderated beam (see Fig. 4.11).

Nevertheless, simplified considerations were made to estimate the minimal diameter of the electrodes located in the exit branch. The positrons escape from the magnetic field at a point where the field strength is sufficiently low. For the following estimation it is assumed, that this point is at a distance of about 125 mm from the re-moderation crystal. The field strength there is denoted with B_1 . The operational field of the electric lens which focuses the free diverging beam into the magnetic transport field is—in a rectified model—about 250 mm away from the crystal. Hence, the distance z within the beam diverges freely is about 125 mm. The re-moderated positrons are emitted perpendicularly to the crystal surface and deviations from this direction are only thermally induced. Therefore, the maximum transversal energy $E_{\perp 0}$ of these positrons can be estimated to be about 0.1 eV. The area from which the positrons are emitted depends on the spot size d_0 of the focus of the primary beam. Considering the simulations this diameter can be up to 10 mm in the worst case. The simulations give also the reasonable value of $B_0 \approx 1.5$ mT for the magnetic flux density at the crystal. Because of the adiabatic transport of the re-emitted positrons from the crystal surface to the breakaway, the initial diameter d_0 and transversal energy $E_{\perp 0}$ are converted to the values d_1 and $E_{\perp 1}$ according to the ratio of B_0 and B_1 . The transversal momentum

ΔE_{\perp} which is transferred to the positrons during the transition into the field free area is given by Eq. (3.30). As the longitudinal energy of the re-moderated and the primary beam are coupled by the magnetic dipole field, the ratio of the longitudinal energies has to be 1:25. With this assumptions the diameter of the re-moderated beam in front of the electric lens can be estimated as follows:

$$\begin{aligned} D &= d_1 + \Delta d \\ &= d_0 \frac{B_0}{B_1} + 2z \sqrt{\frac{E_{\perp 1} B_1 / B_0 + \Delta E_{\perp}}{E_{\parallel}}} \end{aligned} \quad (4.6)$$

This diameter as well as the two summands d_1 and Δd for an initial diameter $d_0 = 5$ mm are plotted in Fig. 4.10 in dependence of B_1 . In the same figure also the diameter D for several initial diameters d_0 is shown. Since the electrodes at the exit have a diameter of 38 mm a re-moderated beam with an initial diameter which is larger than roughly 8 mm would not pass according to this estimation. For a deeper understanding of the passing of the re-moderated beam numerical simulations are necessary.

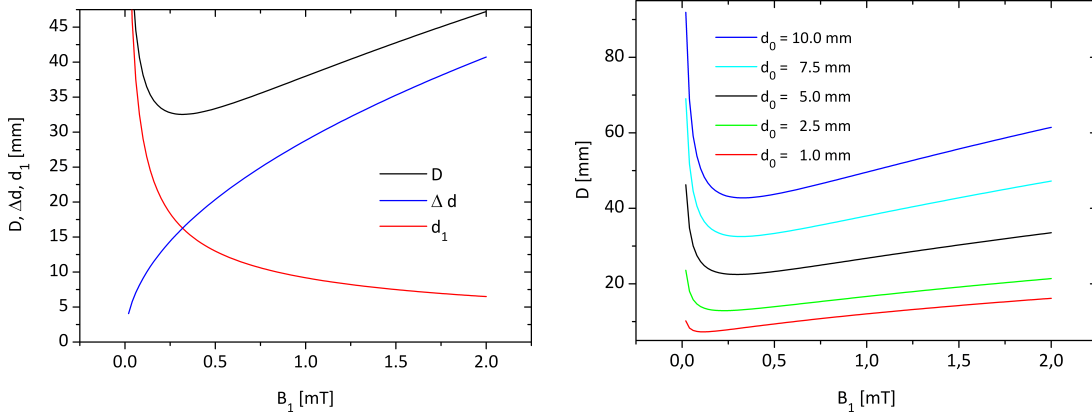


Figure 4.10: Left: Diameter $D = d_1 + \Delta d$ of the re-moderated beam in dependence of the magnetic induction B_1 at the point, where the positrons break away from the field lines of the magnetic lens. d_1 is the diameter of the positron beam at the breakaway point and Δd is the increase of the diameter due to the free diverging of the beam until it is focused by the electric lenses at the exit.

Right: Diameter D plotted for different initial diameters d_0 , which are determined by the focus of the primary beam.

For the simulations of the re-emitted beam, a rectified model was used for the same reasons as in the case of the primary beam. The simulated trajectories start in a distance of 0, 2.5 and 4.25 mm from the center axis and the initial transversal energies were set to -0.1 and +0.1 eV. As shown in Fig. 4.11, for these conditions the positrons reach the exit of the re-moderator, and they are focused well into the magnetic transport field. In the detailed view in right side of the same figure, it can be seen, that

4 Positron beam preparation at NEPOMUC

the positrons which are emitted at the outermost radius and with their initial velocity pointing outwards, are not guided adiabatically from the beginning. But since all simulated positrons have the same gyration radii within the magnetic guiding field, this additional transversal momentum seems to be negligible in comparison to the transversal momentum all positron gain during the transition from and into the magnetic fields and by the focusing due to the electrical lens.

Influence of the magnetic dipole field

So far, the deflection by the magnetic dipole field has not been regarded in the discussion of the positron paths. This was possible, because the other components of the re-moderator are placed and designed in such a way, that the fields which they create is sufficiently small in the area of the dipole and therefore do not perturb the functionality of the dipole and vice versa. For instance, the absolute value of the magnetic flux density of the magnetic single pole lens is below 200 μT at the center of the deflection coil when it is adjusted to focus a 1 keV beam. In order to reduce the magnetic field to zero, a correction coil in this area creates an opposed field. Other examples are the magnetic transport fields. Not only the transport field of the primary beam is terminated by the high permeability grid, but also the penetration of the transport field for the re-moderated beam is minimized by a high permeability aperture and adequate leading of the field lines outside the coils. Further, already in the work of Straßer it was ensured, that the dipole field itself is strongly localized and that there is no interference with other electric and magnetic fields [110]. In this work and in [111] the deflection for the primary and re-moderated beam was simulated, and it was shown that both beams are bent at the same magnetic field strength according to the requirements of the setup.

4.1.3 Experimental results

After first measurements in the laboratory, the re-moderator setup was connected to the NEPOMUC beam line short after the first accessible position. For the detection of the re-moderated positrons, a micro channel plate (MCP) together with a phosphor screen was connected to the beam line about 4 m behind the re-moderator. The MCP was used as annihilation target and together with a CCD camera for the determination of the beam profile. The annihilation radiation was detected with a NaI scintillator which was shielded by a tungsten collimator. From the amplified detector signal was with the help of a single channel analyzer a counting rate derived which was used to optimize the parameters of the re-moderator. The intensity of the NEPOMUC primary beam was determined with the aid of a permanently installed annihilation target, which can be moved into the path of the primary beam by a linear motion feedthrough. This target consists of a honeycomb structure in front of a solid plate. Both is made from aluminum in order to reduce the fraction of reflected positrons.

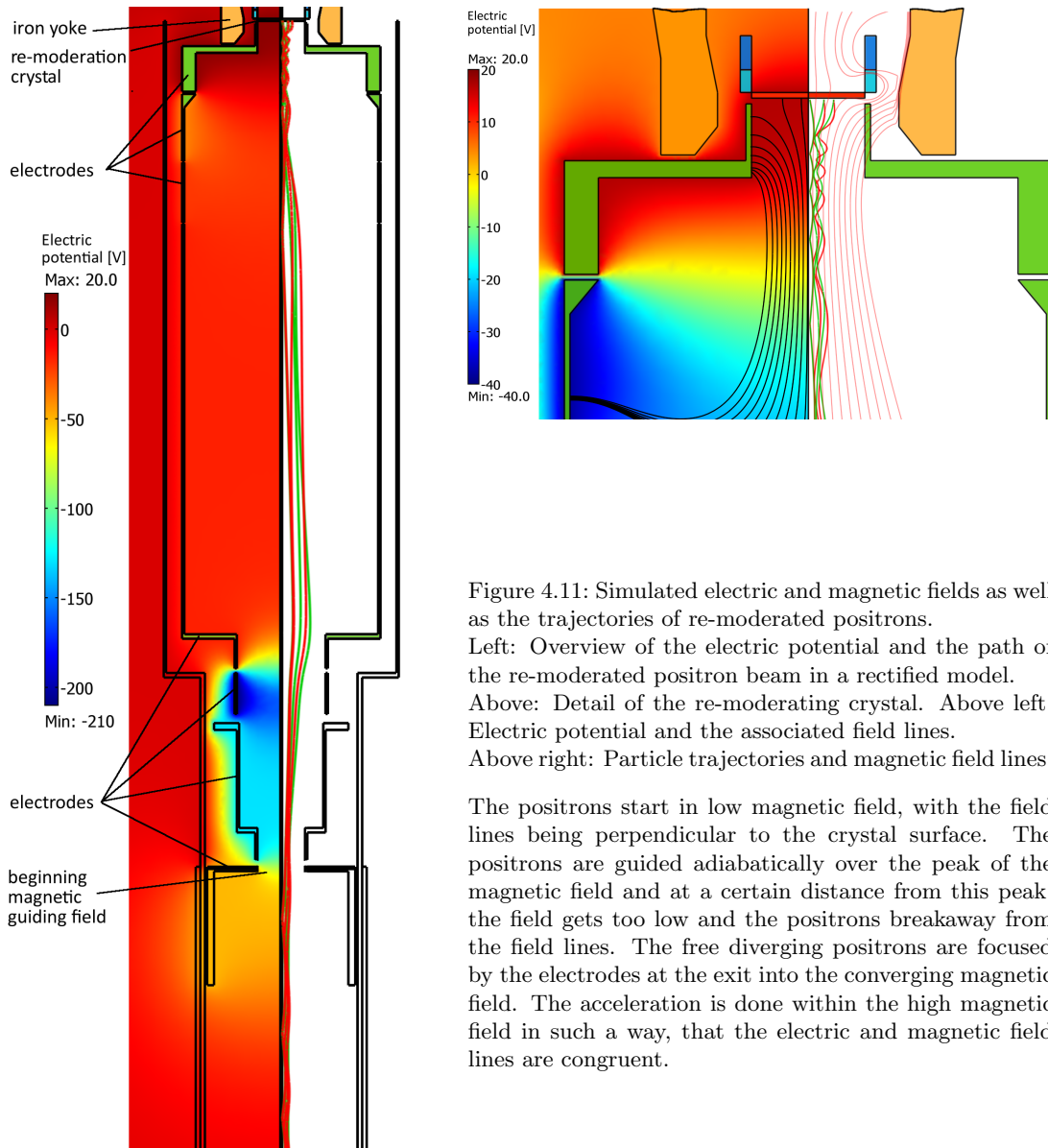


Figure 4.11: Simulated electric and magnetic fields as well as the trajectories of re-moderated positrons.
 Left: Overview of the electric potential and the path of the re-moderated positron beam in a rectified model.
 Above: Detail of the re-moderating crystal. Above left: Electric potential and the associated field lines.
 Above right: Particle trajectories and magnetic field lines.

The positrons start in low magnetic field, with the field lines being perpendicular to the crystal surface. The positrons are guided adiabatically over the peak of the magnetic field and at a certain distance from this peak, the field gets too low and the positrons breakaway from the field lines. The free diverging positrons are focused by the electrodes at the exit into the converging magnetic field. The acceleration is done within the high magnetic field in such a way, that the electric and magnetic field lines are congruent.

4 Positron beam preparation at NEPOMUC

After manual and automatic optimization of the parameters of the NEPOMUC source and of the re-moderator the intensities of both beams were measured. For the quantitative determination of the absolute beam intensity a ^{22}Na calibrating source was used, with evaluating the energy spectra of the annihilation radiation (see Fig. 4.12). Therefore, three effects have to be regarded: First, the ^{22}Na source emits simultaneously with each positron⁶ a 1275 keV γ -quantum which causes Compton background in the energy range of the 511 keV annihilation line. Hence the spectrum of the sodium source was corrected by linear subtraction of this Compton background. Second, due to the high intensity of the primary NEPOMUC beam, pile-up events have to be taken into account. In the case of the sodium source the evaluation of the pile-up events is not possible, since they are covered by the dominant Compton background of the 1275 keV γ -quanta. Since the source is relatively weak there are only very few pile-up events. At last all spectra have to be corrected for the background radiation caused by other experiments nearby the re-moderator but also caused by the re-moderator and NEPOMUC itself.

Intensity of the beams and total re-moderation efficiency

In the case of the NEPOMUC primary beam, the Compton background in the ^{22}Na spectrum was subtracted and the pile-up events in the beam spectra were taken into account. The evaluation resulted in an absolute intensity of the former NEPOMUC beam⁷ of $5.2 \cdot 10^7 \frac{e^+}{s}$. In the case of the re-moderated beam, the situation is different. Due to a larger solid angle of the detector, pile-ups are not only observable in the annihilation spectrum of the beam but might be also relevant in the spectrum of the source. In the beam spectrum they contribute about 5 % to the total number of events. Since it is not possible to identify the contribution of the pile-ups in the spectrum of the source, a direct comparison is difficult. Therefore, only an upper and a lower limit of the absolute beam intensity can be given by regarding and not regarding the pile-ups in the spectra of the beam (hatched area in Fig. 4.12). It has to be mentioned, that the real lower limit might be even smaller because the potential pile-up events in the sodium spectra were not regarded for the determination of the Compton background and therefore, this background might be overestimated. The analysis results in an absolute intensity of the re-moderated beam between $3.3 \cdot 10^6$ and $3.4 \cdot 10^6 \frac{e^+}{s}$. Therefore, the different treatment of the pile-up events lead to a deviation of only about 3 %. By using the intensity values of the primary and the re-moderated beam the total efficiency of the re-moderation setup can be assigned between 6.3 and 6.8 %.

⁶A very small amount (< 0.06 %) of the positrons are emitted without the emission of the 1275 keV-quantum.

⁷The measurements were made in April 2007. At this time, the old platinum structure was still in operation, which produced less positrons than the new structure, which was built in January 2008. Further, the old structure had to be cleaned with the help of oxygen gas from time to time to attain the maximum intensity. This was not made before these measurements in order to ensure a constant positron production rate.

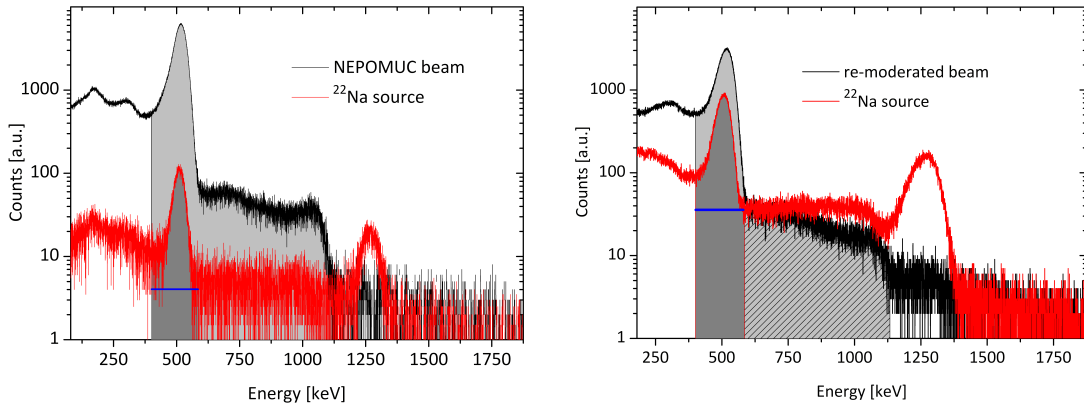


Figure 4.12: Background corrected energy spectra of the annihilation radiation of the positrons of the primary beam, the re-moderated beam and of the positrons from a ^{22}Na source placed at the corresponding annihilation targets. These spectra were used to determine the intensities of the primary and the re-moderated beam.

Due to thermal problems at the source section of NEPOMUC, the platinum structure and the electric lenses had to be renewed. Due to improvements at these parts, the NEPOMUC beam provides up to $9 \cdot 10^8 \frac{e^+}{s}$ since January 2008 [12]. Hence the re-moderated beam has an calculated intensity of more than $6 \cdot 10^7 \frac{e^+}{s}$.

The maximum intensity, which is reached short after the heat treatment of the re-moderation crystal, decreases due surface contamination. For some experiments it is important, that the beam intensity remains stable during a longer period. To know the timescale of the decline, the intensity was recorded over 600 min. As shown in Fig. 4.13 there are two time components. The short decline rate leads to an intensity drop of 11 % within about 11 min, and the longer reduces the intensity to about 83 % of the maximum value after the heat treatment within about 100 min. After this time the intensity remains nearly stable even for several months. The increase of the intensity immediately after the reconditioning is attributed to the cooling of the crystal.

Intensity distribution and beam profile

The intensity distribution was measured within a magnetic transport field at a field strength of about 5 mT, using the MCP and phosphor screen setup together with a CCD camera. Several parameter sets for the re-moderation and beam transportation for different energies of the re-moderated beam were found and lead to similar results for the intensity and the intensity distribution. A typical distribution and the related beam profile is shown in Fig. 4.14. By appropriate adjustment of the magnetic transport field, the beam can be guided over a distance of 15 m and more (see Fig. 4.1). However, there are some locations at the beam line where the beam is guided only

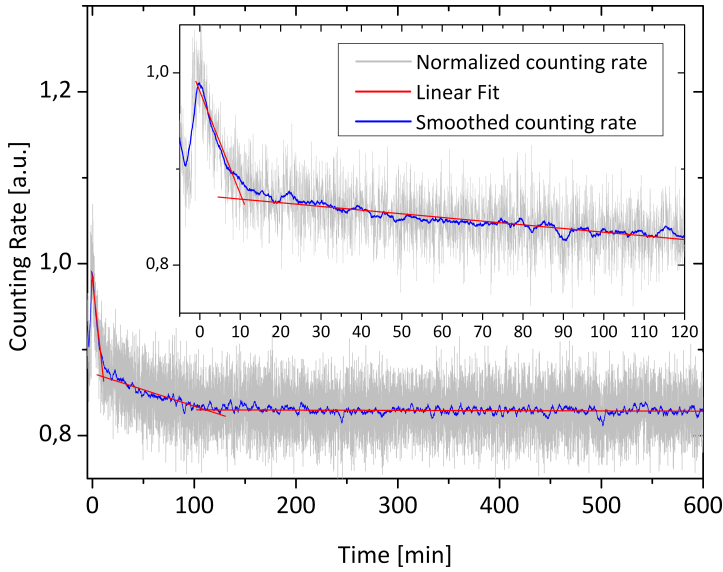


Figure 4.13: After reconditioning the re-moderator crystal, the intensity of the re-moderated beam decreases linearly with two time constants of 11 min and 89 min to a saturated level of about 83 %. The increase at $t < 0$ is attributed to the cooling of the hot crystal.

imperfectly. E.g. there is a beam switch which is used to guide the beam to the different positron experiments and which involves highly curved bends and entails also high gradients in the longitudinal magnetic field. Hence, intensity losses of a factor of two have been observed. In some cases also the shape of the beam was affected or in the case of stronger, localized perturbations the entire beam began to gyrate.

Energy distributions and brightness of the re-moderated beam

During one measurement campaign for the SPM interface, the longitudinal energy spread was measured by applying a retarding potential at an electrode within a magnetic transport field of roughly 5 mT. Behind this electrode the beam intensity was measured in dependence of the retarding potential, what is equal to the integrated energy distribution. The derivative of this distribution, which is shown in Fig. 4.15, has a width of about 2.5 eV (FWHM). This value was confirmed by similar measurements at the PLEPS lifetime spectrometer. The distance between the re-moderator and the experiments were in both cases about 15 m, and the beam had to pass the beam switch. Since over this distance the mentioned intensity loss was also observed, it is assumed, that the relatively large energy spread is caused to a large extent by the imperfect beam transport from the re-moderator to the experiment. Nevertheless, for the estimation of the brightness enhancement, this value will be regarded as an upper limit. The lower limit of longitudinal energy spread right after the re-moderator is assumed to be less than 1 eV. Since the energy is conserved, the transversal energy spread have to be in the same range.

As the longitudinal energy spread of the primary NEPOMUC beam was measured at

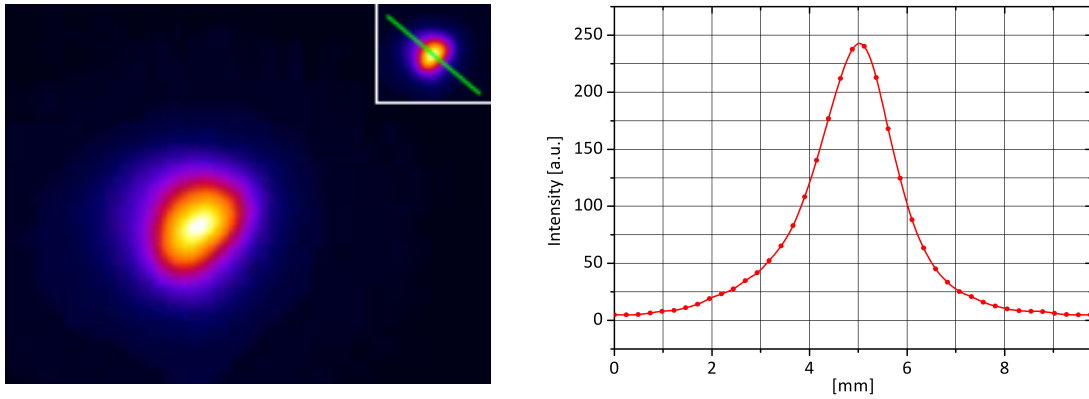
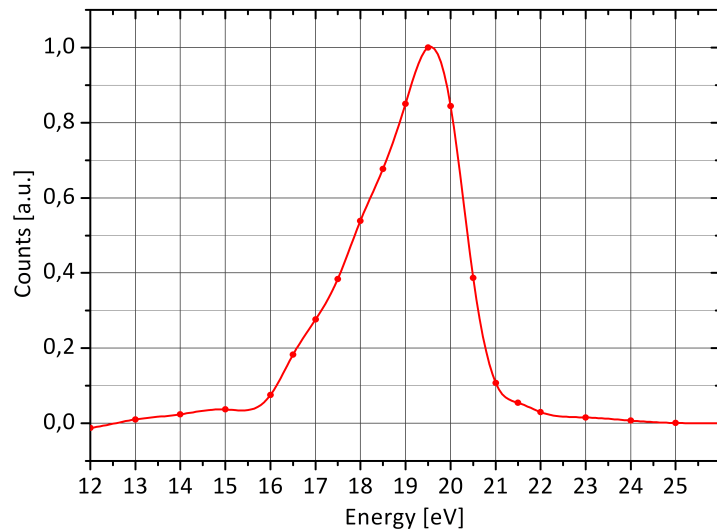


Figure 4.14: Left: The intensity distribution of the re-moderated beam. Right: Beam profile along the line marked in the inset, at an energy of the re-moderated beam of 32 eV. Similar beam profiles with a diameter of less than 2 mm (FWHM) were observed at several other energies (e.g. 20, 50, and 200 eV).

Figure 4.15: Energy distribution of the re-moderated beam at the so called open beam port of the NEPOMUC positron beam facility (see Fig. 4.1). The distribution was measured with the aid of a retarding potential tube within a magnetic transport field.



4 Positron beam preparation at NEPOMUC

the first accessible position, also the intensity distribution was determined. The beam consist of a intense center with a diameter of 7 mm (FWHM) and a broader base of 20 mm (FWTM) [104]. Since the contribution of the base to the total intensity is small, only the center is taken into account. With the measured and assumed values, the brightness and brightness enhancement can be estimated roughly:

$$\begin{aligned}
 B_{\text{re-mod}} &\approx 5.9 \cdot 10^6 \dots 1.5 \cdot 10^7 \left(\frac{\text{c}}{\text{eV m}} \right)^2 \frac{1}{\text{s}} \\
 B_{\text{re-mod}}^* &\approx 2.4 \cdot 10^6 \dots 1.5 \cdot 10^7 \left(\frac{\text{c}}{\text{eV m}} \right)^2 \frac{1}{\text{seV}} \\
 \frac{B_{\text{re-mod}}}{B_{\text{NEP}}} &\approx 16 \dots 40 \\
 \frac{B_{\text{re-mod}}^*}{B_{\text{NEP}}^*} &\approx 320 \dots 2000
 \end{aligned} \tag{4.7}$$

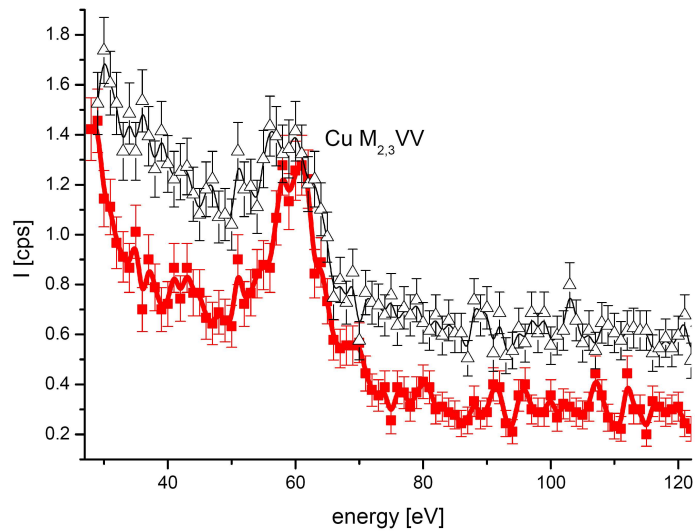
Hence, if the longitudinal energy spread is not taken into account the re-moderator a provides a beam which is in the best case about 70 times brighter than the beam provided by a well designed laboratory beam. If the longitudinal energy spread is also regarded, the re-moderated NEPOMUC beam might be 7 times brighter but is at least as bright as that one provided by the laboratory setup. Further, it can be seen that the brightness gain is especially high if the longitudinal energy spread is taken into account. This arises from the fact, that the primary beam is difficult to focus to a small spot size and that therefore the reduction in the transversal phase space volume is relatively low. The reduction in the longitudinal direction, on the other hand, is only influenced by the properties of the re-moderation process itself and the extraction of the re-moderated beam.

Improvement for the spectrometers

The positron annihilation-induced Auger electron spectrometer (PAES) and the coincidence Doppler broadening spectrometer (CDBS) are connected to the NEPOMUC beam facility. Both are no typical experiments which are reliant on a high brightness beam but nevertheless they profited from the increased brightness. Both extract the positron beam from the magnetic transport field and focus it electrostatically onto the sample.

PAES has no entrance aperture and was developed for beam conditions as usually provided in the laboratory. This is particularly true for the magnetic field termination device and for the electrodes which are used to transport and focus the beam. Due to the large extension of the NEPOMUC primary beam, parts of the beam could not be focused onto the specimen and annihilated elsewhere inside the spectrometer e.g. at the transport electrodes and the vacuum chamber. This lead to a high background in the Auger spectra. By installing the re-moderator the beam became dimensions as

Figure 4.16: PAES spectra of a polycrystalline copper foil recorded within only 3 h. Once by using the primary NEPO-MUC positron beam (\triangle) and once by using the re-moderated beam (\blacksquare). In the latter case the background in the spectra was nearly reduced entirely (for details of these spectra see [112]).



common in the laboratory, but with much higher intensity. Hence, the PAES spectra can now be recorded within a short time, but with a much lower background (see Fig. 4.16) [112, 113].

With the CDB spectrometer lateral resolved measurements are possible. The spectrometer has a variable entrance aperture, which is used to enhance the lateral resolution to less than 1 mm. Because of the higher brightness the count rate at high resolutions was increased by about 60 % [114, 115].

4.2 The SPM interface

The SPM interface is supposed to replace the source section and the beam preparation column of the existing SPM and must therefore provide a beam with similar or even improved properties. To understand which demands the interface has to fulfill, in the first part of this section the SPM is briefly presented. The design of the interface is explained, by accentuating the key features and design principles but also the critical properties of the existing SPM.

4.2.1 The SPM project and the design of the SPM interface

The Munich SPM is the result of a cooperation between the Dipartimento di Fisica of the university of Trento in Italy and the Institut für Nukleare Festkörperphysik of the university of the federal armed forces in Munich, Germany. The functioning

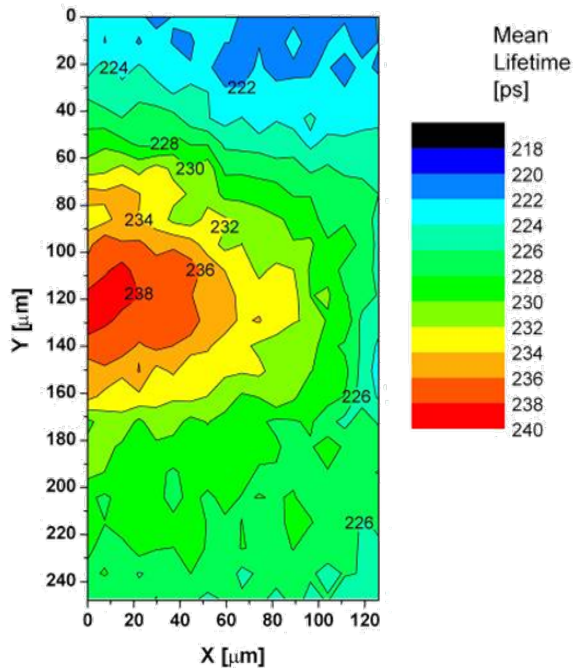


Figure 4.17: Two-dimensional lifetime map measured with the Munich SPM, which shows the mean lifetimes distribution around the tip of a fatigue crack in an Al 6013 sample. From this measurement it was concluded what kind of defects were created due to the cyclic load which was applied onto the specimen (From [10]).

was demonstrated during the PhD work of David in 2000 and since then, several measurements have been performed [6, 9, 10, 99]. The maximal lateral resolution is about $1 \mu\text{m}$ and the depth resolution is given by the Makhovian implantation profile (see Sec. 2.2), where the maximal implantation energy is 20 keV. The time resolution which is determined by the width of the positron bunches and the time resolution of the detector system is about 255 ps. Hence, lifetime measurements can be performed depth and lateral resolved, whereby three-dimensional defect maps are measured. This makes the SPM to an unique tool in solid state physics. As an example for a typical result of an SPM measurement a two-dimensional positron lifetime map of a fatigue crack in an Al 6013 sample is shown in Fig. 4.17.

Unfortunately, such measurements are very time consuming. Not only recording of such a lifetime map lasts about one to two weeks also the adjustment of the SPM before performing such measurement lasts generally about the same time. This time is needed for the reconditioning of the moderation crystals, the adjustment of the beam transport, the focusing, the optimization of the beam bunching, the tuning of the detector system and finally identifying the region of interest on the sample. Especially the last point and the focusing needs a lot of time because this tasks require to record a lot of test images and line scans of reasonable sizes. In contrast to a Scanning Electron Microscope (SEM), where each pixel of an image is recorded within a fraction of a second, this lasts at the SPM at least several minutes. The time difference and

also the difference between the attainable resolutions arise from the different particle sources. An electron source used in a SEM provides a beam with a brightness which is many orders of magnitudes larger than the brightness of a typical laboratory positron beam or even of the re-moderated positron beam at NEPOMUC; e.g. a LaB₆ single-crystal cathode cone with a microflat tip with a diameter of 15 μm emits more than $8 \cdot 10^{14} \frac{e^-}{\text{s}}$ ⁸. This enormous intensity emphasizes the main problem in the design of a positron microbeam system and why not all concepts of a SEM can be copied. The design of the SPM obeys the constraints which arise from the low positron intensity as shown in the following.

The SPM setup

The SPM can be divided into the source section (①,②), the beam preparation column (③–⑤) and the last optical column (⑥–⑫) (see Fig. 4.18). The two columns are connected via a re-moderation stage ⑧, which is in the following regarded as a part of the last optical column. In both columns the beam transport is fulfilled mostly electrostatically and only for few dedicated tasks magnetic fields are used in addition. In the source section ①, positrons from a ²²Na source are moderated by a W(100) foil with a thickness of 1 μm . The sodium source had usually a strength of less than 30 mCi. By assuming a total moderation efficiency of $5 \cdot 10^{-4}$ and regarding the positron yield of about 90 %, a beam with an intensity of less than about $5 \cdot 10^5 \frac{e^+}{\text{s}}$ and with a diameter of more than about 3 mm is created. This beam is bent by a magnetic dipole field ② into the beam preparation column.

This column converts the continuous beam into a bunched beam by two steps in order to combine the opposed aims of short pulses and high efficiency. In the first step, a sawtooth like modulation function with a small amplitude is used to create relatively long bunches of about 2 ns (FWHM). This pre-buncher ③ is implemented as a three electrode buncher, where the energy modulation occurs at the first gap. At the second gap the positrons are accelerated in order to conserve the time focus. Therefore, the drift tube has to be sufficiently long so that the time focus is in front of the second gap. The large extension of the drift tube leads to a high capacity and hence to low modulation amplitudes. However, the relatively low amplitude as well as the relatively long bunches are of minor importance because this device is intended as a pre-buncher, which creates efficiently bunches which are sufficient short to be accepted entirely by the subsequent stage. Since the positrons pass the pre-buncher with a low kinetic energy of 22 eV there has to be a magnetic transport field which is terminated at the entrance and at the exit by apertures which have a high permeability.

The subsequent sine wave buncher ④ is implemented as a $\lambda/4$ -resonator which allows high modulation amplitudes. Because of the sine wave and the repetition rate of 50 MHz this buncher can convert only short pre-bunched pulses into sharp bunches.

⁸Data taken from product catalog of Kimball Physics Inc.

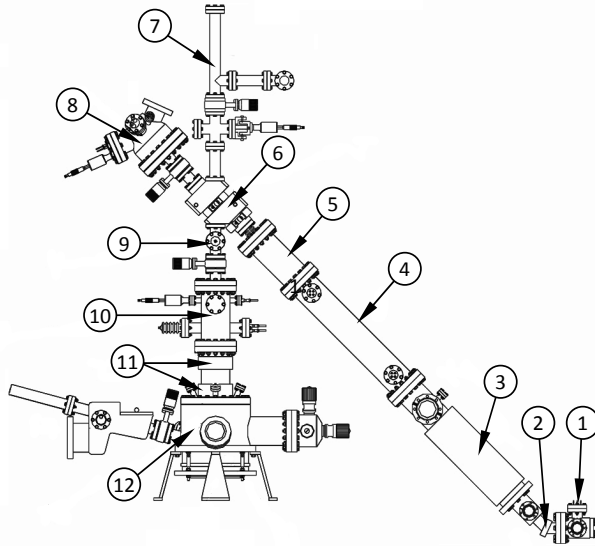


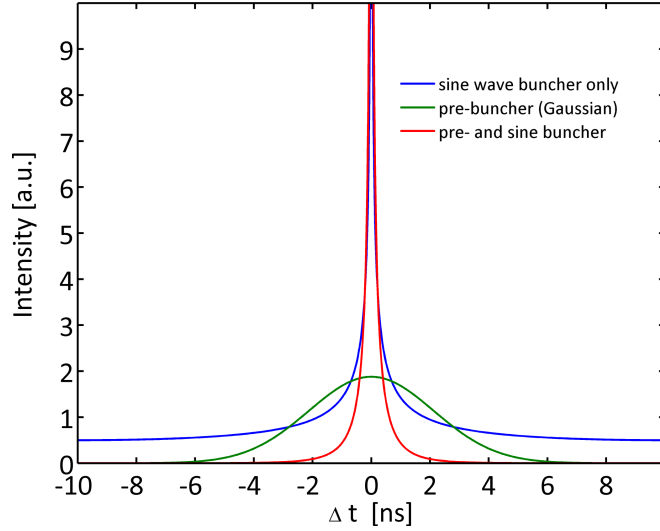
Figure 4.18: Overview of the existing SPM: In the source section ① the positrons emitted by a ^{22}Na source are moderated in a W(100) foil. The resulting beam is bent by a magnetic dipole ② into the beam preparation column, where it is pulsed by a combination of a pre-buncher ③ and buncher ④. In order to reduce the remaining background between the bunches, an additional chopper is located also in ④. The bunched beam is accelerated ⑤ to a kinetic energy of 5 keV, guided through the beam switch ⑥ toward the re-moderator ⑧. The beam switch bends the slow re-moderated beam into the last optical column, which consists of a further buncher ⑨, the main accelerator ⑩, the scanning coils ⑪ and the specimen chamber ⑫. With the help of an electron gun ⑦ also electron images can be recorded.

Since the pre-buncher provides sufficiently small pulses the sine wave bunching is very efficient, and therefore, the background becomes accordingly low (see Fig. 4.19). Because of imperfections during the pre-bunching and sine wave bunching there is still a background between the pulses, which is suppressed by a chopper, which is also located in the first column. The concept of using a combination of a high efficiency pre-buncher and a high amplitude sine wave buncher is reused in the design of the SPM interface.

After these bunching units, a re-moderation stage follows ③. The idea of re-moderation is based on the fact, that the additional momentum which is transferred by the focusing is eliminated during the thermalization of the positrons leading to a reduced phase space volume. Because the bunchers can be regarded as lenses in the time domain this re-moderation stage reduces not only the lateral phase space volume but also the longitudinal phase space volume which is related to the time domain. Only due to the reduced longitudinal energy spread a further reduction of the pulse duration by a buncher ③ is possible. Also this concept was copied for the design of the interface.

Since the source section is set to a potential of +5 kV a beam with a kinetic energy of 5 keV with respect to ground potential is created. This energy was chosen, since the maximum re-moderation efficiency is attained if the the primary beam is implanted with this energy into the re-moderation crystal. In principle this implantation energy could be also archived if the primary beam has a lower kinetic energy but in this

Figure 4.19: Time spectrum generated by an ideal sine wave buncher according to Eq. (3.55), the assumed spectrum of a pre-buncher and the time spectrum of the sine wave buncher if the primary beam is pre-bunched. For the pre-buncher spectrum a Gaussian distribution with a width of 5 ns (FWHM) was used. Due to the pre-bunching the sine wave buncher creates short pulses with low background between the bunches. (For the plots the same values were used as for Fig. 3.24.)



case an accordingly high negative potential has to be applied at the re-moderation crystal. However, this would also reduce the maximum final energy for implanting the positrons into the sample and it is impracticable without considerable changes at the insulation of the re-moderation crystal. Because of installations which enable the cooling of the re-moderation crystal with liquid nitrogen there is no possibility to change this situation without a completely new design of the re-moderator. Further not only the re-moderator but also the beam switch, and some of the following parts would have to be modified considerably. To avoid this major changes the beam which is provided by the interface has also to have a kinetic energy of 5 keV with respect to ground potential.

One main component, which enables the SPM to reach the high lateral and temporal resolution, is the re-moderation stage, which acts as a high brightness pulsed positron source for the last optical column. But in order to attain a spot size of 1 μm the phase space volume has to be reduced further. Up to now this is done by apertures, which is due to the low positron intensity, an inappropriate method. Therefore, the interface should provide a beam with a smaller phase space volume than the preparation column. Further, even in the case that the NEPOMUC re-moderator might provide a beam which is comparable with the beam created by the source section of the SPM, it was from the beginning assumed, that the phase space volume of this beam would increase during the transport to the interface. The measurements at the open beam port and at PLEPS supported this assumption. To ensure that the SPM can attain the former or even higher spatial resolution, although under the circumstance that the interface is provided with a beam which has a considerable larger phase space volume, an additional re-moderation stage was foreseen for the interface.

4 Positron beam preparation at NEPOMUC

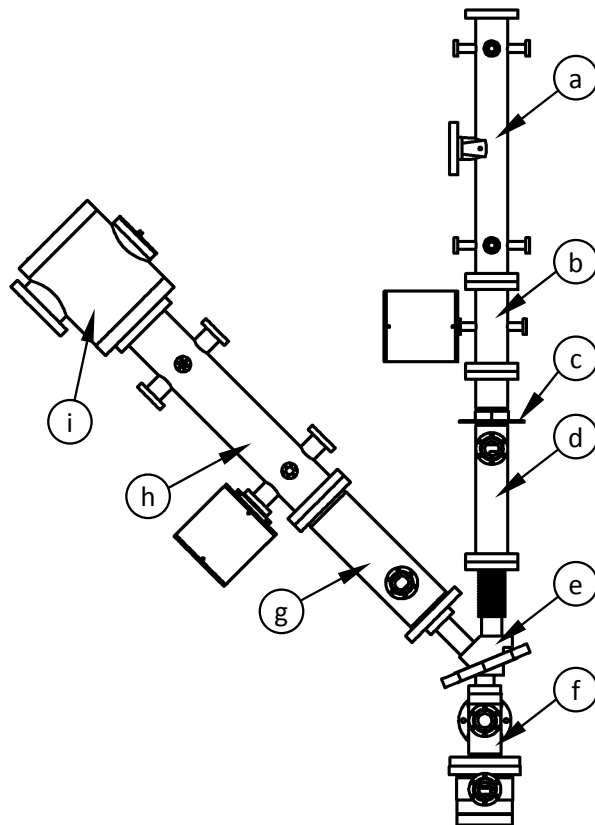
This additional re-moderator enables also a convenient solution to create a beam with a kinetic energy of 5 keV with respect to ground potential. Also this re-moderator operates with the highest efficiency, if the positrons are implanted with 5 keV. Therefore and because the re-moderated beam of NEPOMUC has an energy of only 20 eV in routine operation, the crystal of the re-moderator in the interface has to be set to about -5 kV. Hence, the energy of this two fold re-moderated beam has to be raised by 10 keV in order to match the demands of the last column of the SPM. Hence, the additional re-moderator seems at the first glance contra productive for the aim to provide a 5 keV beam. But if a similar buncher combination as used in the beam preparation column is placed in front of this re-moderator, the crystal acts as a pulsed high brightness positron source in the same way as the SPM re-moderator. Because of the pulsed structure and the sharp energy of this beam, rf-acceleration techniques can be applied to raise the kinetic energy to the desired level. This rf-acceleration, however, is not within the scope of this work.

Overview of the SPM interface

Concluding the remarks of the last paragraphs, a concept for the SPM interface can be derived (see Fig. 4.20). The first device should be a high efficiency pre-buncher with a small electrode on which a sawtooth like modulation function is applied. This buncher is followed by a high amplitude sine wave buncher, which ensures short bunches. In a subsequent re-moderation stage not only the lateral phase space is reduced but also the longitudinal energy spread induced by the bunchers. For the re-moderator, the proofed concept of the NEPOMUC and SPM re-moderator is used. The magnetic transport field has to be terminated, since in this concept the beam transport is mainly electrostatically accomplished. On the other hand, a magnetic transport field is necessary at the drift tube of the pre-buncher, because of the low energy of the positrons there. Hence the magnetic field termination is realized between the bunchers and the re-moderator. Behind the re-moderator the beam transport is performed entirely electrostatically, because this simplifies a chopper design enormously, and it avoids the perturbing injection and extraction in and from a magnetic field. In order to attain very short pulses and to prepare the beam for the rf-acceleration, a further buncher is placed between re-moderator and accelerator. The beam transport through the SPM interface and the single devices except the rf-acceleration are presented in detail in the following section.

To ensure a stable operation when the SPM is implemented at the FRM II there are besides the positron optical components of the interface some additional elements necessary. Up to now, the SPM is located in a separated, own laboratory with no perturbing mechanical vibrations. Because at the FRM II the situation is quite different a vibration damping system was foreseen. Commercially available damping systems allow only setups with a low lying center of gravity in order to avoid dynamic instabilities. To avoid such instabilities also in the case of the heavy and large SPM setup

Figure 4.20: The components of the SPM interface. A pre-buncher (a) creates pulses which are short enough to be accepted by subsequent high amplitude sine wave buncher (b). After the extraction of the positrons from the magnetic transport field (c) the positrons are accelerated (d) to about 5 keV and guided through the beam switch (e) to the re-moderation stage (f). The re-moderated beam is accelerated to about 200 eV and bent by a magnetic dipole field toward the second column of the interface. An electric lens (g) transports the beam toward a further buncher (h) which prepares the beam for the rf-acceleration (i). A chopper which is also installed in (h) eliminates the remaining background between the pulses. At the end of this interface the optical column of the SPM will be connected.



a rigid framework was designed which carries the whole setup and ensures that the center of gravity is below the pivot point defined by the dampers (see Fig. 4.21). The SPM is already protected from electromagnetic perturbations by a double walled mu-metal housing. An extension of this housing was build which encloses the parts of the interface where the beam is guided electrostatically.

4.2.2 The bunching units of the SPM interface

4.2.2.1 The pre-buncher

The pre-buncher uses a sawtooth for the energy modulation at one gap. At the pre-buncher of the existing SPM, the wrong energy modulation at the second gap of the buncher electrode is avoided by superimposing a strong accelerating field in addition to the time dependent electric field. This approach demands a long buncher tube with an accordingly high capacitance. In order to avoid this high capacitance and hence to enable in the future higher bunching amplitudes another approach was chosen for the new sawtooth pre-buncher. As shown in Sec. 3.6.1 if the transit time τ for the distance d over which the particle with the velocity v_0 is affected by the time depending field is $\tau = d/v_0 = 2\pi/\omega = 1/f$ the total energy modulation gets zero. Since the repetition rate f at the SPM is 50 MHz the transit time has to be 20 ns. With the sawtooth function generator of the SPM provides a peak to peak amplitude of about 5 V at 50 Ω . If the bunch should have the minimal temporal extension in a distance of about 40 cm the kinetic energy of the reference particle within the drift must be approximately 19.2 eV according to Eq. (3.53). If the positrons have the same energy at the buncher electrode it follows that the field of the second gap has to be spread over a distance of $d \approx 20 \text{ ns} \cdot 2.60 \text{ mm/ns} = 52 \text{ mm}$. Of course the energy within the buncher and the following drift have not to be equal, and small deviations from the estimated lengths can be tolerated by matching the energy accordingly.

The spread of the electric field can be achieved by two methods. One is to increase the diameter of the buncher electrode at the second gap so that the penetration of the field gets accordingly large (see also Fig. 3.26). The other method is to spread the potential difference at the second gap to several gaps by introducing further electrodes on which a subsequent falling amplitude is applied (see Fig. 4.22). This method is used at the interface and has the advantage that the total capacity can be kept low. Moreover, the equal diameter of the electrodes simplifies the accurate alignment of all positron optical elements of the pre-buncher. Hence, in the present design the drift tube is used as mechanical support for all electrodes (see Fig. 4.23).

Time dependent trajectory calculations were made in order to proof the concept. The axial symmetric application modes of COMSOL were used to keep the time for the simulations reasonable low. Moreover, the electric fields and the effect of them onto the particles were supposed to be quasi-static because the dimensions of the areas,

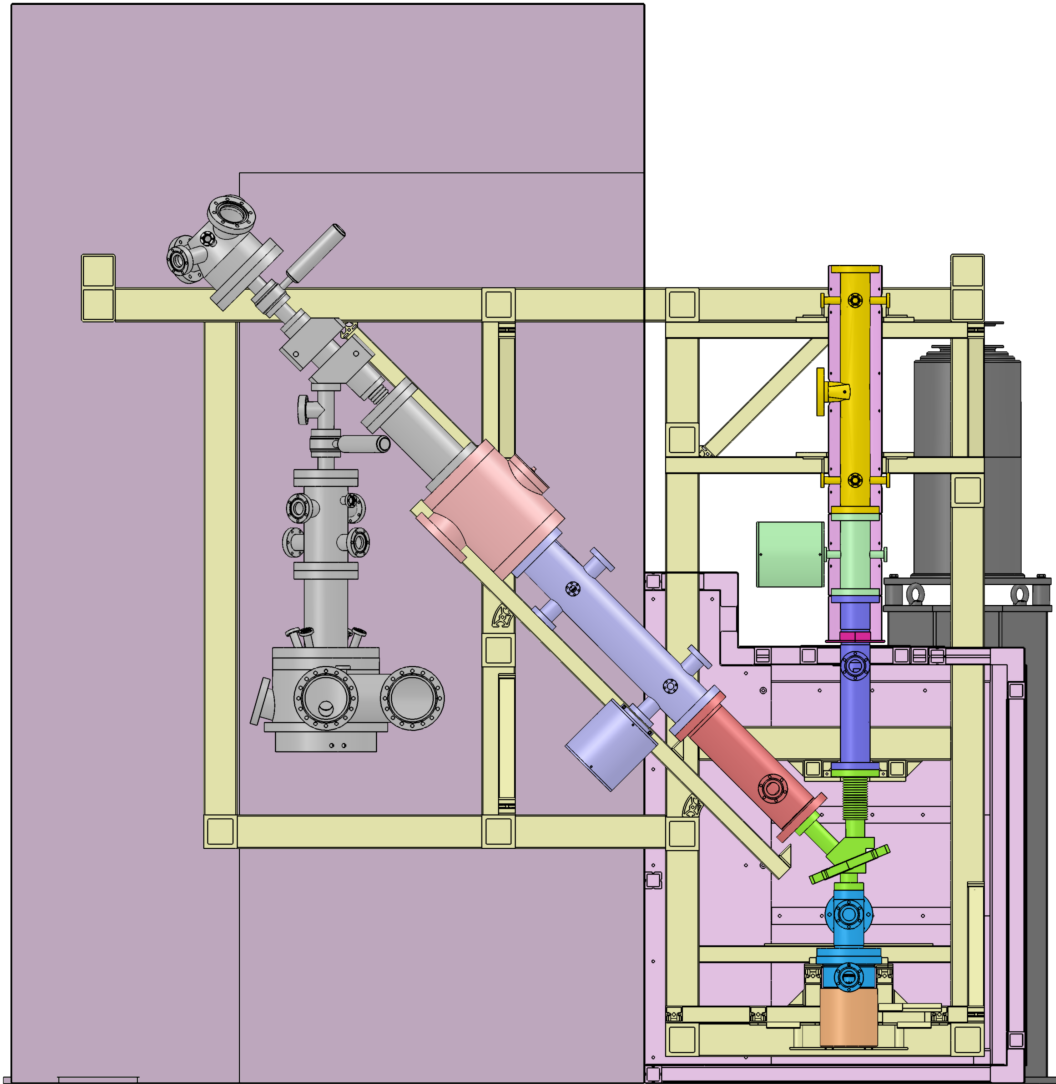


Figure 4.21: The last column of the SPM (gray) and the SPM interface (colored vacuum housings) are carried by a rigid framework (yellow). This framework is supported by four commercial vibration dampers (black; only one is shown) which are mounted on the top of concrete pillars. This setup ensures that the center of gravity is below the pivot point defined by the dampers and hence no dynamic instabilities can occur. The existing double walled magnetic shield (darker pink; only schematic) is extended by a also double-walled housing (pink).

4 Positron beam preparation at NEPOMUC

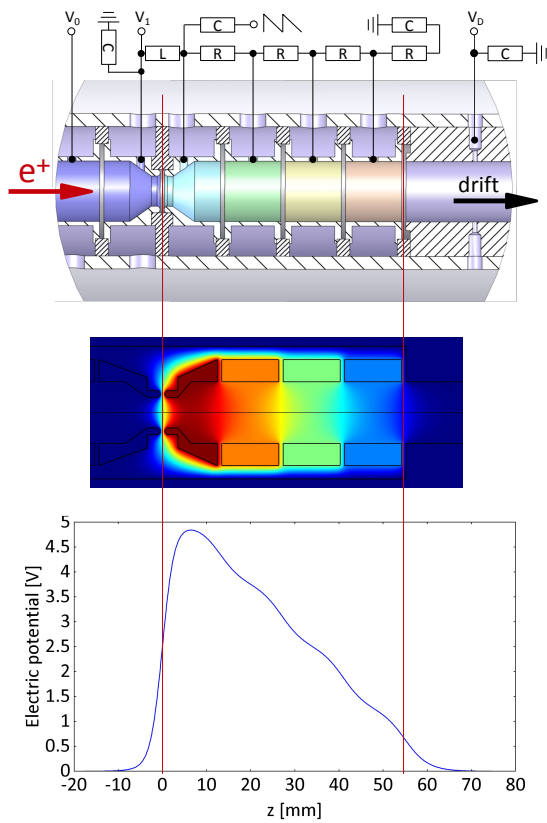


Figure 4.22: Above: Construction and circuit of the pre-buncher (Colors are only for illustration purpose).

Center: Potential distribution at the moment when $V_{\text{saw}}|_{t_0} = 5 \text{ V}$ and $V_0 = V_1 = V_D = 0$

Below: Potential along the center line of the buncher (same conditions as above).

The additional electrodes spread the potential difference between the first bunching electrode and the drift electrode smoothly over a large distance. By matching the transit time of the positrons the mean energy modulation over this distance gets zero. Hence only the time dependent potential difference at the first gap account to the beam bunching.

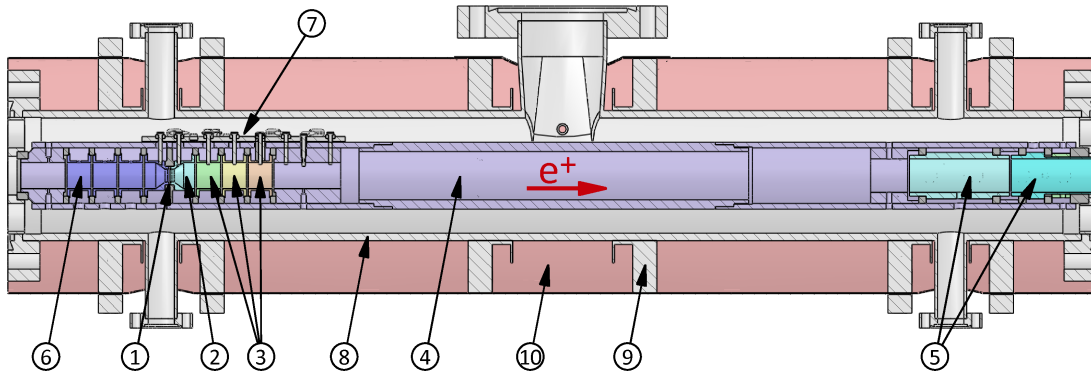


Figure 4.23: Cross section of the pre-buncher: ① is the active buncher gap, where the energy modulation occurs. The additional electrodes ③ are used to spread the potential difference between the first buncher electrode ② and the drift tube ④. Further electrodes ⑤ are used to accelerate the positrons to an appropriate energy for the following buncher. The electrodes ⑥ in front of the buncher gap can be used to decelerate the incident beam in several steps to the low energy which is necessary for the pre-bunching. To ensure that the sawtooth function is as less perturbed as possible the resistors, capacitors, and inductors which are used to couple the dc voltage and rf signals into the electrodes are placed as near as possible to the electrodes onto a vacuum compliant board ⑦. ⑧ is the vacuum chamber on which the support ⑨ for the magnetic shielding ⑩ is mounted.

where the fields have to propagate are small and the speed of the particles is low. The simulations are based on the geometry shown in Fig. 4.22 and 4.23. The diameter of the electrodes at the first gap is 7 mm and that of the subsequent electrodes is 14 mm. Each electrode is 13 mm long and the space between each is 1 mm. Therefore the distance between the first gap and the last gap is 56 mm. Before the trajectory calculations were performed, the field distribution was analyzed. As shown in the center and lower part of Fig. 4.22 the chosen geometry results in an approximately linear potential drop over a distance of about 55 mm if the voltage which is applied to the electrodes decreases also linearly. The reason for the deviation of the maximum potential at the centerline within the first electrode from the applied voltage, is due to field penetration effects. Because the deviation is very small, this is not regarded further.

For the trajectory simulations a sharp beam energy was assumed, and for the energy modulation the real sawtooth as provided by the existing sawtooth generator was used [116]. The kinetic energy of the reference particle within the additional electrodes was 22 eV. At the last gap this energy was increased to 39 eV by a static electric field. As shown in Fig. 4.24 this configuration leads to a time focus at a distance of about 370 mm from the first buncher gap. Because of the real sawtooth function and the perturbing transit time effects at the first gap not all particles meet the temporal focus.

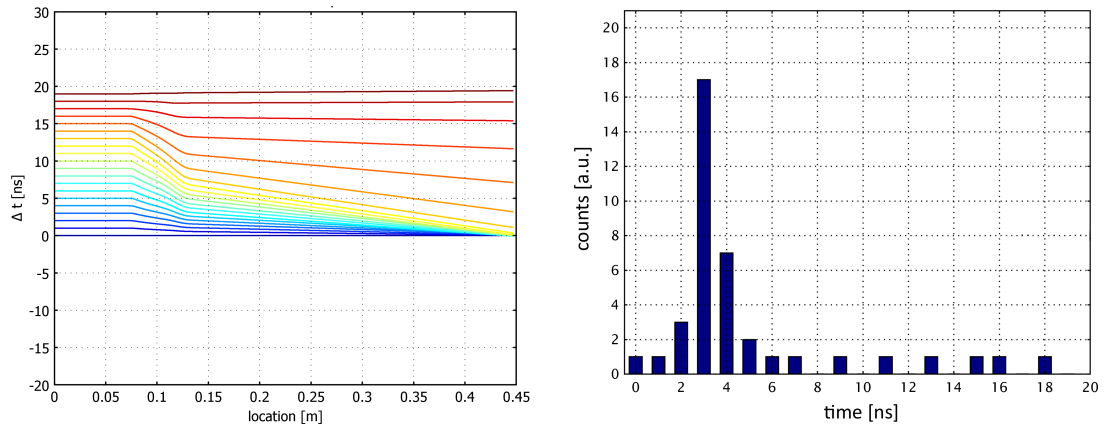


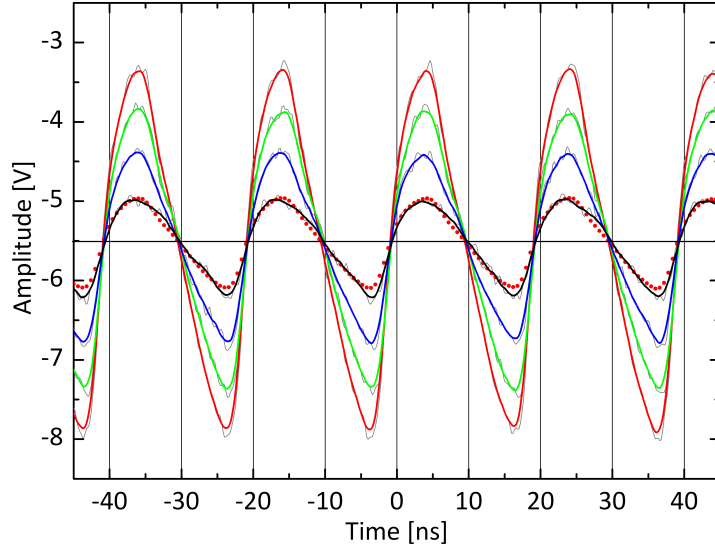
Figure 4.24: Left: The time differences of the particles to a reference particle in dependence of the drift distance. Before the energy modulation, the time difference of the monoenergetic positrons is constant. Since for the energy modulation a real sawtooth is used which has a rising edge of about 5 ns and a falling edge of 15 ns the time difference to the reference particle gets not for all particles smaller. At the last gap the slope changes again due to a slight and time independent acceleration, leading to a shift of the time focus. Left: Time histogram of the bunched beam at the time focus.

For the performance of the pre-buncher it is important, that the the field which occurs at the gaps between the electrodes has actually the sawtooth like time dependence. As described in section 3.6.1 this can be a challenging task because the electrodes have a certain capacitance and inductance perturbing the signal. Also it is to avoid that the rf-signal couples unintentionally to other electrodes whereby the energy of the beam might be unintentionally modulated. Hence for the pre-buncher electrodes, a small board was developed which carries all components for the electric circuit (see circuit in Fig. 4.22) which is used to supply the constant and time dependent voltages for the electrodes and which is placed as near as possible to the electrodes inside the vacuum. Due to the low capacity and the further precautions the modulation voltage could be coupled to the electrodes with only very small perturbations (see Fig. 4.25).

4.2.2.2 The first sine wave buncher

The beam which is now pre-bunched into pulses of the length of a few nanoseconds is accelerated to about 410 eV and enters the first sine wave buncher. This one is built up as a three electrode buncher, with the bunching electrode also acting as the capacitance in a RLC circuit. A scheme is shown in Fig. 3.25 in Sec. 3.6.1 where also the bunching principle is explained. Here, the details of the implementation are exposed (see Fig. 4.26). The design is very similar to that of the buncher used at the PLEPS with the main difference, that the coil which is used to build up the RLC circuit is placed outside the vacuum [117]. This enables a more compact setup and the

Figure 4.25: The voltages at the nearest accessible point of the bunching electrodes as measured with the probe of an oscilloscope (solid lines are smoothed) and the signal of the first electrode divided by a factor of four (dashed line). The bunching signals sustains only little perturbation due to the coupling onto the electrodes, and the scaling matches perfect.



possibility to modify the coil during the operation of the system without breaking the vacuum.

The usage of a RLC circuit has mainly two advantages: Firstly, it enables the creation of high modulation amplitudes by using compact and stable electronic amplifiers which have to provide only low power. Secondly, it avoids coupling problems and ensures an unperturbed sine wave at the gaps. For the dimensioning of the RLC circuit it is necessary to know the desired bunching amplitude as well as the capacitance and the resistance of the system.

With Eq. (3.60) it is possible to calculate the voltage difference at the first gap and hence the amplitude of the sine wave which has to be applied at the center electrode in order to attain a time focus in a certain distance. By supposing a 120 mm long buncher electrode, a drift of about 300 mm and an energy of the reference particle of 410 eV within the buncher electrode and the drift tube, a particle that reaches the first buncher gap 1 ns too late or too early has to be accelerated or decelerated by 16.4 eV. Therefore, the sine wave, which induces the voltage difference at the gap, must have an amplitude \hat{U} of about 55 V.

The eigenfrequency of a RLC circuit with the total capacitance C and the total inductance L is given by:

$$f_0 = \frac{\omega_0}{2\pi} = \frac{1}{2\pi\sqrt{LC}} \quad (4.8)$$

To use the resonant amplification, the eigenfrequency of the buncher RLC circuit must be equal to the base frequency of the system which is 50 MHz. The capacitance is given due to the construction and, as shown below, this should be as low as possible

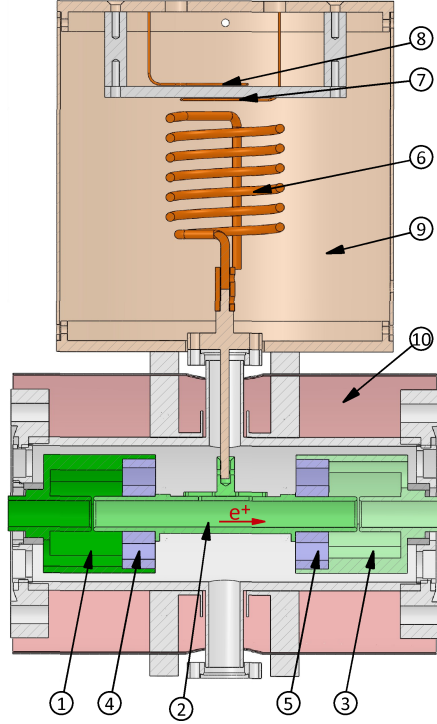


Figure 4.26: Cross section of the first sine wave buncher. The entrance and exit electrodes ①, ③ provide via Macor isolators ④, ⑤ the mechanical support for the buncher electrode ②. The coil ⑥ of the RLC circuit as well as the coupling and pick-up coils ⑦, ⑧ are located outside the vacuum within a copper shielding ⑨. To avoid perturbations due to magnetic stray fields the buncher is shielded by mu-metal ⑨ in the same way as the pre-buncher .

in order to attain a high amplification. Hence, the matching of the eigenfrequency to the base frequency has to be done mainly by adapting the inductance of the coil.

In order to achieve a high amplification, the RLC circuit must have a high quality factor Q . This factor is defined as the ratio of the maximal stored energy and the (effective) power loss of the system multiplied with the angular frequency, and is equal to the amplification if the RLC circuit is operated at the resonance. This value can be calculated easily e.g. for the time when the energy is stored entirely in the magnetic field of the coil:

$$Q = \omega_0 \frac{1/2 L \hat{I}^2}{1/2 R \hat{I}^2} = \omega_0 \frac{L}{R} = \frac{1}{\omega_0 RC} \quad (4.9)$$

The last transformation was obtained by inserting the resonance condition (4.8) in the rearranged form $L = 1/(\omega_0^2 C)$. It shows, that the resistance R and capacitance C have to be small in order to attain a high amplification.

The capacitance of the system is the sum of several single capacitances as the buncher electrode, the supply line and the feedthrough. Other capacitances as the capacitance of the resonator coil do not account to the total capacitance because this one is not

in series but parallel to the inductance. In order to proof, whether the construction provides a sufficiently small capacitance a finite element simulation was made with the help of COMSOL Multiphysics. This simulation yielded a capacitance of about 21.2 pF, where a main contribution for this value arose from the high relative permittivity $\epsilon_r = 6$ of the Macor insulation elements which hold the center electrode. By setting the relative permittivity from the realistic value of 6 to a hypothetical value of 1 the total capacitance is reduced to 10.4 pF. A lower dielectric constant of about 3.7 has e.g. fused quartz. But because this is much harder to machine and a sufficient high quality factor can be also reached by using the ceramic, it was decided to use Macor despite the harmful influence on the capacity. In the simulations, the capacitance of the electrical feedthrough could not be regarded, because the details of the construction and the used materials are unknown. A typical value for the capacitance of such feedthroughs is 80 pF. This high capacitance, which dominates the total value is a further reason, why Macor was preferred as insulating material.

The resistance of the system can be estimated much easier by adding up the single resistances and results in a value of about 0.3Ω . With the total capacitance and resistance the effective power, which has to be provided by the sine wave amplifier in order to attain the buncher amplitude \hat{U} , can be calculated. Therefore, Eq. (4.9) has to be rearranged as follows:

$$P = \omega_0 \frac{L\hat{I}^2}{2Q} = \omega_0 \frac{(\omega_0^2 C)^{-1} (\omega_0 C \hat{U})^2}{2Q} = \omega_0 \frac{C\hat{U}^2}{2Q} = \frac{1}{2} \omega_0^2 R C^2 \hat{U}^2 \quad (4.10)$$

By inserting the estimated values and the capacitance gained by the simulation a power of about 0.42 W can be calculated, what is less than the maximum power of 1 W provided by the used amplifiers.

After building up the buncher and tuning the resonance frequency $f_0 = \omega_0 / (2\pi)$ to 50 MHz by adjusting the main coil the resonance curve was measured. From this curve, the Q factor can be calculated by dividing the resonance frequency by the bandwidth B , which is given by the width of 2σ of the resonance curve (see Fig. 4.27):

$$Q = \frac{\omega_0}{B} = \frac{f_0}{f_2 - f_1} = \frac{50}{50.27 - 49.71} \approx 89 \quad (4.11)$$

This is about 21 % less than the theoretic value, which can be estimated by using Eq. (4.9) to 106. The difference can be attributed to the coupling and possibly to higher total resistance and/or capacitance [117].

The spread of the final temporal focus can be estimated by considering the aberrations, which are mainly determined by the energy spread and the pulse length of the pre-bunched beam. The energy spread composes of the energy spread of the initial beam

4 Positron beam preparation at NEPOMUC

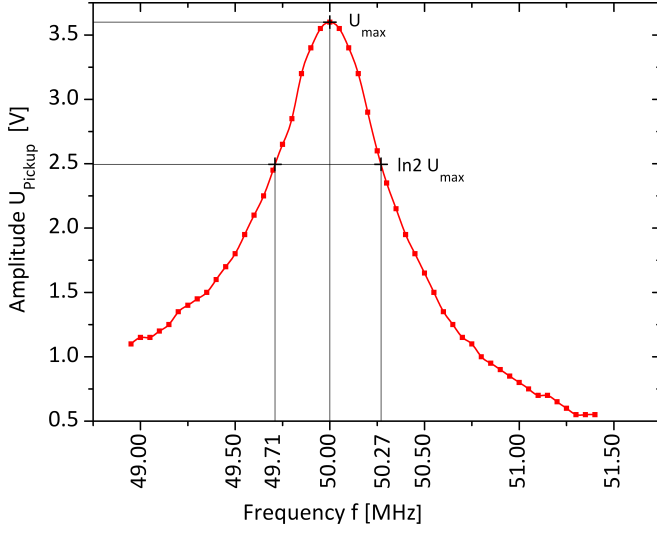


Figure 4.27: The resonance curve of the first sine wave buncher. The resonance frequency divided by the bandwidth is equivalent to the Q factor and reaches for this buncher a value of about 89.

and the energy spread induced by the pre-buncher. Because this energy spreads are unrelated the resulting spread is given by the root-mean-square value. The energy spread of the primary beam is roughly 2.2 eV (FWHM) and the spread caused by the pre-buncher is about 2.3 eV (FWHM) and hence the energy spread of the pre-bunched beam can be estimated to 3.2 eV (FWHM). This energy spread leads according to Eq. (3.65) to a chromatic aberration of 129 ps. The pulse length of the pre-bunched beam can be estimated from the simulations to less than 2 ns. This leads according to Eq. (3.64) to a spherical aberration of about 13 ps. Because this aberrations are unrelated the total aberration is given also by the root-mean-square value which calculates to 130 ps (FWHM) (see Tab. 4.1).

		FWHM	FWTM
ΔE_1	[eV]	2.2	5
ΔE_2	[eV]	2.3	4.6
ΔE_{tot}	[eV]	3.2	6.8
$\Delta \tau_c$	[ps]	129	276
Δt	[ns]	2	4
$\Delta \tau_s$	[ps]	13	102
$\Delta \tau_{\text{tot}}$	[ps]	130	294

Table 4.1: The calculated bunching aberrations ($\Delta \tau_c$, $\Delta \tau_s$, $\Delta \tau_{\text{tot}}$) and the beam parameters which influence this aberrations. ΔE_1 is the energy spread of the primary beam and ΔE_2 is that one induced by the pre-buncher. Δt is the duration of the pulses after the pre-bunching.

4.2.2.3 The second sine wave buncher

The first two bunching units are designed in such a way to create a time focus at the re-moderating crystal. The time structure remains during the re-moderation process nearly constant. The broadening which is caused by the time variation of the thermalization and back diffusion of the positrons is in the range of few picoseconds and can hence be neglected. After the re-moderation, the pulsed positron beam is guided to the next unit, which consists of a further sine wave buncher and a chopper (see Fig. 4.28). The buncher works in the same way as the previous with the differences, that there is no magnetic transport field and that the geometrical dimensions are slightly different. Since the distances between the buncher electrode and the supply line to the vacuum chamber are larger, the capacitances related to this elements are lower than at the previous buncher and hence the quality factor should be higher. The measured value of about 83, however, is slightly lower as the quality factor of the first sine wave buncher (see Fig. 4.29). This is probably caused by a different electrical feedthrough which is used for this buncher.

Since the buncher electrode is again 120 mm long the kinetic energy within this tube has to be also about 410 eV. This energy should have the positrons also within the buncher drift to avoid a potential difference and hence lens effects at the gap between the buncher electrode and the drift tube. If the time focus should appear in a distance of 400 to 500 mm from the second buncher gap the buncher amplitude \hat{U} has to be between 30 and about 40 eV. As this is even less as in the case of the first buncher this amplitude can be attained with the existent amplifiers.

4.2.2.4 The beam chopper

The pre-buncher is operated with a real sawtooth and hence not all positrons of the continuous beam are compressed into the pulses of the beam. Therefore, this positrons can not be bunched by the subsequent sine wave bunchers, either, and lead to a background in the time spectra. To attain a high peak to background ratio a chopper is necessary, which removes the positrons between the pulses. The chopper cabinet is located in front of the buncher electrode and consists of two half shells which provide the mechanical support for the chopper plates and ensures that the electrical deflection field is located between the chopper plates. On both chopper plates a square signal is applied, where one signal is inverted to the other (see Fig. 4.30). A chopper is used to deflect the beam for a certain duration to such an extent, that it is stopped by an aperture in a certain distance. For this purpose the chopper transfers transversal energy to the positrons which leads after the drift to a certain displacement. The amount of transversal energy is determined by two factors: Firstly, by the strength of the electric field and secondly, by the transit time within the chopper plates (see also Sec. 3.6.2).

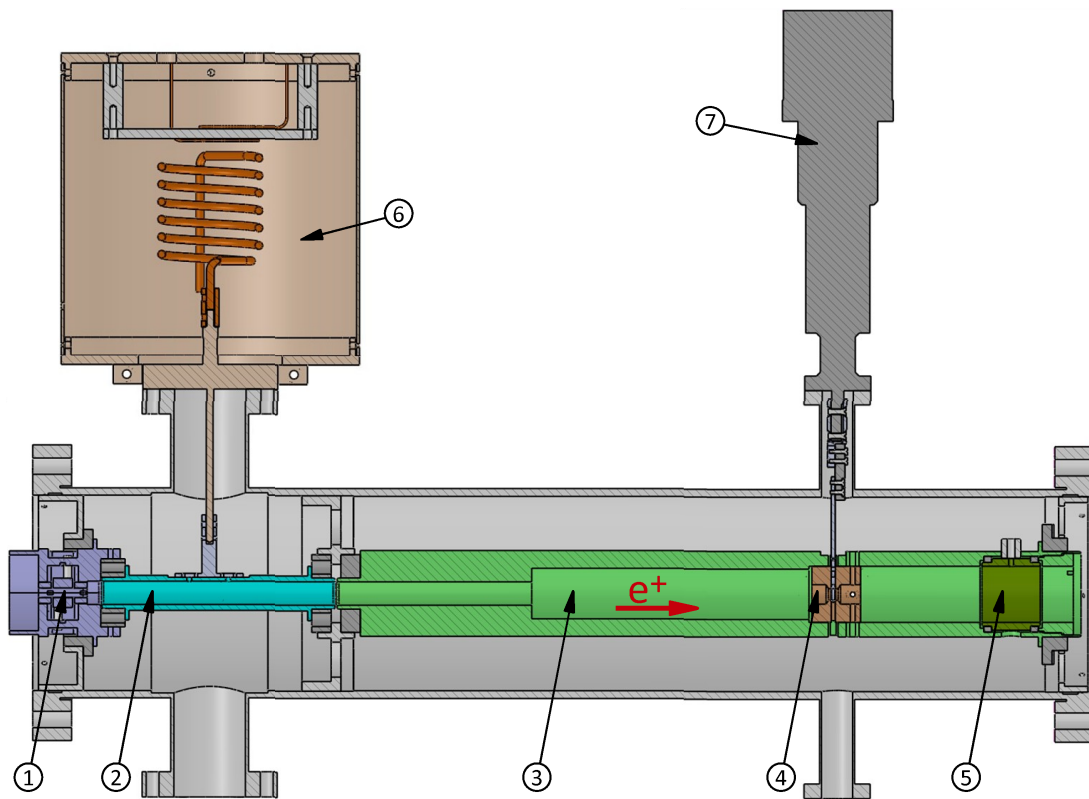


Figure 4.28: Cross section of the device containing the chopper and the second sine wave buncher. At the entrance of the device the chopper cabinet ① is located, which holds the chopper plates. The chopper is followed by the buncher electrode ② and the drift tube ③. This tube is also used as mechanical support for the chopper aperture ④ and an electric transport lens ⑤ which focus the beam into the center of the following beam energy elevator. The diameter of the chopper aperture can be varied by moving different sized holes into the path of the beam remotely with the help of a stepper motor ⑦. In order to keep the background, induced by the annihilation of positrons at the aperture low, this is surrounded by a block of a machinable tungsten-copper alloy. The buncher is build up in the same way as the previous and has therefore also the main coil outside the vacuum ⑥.

Figure 4.29: The resonance curve of the second sine wave buncher. The resonance frequency divided by the bandwidth is equivalent to the Q factor and reaches for this buncher a value of about 83.

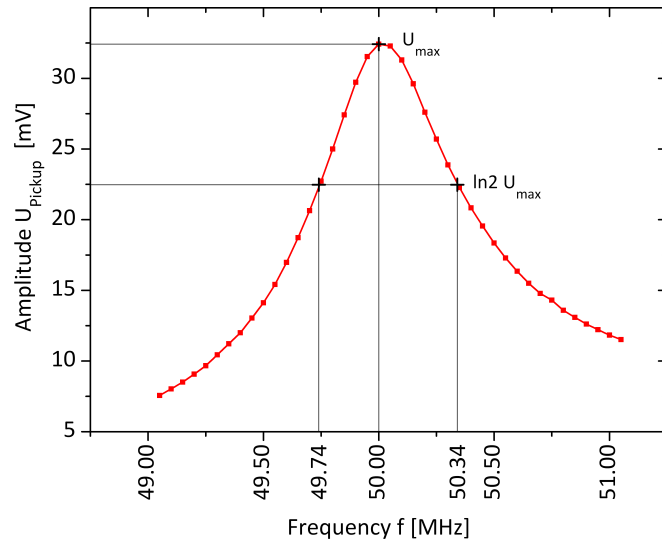
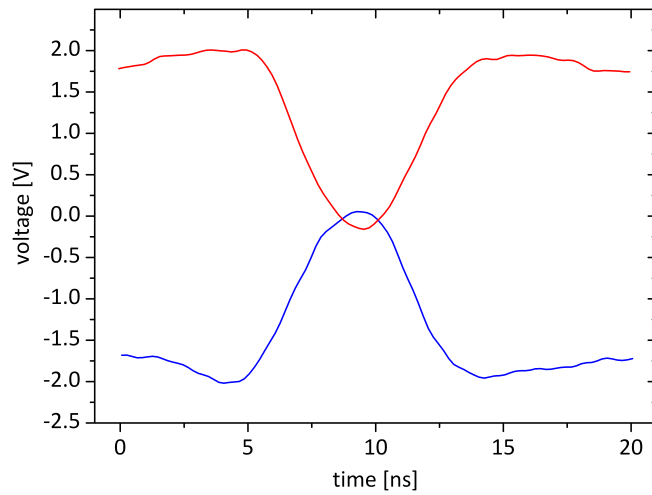


Figure 4.30: Time dependent voltages applied at the chopper plates. Since the chopper plates are operated antisymmetric the potential difference is twice the voltage amplitudes created by the function generator.



4 Positron beam preparation at NEPOMUC

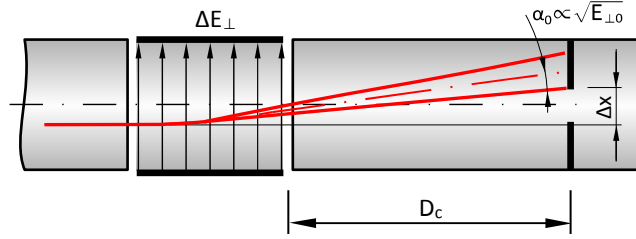
The maximum field strength is limited by the minimal distance between the chopper and the maximum voltage supplied by the function generator. The distance between the plates has to be larger than the beam diameter. On the base of numerical calculations of the positron trajectories, the distance between the chopper plates was set to 5 mm (see 4.2.3.2). The maximum voltage provided by the existent function generator is about 1.75 V and hence the maximum potential difference between the two plates is 3.5 V.

The transit time is given by the ratio between the length of the chopper plates and the longitudinal velocity of the positrons within the chopper. The longitudinal energy within the chopper should be the same as in the subsequent buncher in order to avoid potential differences. Such potential differences would lead to lens effects and hence complicate the beam transport. Since the buncher has a length of 120 mm the velocity has to be 12 mm/ns to ensure a correct energy modulation at the first and the second gap. Because of the fixed velocity the length of the chopper plates is the only free parameter for the variation of the transit time. However, the finite transit time causes that some positrons gain less energy than others. If at the chopper plates an ideal square wave voltage would be applied and the transit time would be infinitesimal short, the gained transversal energy would be also like an ideal square wave. But a finite transit time leads to a smeared energy distribution over time because the potential applied at the chopper plates changes during the passage of a positron and hence the transferred energy varies. E.g. if the chopper plates are 12 mm long 10 % of the positrons of a 20 ns time interval get not the desired transversal energy. As a compromise between a high transferred transversal energy and a low broadening of the energy distribution, a length of 13 mm was assigned.

By using this values and Eq. (3.67) the transferred energy calculates to 50 meV. In order to determine the effects of fringe fields numerical simulation were made additionally, which resulted⁹ in a slightly higher energy of 58 meV. In order to deflect the beam entirely, this value has to be at least as high as the spread of the transversal energy of the beam at the chopper. The positrons have immediately after the re-emission from the re-moderation crystal an energy spread of about ± 50 meV, and since the beam is afterwards adiabatically decompressed, the transversal momentum considerably lower. On the other hand the transversal momentum increases during the break away of the field lines of the magnetic lens at the re-moderator. In order to quantify the transversal energy of the beam in the area of the chopper numerical simulations were made, resulting in transversal energies lower than 10 meV, for two different beam transport scenarios (see below). Hence, the deflected positrons will leave the path of the regular beam at a certain point entirely. It would be desirable if the deflected beam annihilates at the chopper aperture because there the annihilation radiation is shielded by a copper-tungsten block. The deflection after a certain distance could be calculated

⁹This value was attained by simulating a particle entering the chopper at the center. For particles entering at different points the transversal energy differed slightly (± 2 meV).

Figure 4.31: Scheme of the chopper. The lower trajectory has to be deflected at most in order to be stopped by the aperture.



with these numbers and simple geometric considerations (see Fig. 4.31). The deflection after a certain distance is as follows:

$$\Delta x = \sqrt{\frac{\Delta E_{\perp} - E_{\perp 0}}{E_c}} D_c \approx \sqrt{\frac{58 \text{ meV} - 10 \text{ meV}}{410 \text{ eV}}} \cdot 400 \text{ mm} \approx 4.3 \text{ mm} \quad (4.12)$$

Hence, if the transversal momentum of a positron points in the opposed direction to the deflection field before it enters the chopper it is deflected by 4.3 mm. The radius of the chopper aperture is 2.0 mm and the maximum distance from the axis from which a positron can pass the chopper is 2.5 mm. Hence such a *worst case* positron has to be deflected 4.5 mm in order to annihilate at the chopper aperture. Under the considered conditions a small amount of the positrons will pass the chopper aperture and annihilate at an undetermined location.

4.2.3 The beam transport within the interface

In front of the magnetic field termination, the transport is performed adiabatically by a longitudinal magnetic transport field which extends the transport field of the beam line. After the magnetic field termination, the transport is apart from two exceptions electrostatically. One is the magnetic separation of the incident and the re-moderated beam at the beam switch by two dipole fields and the second is the focusing of the incident beam onto the re-moderation crystal by a magnetic single pole lens. Because there is no overlap of electric fields and the magnetic dipole field they can be examined separately. In principle the calculation of the path of the incident beam could be calculated with the tools of the Gaussian optics. Only the presence of elements for which the optical properties are unknown and not available elsewhere e.g. in textbooks, avoids this. Since the situation is similar for the re-moderated beam, both beam paths were examined numerically with the help of COMSOL Multiphysics. Due to the separation of the magnetic dipole field, rectified and rotationally symmetric computer models could be used.

4.2.3.1 The transport of the incident beam

The magnetic transport field is in the same way terminated as in front of the NEPOMUC re-moderator with the differences, that the open diameter is only 7 mm and that the distance between the metallic glass stripes is only 1 mm. Because of the smaller distance between the stripes, the azimuthal momentum, which the positrons gain during the transition into the magnetic field free area, is lower than 90 meV even if the field in front of the field termination is 4 mT. On the other hand, the decreased distance leads to a slightly reduced geometric transmission of about 98 %. Behind the field termination, the beam diverges by an angle given by the ratio between longitudinal and transversal energy. The longitudinal energy should be between 400 and 600 eV because this is the drift energy which the positrons must have after the first sine wave buncher. As already mentioned above, due to the longitudinal energy spread of about 5 eV (FWTM) it is an educated guess that the maximum transversal energy spread of the incident beam is about ± 2.5 eV

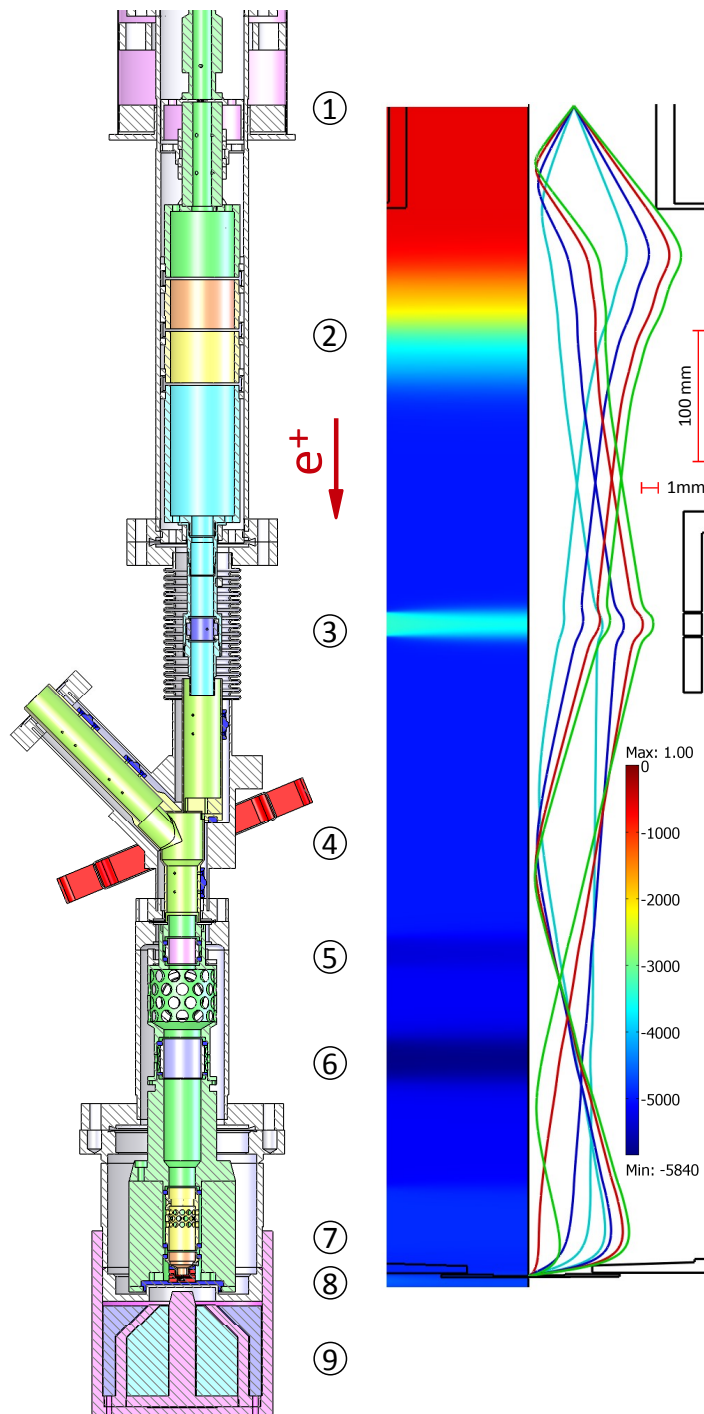
The diverging beam is accelerated within three potential steps to the energy of 5 keV which is used for the implantation of the positrons into the re-moderation crystal. Since the acceleration occurs without a magnetic transport field, the field gradients at the potential steps act as electric lenses. Because the potential difference of about 4600 V is spread over a distance of about 180 mm by the usage of the several electrodes with a large diameter, this assembly has a long focal length. The following field lens ensures that the beam has a small diameter during the pass through the beam switch, and that the illumination of the magnetic single pole lens is not too large. A small diameter at the beam switch is desirable because there is a constriction and a small diameter keeps the aberrations caused by the magnetic deflection low. This lens was not foreseen from the beginning but became necessary due to the the large transversal energy of the beam. In the final step the positrons are focused onto the re-moderation crystal. The magnetic lens consists of two separated coils and iron yokes in order to adjust not only the field strength but also the field gradient (see Figs. 4.32 and 4.33).

For the trajectory simulations shown here, the initial parameters were adapted to the experimentally observed values. Hence the initial radii for the trajectories were set to the HWTM value of the measured beam profile (2.5 mm) and the maximum transversal energy range was extended from a value of ± 0.5 eV which was originally assumed to a higher value of ± 2 eV. An overview of the trajectories is shown on the right side of Fig. 4.32 and the minimal attainable spot sizes are shown in the detailed view of the crystal in Fig. 4.34. The simulation showed that with the combination of electrostatic and magnetic lenses a diameter reduction by a factor of 60 can be attained if the maximum transversal energy is ± 0.5 eV and even with the very high energy spread of ± 2 eV a reduction by a factor of 13 is possible. Further trajectory calculations showed, that the chromatic aberrations lead only to a negligible blur even of the smallest simulated spot and even if a very high longitudinal energy spread of ± 25 eV was assumed which

Figure 4.32: Left: Components of the interface which are passed by the incident beam after the magnetic field termination.

Right: The electric potential and the positron trajectories within a rectified and rotationally symmetric model. In order to provide a better overview, the transversal dimension is scaled by a factor of 10.

The acceleration electrodes ② focus together with the Einzel-lens ③ the beam which diverges after the magnetic field termination ① toward the operating field of the magnetic single pole lens ④. The action onto the incident beam by the Einzel-lenses ⑤, ⑥ and the extraction electrodes ⑦, ⑧ are only low, due to its high energy.



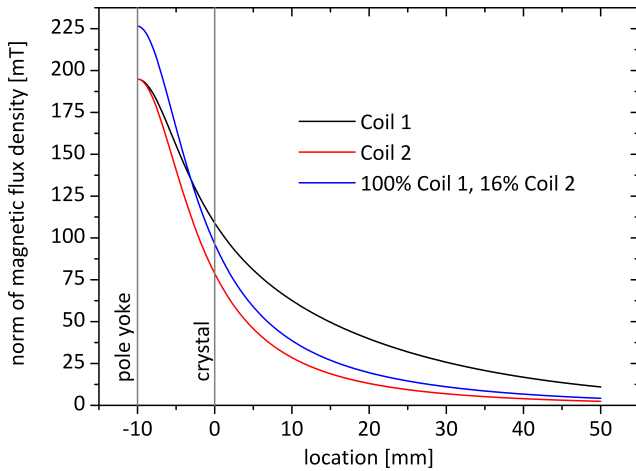


Figure 4.33: The single pole lens consists of two separated coils and iron yokes in order to adjust the field strength and the field gradient. Therefore, during operation it can be selected whether the lens should have low aberrations and a low acceptance or vice versa. In the first case the field has to be strongly located and therefore the field gradient has to be high. In the second case the field has to be long reaching and hence the field strength has to increase slowly.

might be induced by the bunchers.

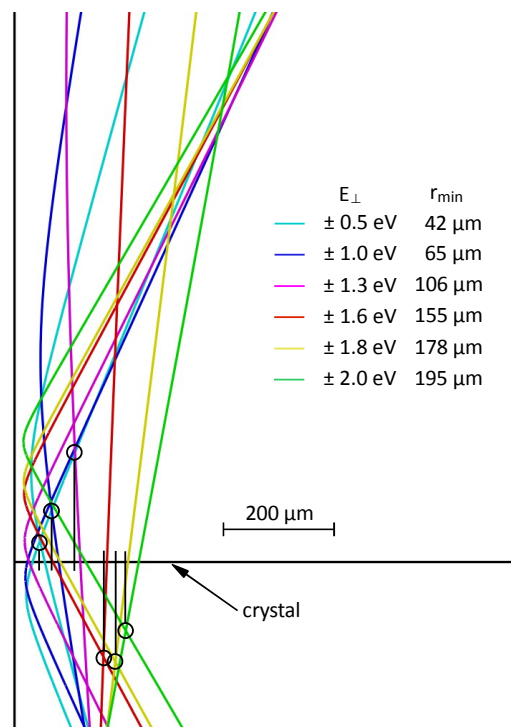
Concluding, the simulations attest that the transport system for the incident beam is capable to image even a beam with a very high transversal momentum down to a reasonable small spot size. Further, the de-magnification gets very high if the transversal energy spread of the incident beam becomes in the range which should be attainable if the re-moderated NEPOMUC beam is transported entire adiabatically to the SPM interface.

4.2.3.2 The transport of the re-moderated beam

The transport of the re-moderated positron beam is performed mainly with the help of electrostatic Einzellenses (see Fig. 4.35). Only the deflection of the beam into the second column of the interface is performed by the magnetic dipole field. The situation is very similar to that of the re-moderated beam at the NEPOMUC re-moderator with the difference, that in the case of the interface there are more Einzellenses and that the re-moderation crystal is located within the strong and diverging field of the magnetic single pole lens. This position was selected, because thereby a shorter focal length and lower aberrations can be attained. In contrast to the NEPOMUC re-moderator, the spot size at the crystal of this re-moderator and hence also the diameter of the beam at the breakaway from the magnetic field lines is much smaller. Therefore, the the azimuthal momentum transferred to the positrons at the breakaway point is much lower (see also Sec. 4.1.2 P. 68).

The initial values for the simulation of the trajectories are based on the spot sizes of the incident beam at the re-moderation crystal according to the previous simulations (see. Fig. 4.34) and on a maximum transversal energy of ± 50 meV. From the several

Figure 4.34: Detailed view of the simulated trajectories. The black circles mark the minimal spot sizes which can be attained for beams with different maximum transversal energies. Because the lens excitation was kept constant for all trajectories the minimal radii for the beams with low initial transversal energies are slightly in front of the re-moderation crystal and for those with higher transversal energy these radii appear behind the crystal.



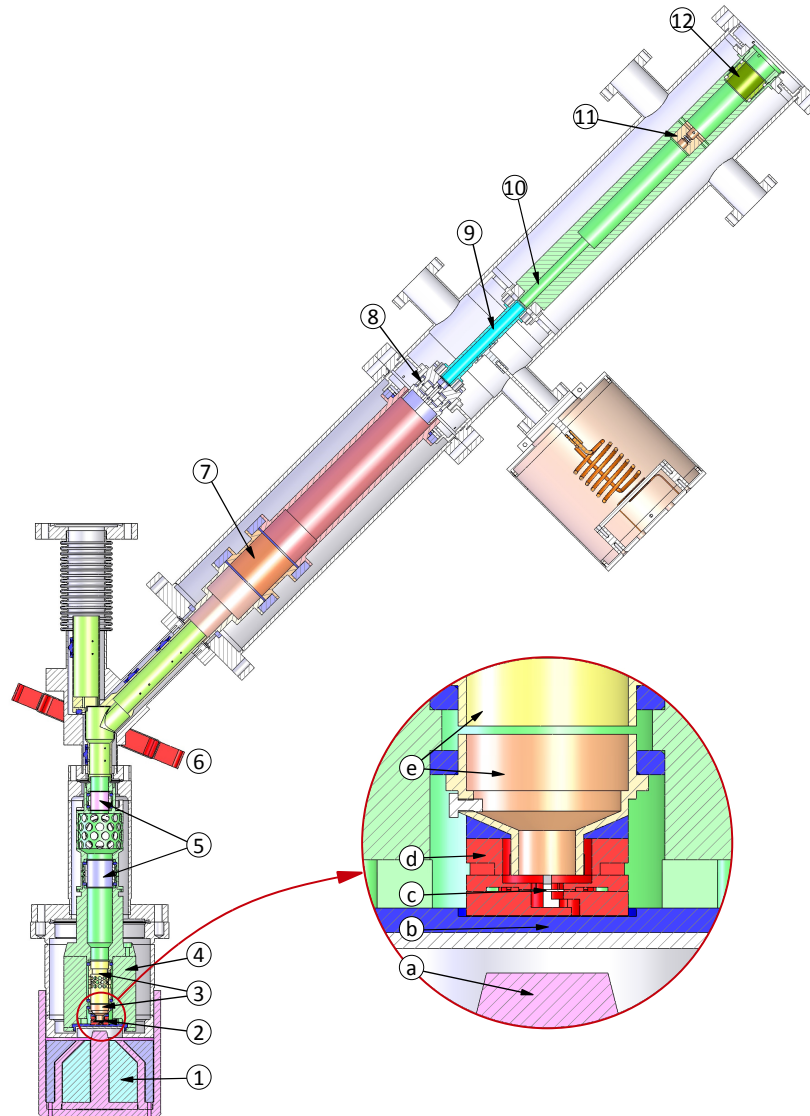


Figure 4.35: Components of the interface passed by the re-moderated beam: The positrons re-emitted from the crystal ①,Ⓒ are accelerated by the electrodes ③Ⓔ within the high magnetic flux of the single pole lens ①Ⓐ. After the breakaway of the positrons from the magnetic field lines of the single pole lens ①Ⓐ the beam transport is accomplished mainly by electrostatic Einzellenses ⑤⑦⑫. Only the deflection of the beam into the second column of the interface is performed by a magnetic dipole field ⑥. The chopper ⑧, the buncher electrode ⑨ and the drift tube ⑩ are used to enhance the pulse structure of the beam further. In order to shield the γ -radiation which originates from the annihilation of positrons in the re-moderation crystal and at the chopper aperture, both are surrounded by a machinable tungsten alloy ④Ⓘ.

simulations, two beam transport scenarios are shown in Fig. 4.36. On the left side of each figure a beam transport is shown, which avoids large opening angles, and hence only little aberrations are evoked. But this transport is only possible if the spot size on the re-moderation crystal is small and hence the diameter of the beam keeps small over the full path. Critical points are a constrictions at the beam switch (see below), the small distance of the chopper plates and the chopper aperture. This scenario allows to transport positrons which stem from a spot on the re-moderation crystal which has a radius smaller than $110\ \mu\text{m}$ and hence from an incident beam with a maximal diameter of $5\ \text{mm}$ and a transversal energy spread narrower than about $\pm 1.3\ \text{eV}$. Because of the larger energy spread of the incident beam, an alternative scenario was worked out which allows also the lossless transport of a re-moderated beam which stems from an incident beam with a transversal energy of $2\ \text{eV}$. This scenario creates more intermediate images whereby the opening angles and hence the aberrations become larger.

Beside the lower aberrations, the first scenario enables to keep the energy constant within the chopper cabinet, the buncher electrode and the drift tube and at the value which is necessary for the correct energy modulation at the first and second buncher gap. This avoids potential steps and hence a unintended focusing of the beam, which is deflected by the chopper, trough the copper aperture. The two scenarios presented here demonstrate, that with the setup at least two very different beam transports can be achieved which satisfy the demands of a broad range of parameters of the incident beam.

4.2.3.3 The positron beam switch

Since now only the rectified beam paths have been examined. The design and the research of the influence of the dipole coils at the beam switch was the subject of a diploma thesis whose results are presented here [111]. The aim of the beam switch is to separate the incident beam from the re-moderated beam by a magnetic dipole field. If only one dipole is used, which acts on both beams the geometry of the re-moderator has to be shaped according to the deflection angles. Hence the axis of the part, where both beams are guided, has to be inclined to the axis of the incident beam and to the axis of the re-moderated beam. Beside this method, which is implemented at the NEPOMUC re-moderator, there is the possibility to install a second dipole, which acts only on one beam and in the contrary way to the first dipole. Due to this, the axes of the beams in front and after this two dipoles are not inclined but have a parallel offset. This concept is used for the incident beam at the beam switch at the SPM interface and has the advantage of a simpler mechanical setup.

Independent from the concept, the quality of the deflected beams depends essentially from actual distribution of the magnetic deflection fields. One kind of aberrations arise from higher moments in the field distribution. E.g. a quadrupole contribution leads to a

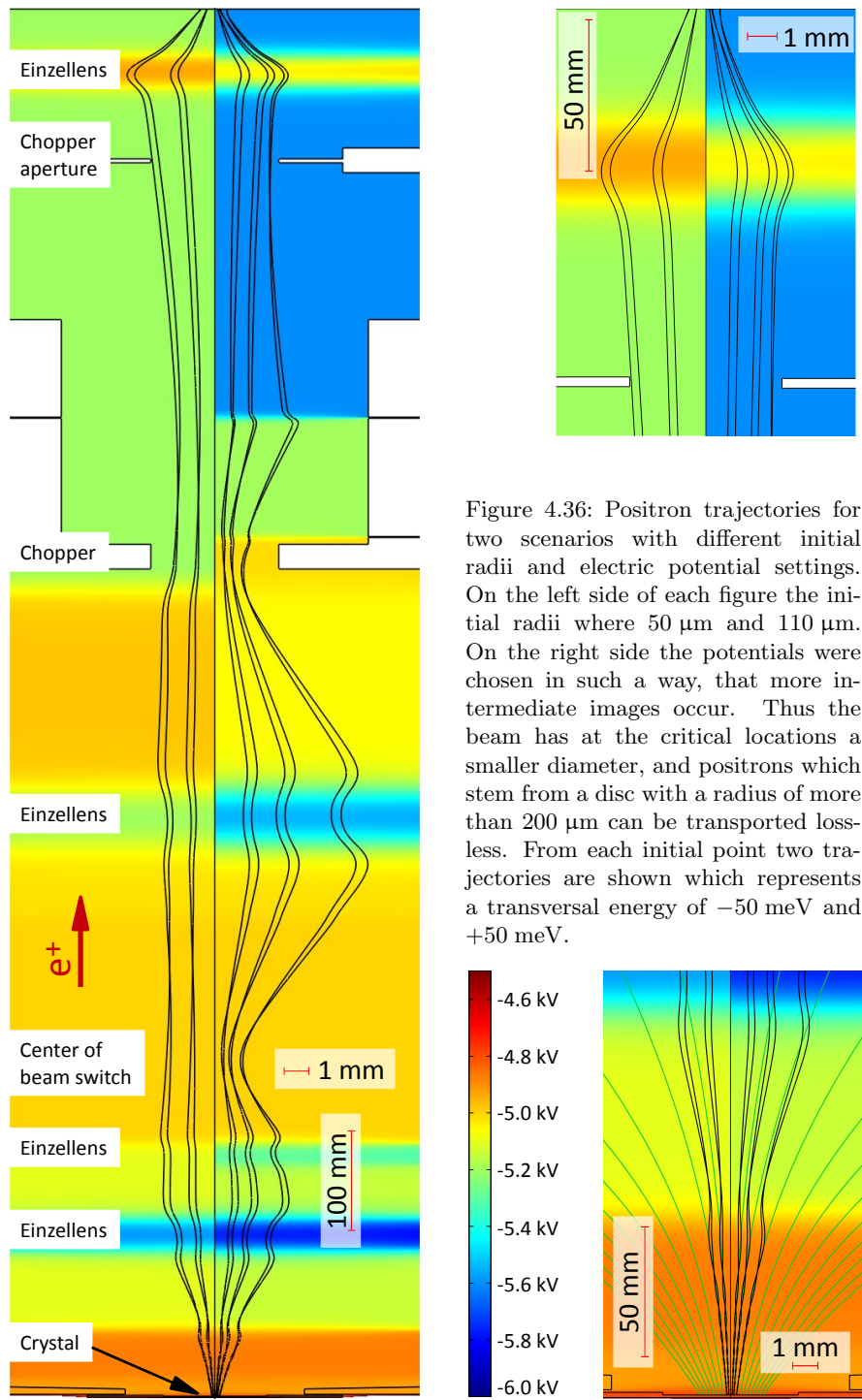
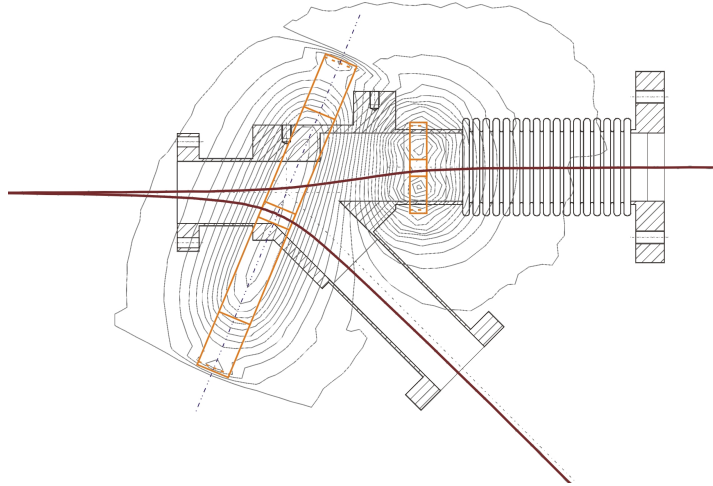


Figure 4.36: Positron trajectories for two scenarios with different initial radii and electric potential settings. On the left side of each figure the initial radii were $50\ \mu\text{m}$ and $110\ \mu\text{m}$. On the right side the potentials were chosen in such a way, that more intermediate images occur. Thus the beam has at the critical locations a smaller diameter, and positrons which stem from a disc with a radius of more than $200\ \mu\text{m}$ can be transported lossless. From each initial point two trajectories are shown which represents a transversal energy of $-50\ \text{meV}$ and $+50\ \text{meV}$.

Figure 4.37: Setup of the beam switch and the trajectories of the incident and re-moderated beam. The contour lines represent the norm of the component of the magnetic flux density which is perpendicular to the drawing plane. Onto the incident beam act both magnetic fields and since they are opposed the beam is shifted by 15 mm. The re-moderated beam is only affected by the field of the larger coil and hence deflected by 45° (from [111]).



focusing in one direction and to a defocusing of the beam in the perpendicular direction. A reduction of this higher order contributions in the area passed by the can be achieved by guiding the magnetic field within a material with a high magnetic permeability and keeping the distance between the two pole shoes small. Other aberrations are caused due to the extension of the field and from the beam properties. In order to deflect a beam with a finite spatial and angular distribution uniformly, an equal field has to act onto each particle and all particles have to cover the same distance within the field. The easiest approach to achieve this is to minimize the field extension so that the influence of different paths within the field get also minimal.

In order to prove whether the initial and the re-moderated beam passes the switch appropriately and to estimate the aberrations, which are induced by the deflection, numerical simulations of the beam paths were made, with the actual field distributions being used [111]. As shown in Fig. 4.37 appropriate locations and excitations of the deflecting coils were found which lead to an offset of the incident beam of 15 mm and deflects the re-moderated beam by 45° . Further, it can be seen, that there is a point where the re-moderated beam becomes very close (≈ 5 mm) to the vacuum chamber and hence the beam has to be sufficiently narrow at this point and the potential tubes have to be carefully arranged. The potential tubes reduce the inner with by approximately 3 mm and hence the beam radius has to be smaller than 2 mm at this point, what is reached by both presented beam transport scenarios.

The perturbing influence of the coils was examined by regarding a finite extension of the beams within the middle plane perpendicular to the magnetic field. For the re-moderated beam it could be shown, that the deflection leads to a diverging of the beam within this plane and that a focused beam is less perturbed than a parallel beam (see Fig. 4.38). This perturbation is ascribed to a quadrupole contribution of

4 Positron beam preparation at NEPOMUC

the magnetic field and hence can be corrected by an additional quadrupole element. The incident beam should be shifted by 15 mm and no angular alteration should be induced. As shown in Fig. 4.39 this is achieved for a sufficient small beam. In both cases, a correction of the aberrations is not necessary, because the beams are focused toward the beam switch and hence the diameters are sufficiently small.

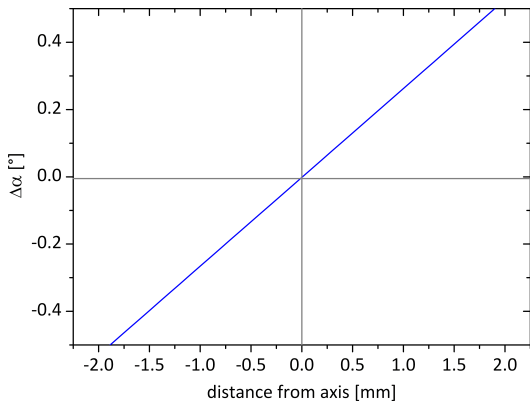


Figure 4.38: Deviation from the reference angle of 45° . A negative value means a larger deviation and positive value a lower deviation. Thus a large scaled re-moderated beam is defocused by passing the beam switch.

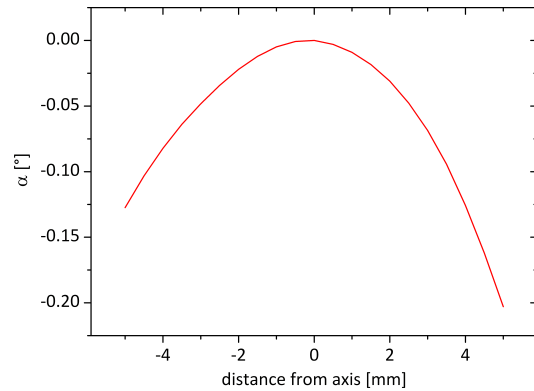


Figure 4.39: Angular distribution of the incident beam after passing the beam switch. Positrons which are radially far apart from the reference particle are skewed in the same direction.

4.2.4 Experimental results

During several measurement campaigns both, the efficiency of the beam transport including the re-moderation and the bunching performance were measured. A comprehensive overview of these measurements is given in the following.

4.2.4.1 Performance of the beam pulsing components

For the measurement of the spatial intensity distribution of the beam, a MCP was mounted behind the chopper drift. In order to avoid vacuum breaks and time consuming modifications of the system during the measurement campaigns the MCP served also as annihilation target. The annihilation radiation was used for the determination of the beam intensity and as timing signal for lifetime measurements which were accomplished to proof the bunching properties of the interface.

A MCP is made of glass whereby the front and the back is coated by a metallic alloy. Since this layers are very thin and the open area ratio of a MCP is typical more than

60 % there is a high probability that the positrons are implanted into the glass body. In glass the positron lifetime is increased due to positronium formation and thus the lifetime spectra will be broadened by this long lifetime. The measured lifetime spectra are the convolution of the unknown positron lifetimes and the resolution function of the system. Since the positron lifetimes appear due to the reversed timing only at the left side of the time peak the right side is broadened solely by the timing resolution of the system. Usually the FWHM of the peak is used as a figure of merit which characterizes this resolution. Since the FWHM can not be derived directly due to the long and unknown lifetime at the left side of the peak it is estimated by doubling the HWHM value of the right side.

This $2 \times \text{HWHM}$ value results from the time resolution of the detector system and the time spread of the bunches created by the interface. The detector system consists of a BaF_2 scintillator coupled to a XP2020Q photomultiplier from Photonis (see Fig. 4.40). The high voltage supply and the readout of the signal is made by the same base which is also used e.g. at the PLEPS. The measurement setup is divided into a fast branch, which measures the time between start and stop signal, and a slow branch, which selects only unperturbed events from the 511 keV photo peak. The fast signal from the base is feed directly to a constant fraction discriminator (CFT, Canberra 2128) and the slow signal is first amplified (Ortec 855) and than with the help of a single channel analyzer (SCA, Ortec 551) used to select 511 keV events and to open the gate of the analog to digital converter (ADC, Fast ComTec 7070) in the case of a valid event. The fast logical signal from the CFT is used as start signal for a time to amplitude converter (TAC, Canberra 2145) but also to gate the fast gate logic (FGL). When ever the gate of the FGL is open it derives from the sine wave of the master oscillator a logical signal which is used as the stop signal for the TAC. The amplitude signals of the TAC are digitalized by the ADC and the digital values are collected by a multi channel analyzer (MCA, Fast ComTec WebMCA). The determination of the time resolution of this detector system is difficult, because there is no calibrated bunched beam system and other common calibration methods need a second detector which has an also unknown time resolution.

Since the width of the pulses of the positron beam and the time resolution of the detector system are uncorrelated the FWHM value of the peak in the time spectra is given by the rms-value of both. In the following, the performance of the pulsing components is illustrated and discussed with the help of the lifetime spectra, which where recorded with the described system (see Fig. 4.41a–e). The shadow peaks in some of the spectra are due to the setup and not a part of the pulse structure. A small amount of the positrons annihilate at the chopper aperture, which was in sight of the detector. Since the positrons are much slower than the γ -quantum, the positrons which annihilate at the MCP are detected later than the positrons which are stopped at the aperture. The time difference exceeds the 20 ns time frame of the spectrum and hence the shadow peak seems to appear at the wrong side of the main peak.

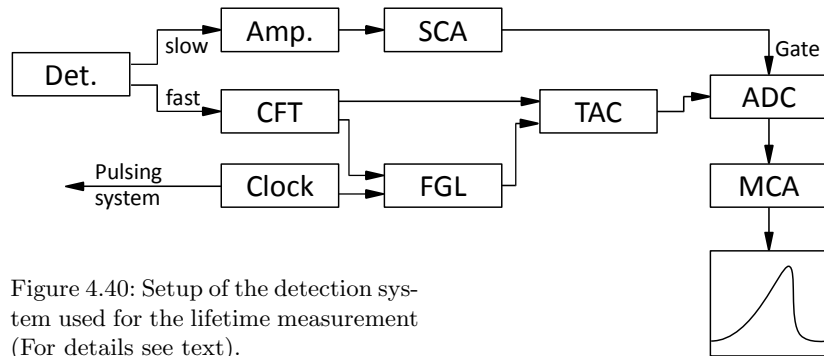


Figure 4.40: Setup of the detection system used for the lifetime measurement (For details see text).

Due to the construction of the pre-buncher and particularly because of the shape of the real sawtooth used for the energy modulation the spectrum of the pre-buncher has an inherent asymmetry, which is not caused by a long positron lifetime (see Fig. 4.41a). The $2 \times \text{HWHM}$ value of this spectrum is about 4.3 ns and the FWHM value is about 5.9 ns. Both values are much longer than the pulse duration predicted by the simulation. This can be explained by the large energy spread of the incident beam, which was about the half of the modulation amplitude. Nevertheless, the pre-buncher is capable to compress about 56 % of the total intensity into the FWHM time frame. A more meaningful estimation of the capability of the pre-buncher is given by evaluating the impact of the pre-buncher onto the spectrum of the first sine wave buncher (see Fig. 4.41b). The two bunchers in front of the re-moderator have to create pulses which are short enough that no or only a very small spherical aberration at the second sine wave buncher occurs. Pulses with a duration of e.g. 2 ns cause a spherical aberration of only 13 ps and can therefore be regarded as short enough. The pre-buncher alone can compress 23 % into this time frame and the first sine wave buncher concentrate 30 % of the total beam intensity into this 2 ns duration. By operating the two bunchers together, this amount is increased to 56 %.

If the first sine wave buncher is operated alone the $2 \times \text{HWHM}$ is about 610 ps. The second sine wave buncher, which is basically a copy of the first one and which is operated only with a slightly different bunching amplitude, attain a peak width of about 520 ps ($2 \times \text{HWHM}$) if it acts onto the dc beam. The lower width is reasonable because the re-moderation in front of the second buncher creates a beam with a very small energy spread and hence the chromatic aberrations are in the range of only a few picoseconds.

Also the spheric aberration which is determined by the pulse width of the incident beam is very low at the second sine wave buncher, if it is operated together with the bunchers in front of the re-moderator. The time focus of the first two bunchers is set onto the re-moderation crystal. Because of the timing resolution of the detector exact pulse length is unknown but is at least lower as the measured $2 \times \text{HWHM}$ value

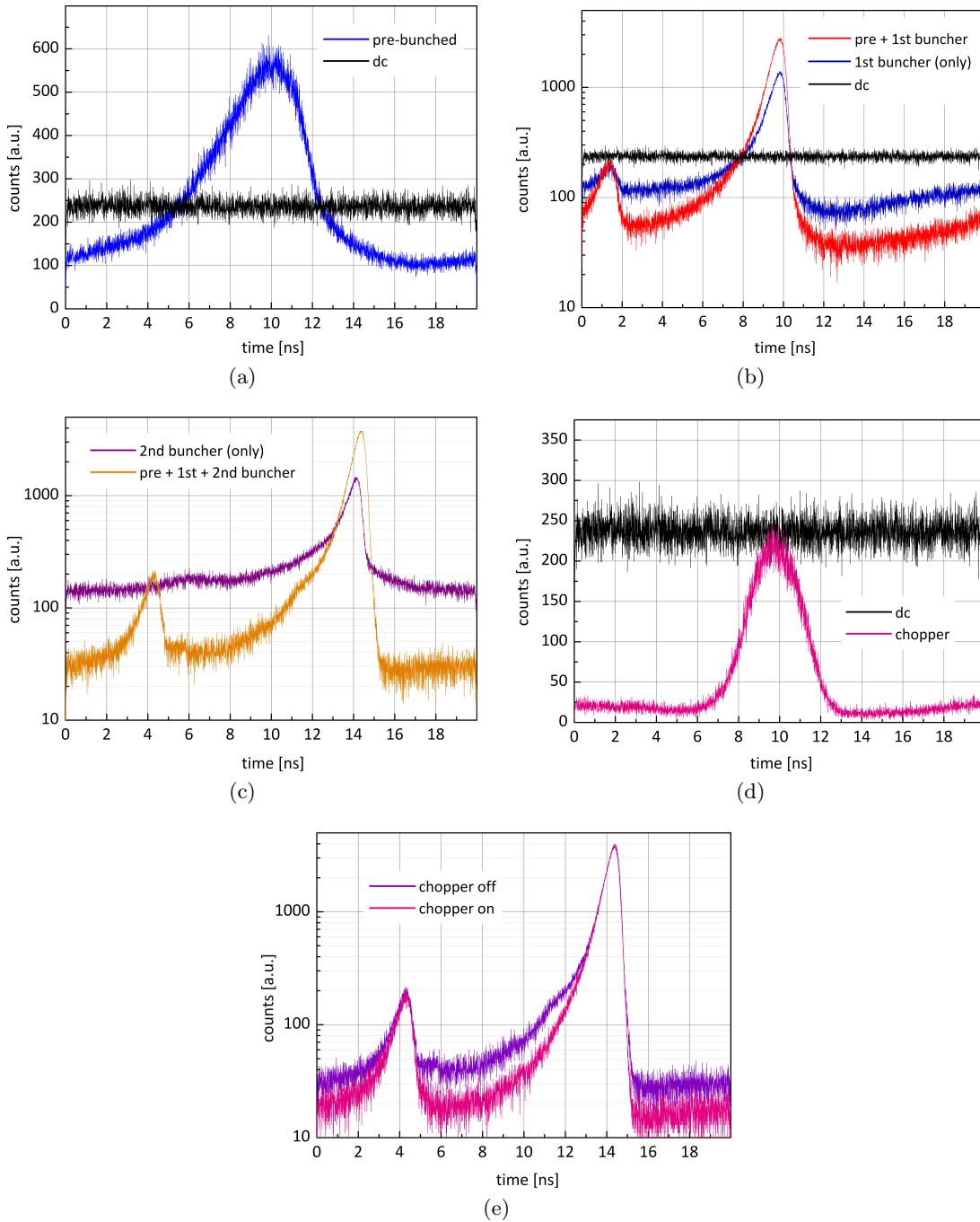


Figure 4.41: Lifetime spectra recorded with a the pulsed beam and a MCP as annihilation target.

4 Positron beam preparation at NEPOMUC

which is 558 ps. Due to the small energy spread of 0.1 eV the width of the pulses is nearly conserved until they reach the second sine wave buncher. Even with an enlarged energy spread of 0.2 eV which might be caused due to perturbing effects e.g. within the beam switch leads to an additional time spread of maximal 40 ps in front of the second sine wave buncher. More harmful are transit time effects caused by different lengths of the trajectories of the positrons. The largest variation of the distance from the re-moderation crystal to the buncher is induced by different deflection radii at the beam switch, which can lead to a maximal difference of the covered ways of 4 mm in the worst case. This would lead to a time spread of about 500 ps. These two effects together with the width of the pulse, created by the two bunchers in front of the re-moderator, would cause a total time spread of about 750 ps in front of the second sine wave buncher. This in turn would lead to a negligible spherical aberration of less than 1 ps. Hence, the second sine wave buncher works essentially aberration-free if operated together with the bunchers in front of the re-moderator and the measured $2 \times \text{HWHM}$ value has to be caused solely by the timing resolution of the detection system. Therefore, in Tab. 4.2 not only the $2 \times \text{HWHM}$ values are given but also the estimated pulse length regarding a time resolution of the detector of 472 ps.

	$2 \times \text{HWHM}$ [ps]	est. pulse length [ps]
pre-b.	5940	5921
1st sine b.	610	386
pre- & 1st sine b.	558	298
2nd sine b.	520	218
pre- & 1st & 2nd sine b.	472	0

Table 4.2: The $2 \times \text{HWHM}$ values of the timing peaks and the estimated pulse lengths achieved by the bunching components separately as well as in combination. Since the second sine wave buncher works essentially aberration free if operated together with the first two bunchers, the measured peak width has to be induced by the detection system.

A further broadening of the measured timing spectra arises due to the tilted channels of the MCP, which leads to a longitudinal variation of the site, where the positrons annihilate and hence a variation annihilation time. To estimate the influence of the tilted channels onto the timing spectra it is assumed, that the penetration depth into the channels can vary up to 0.5 mm. This variation leads together with the mean energy of the positrons at the MCP of 850 eV to a variation in time of about 30 ps. Since this blur is independent from the pulse width it is assigned to the resolution of the detection system.

Beside the pulse length and hence the timing resolution the peak to background ratio is of great importance for lifetime measurements. The combination of a sawtooth pre-buncher and a sine wave buncher ensures short pulses created with high efficiency, and therefore, a high peak to background ratio. As shown in 4.41b the peak of the

spectrum created by the first sine wave buncher raises by a factor of two with the help of the pre-buncher and at the same time the background is reduced by a factor of two. Thus, the peak to background ratio is enhanced by a factor of 4. The situation is similar at the second sine wave buncher. Operated individual, the ratio is about 1:10 and in combination with the first two bunchers this ratio is enhanced to 1:130.

The bunchers do both, raising the peak and reducing the background, whereas the chopper has the only aim to eliminate the background. As shown in Fig. 4.41d the chopper can be adjusted so that only small parts of the dc beam can pass the chopper aperture. In order to achieve this, although with the relatively small voltages applied at the chopper plates, the drift energy had to be reduced from the desired 5600 eV to 5250 eV. However, this leads to an imperfect beam transport intensifying the shadow peak in the spectra. According to the simulations the higher energy would have been necessary to pass also those positron through the chopper aperture which stem from a larger spot size at the re-moderation crystal. Therefore, the situation could not only be enhanced by using a function generator providing a higher amplitude, but also by ensuring a higher quality of the primary beam which enters the SPM interface.

In the chopper spectrum the shadow peak is not observable for following reasons: The aperture, which is made out of stainless steel, had an diameter of 4 mm. It is surrounded by a tungsten block with a 5 mm drill in beam direction. Hence only those positrons appear in the shadow peak which annihilate at the steel sheet. Those which are more than 2.5 mm apart from the center annihilate at the tungsten block and their annihilation radiation is shielded. If the chopper is operated alone most positrons are deflected more than 2.5 mm and only a small amount annihilates at the steel sheet. In the case when the chopper is operated together with the bunchers only a small amount of the beam is deflected because of the pulse structure of the beam. Hence a higher amount annihilates at the steel aperture and becomes detectable. As shown in Fig. 4.41e the chopper is not only able to reduce the background but also a little substructure on the left side of the main peak, which arose due to overbunching (see Sec. 3.6.1). If the chopper is operated together with the bunchers the intensity within the FWHM duration is decreased by only 1 % and thus the peak to background ratio can be doubled again.

With the experimental setup it was possible to demonstrate the background reduction. The background induced by positrons which do not annihilate at the target could not be determined and hence the absolute value of the peak to background ratio is unknown. The largest contribution to this background stems from the positrons which are reflected at the MCP and annihilate at the close surrounding.

The measurements demonstrated that each buncher alone and all components in combination work as desired. Even during the short measurement campaigns it was possible not only to accomplish the demanding beam transport for the first time but also to achieve a timing resolution which is capable for first practice-orientated lifetime mea-

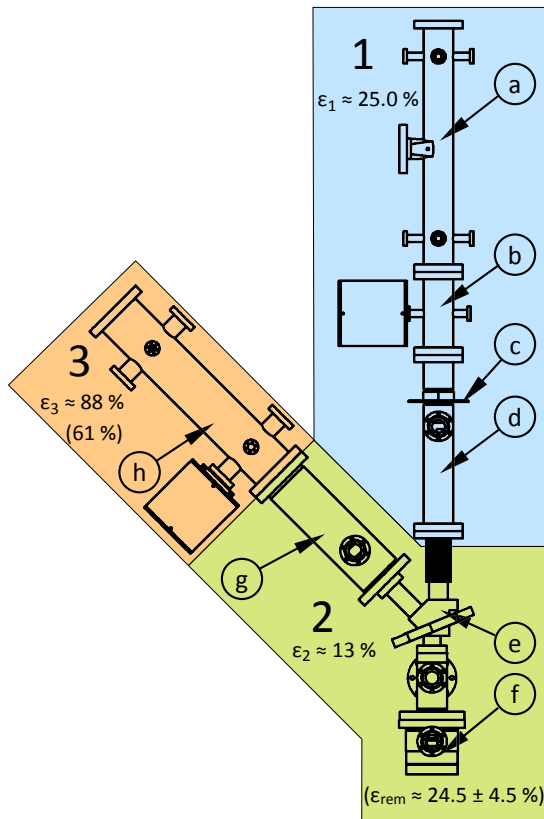


Figure 4.42: The three subsections of the interface for which the transmission efficiency was determined. The large range for the re-moderation efficiency stem from the unknown amount of positrons which are reflected from the re-moderation crystal. Since the transport of the beam behind the re-moderation depends from the spot size of the incident beam at the re-moderation crystal, not only the transmission of the first section would be improved by a brighter primary beam but also the transport through the beam switch and the chopper installations.

- (a) pre-buncher
- (b) 1st sine wave buncher
- (c) magnetic field termination
- (d) pre-accelerator
- (e) beam switch
- (f) re-moderation stage
- (g) linking chamber
- (h) chopper and 2nd sine wave buncher

surements. Also the background reduction afforded by the bunching concept and the chopper work as predicted.

4.2.4.2 Efficiency of the beam transport and the re-moderation.

The efficiency of the beam transport was measured for three subsections of the SPM interface separately (see Fig. 4.42). The first section ranged from the entrance to the end of the accelerator. The second incorporated the transport to the re-moderation crystal, the re-moderation itself, the separation of incident and re-moderated beam and the transport of the re-moderated beam to the beginning of the chopper entrance. The last section covered the transport through the chopper cabinet and the chopper aperture.

The incident beam

Before and after the following measurements had been performed, the intensity and the intensity distribution of the primary beam as provided by the NEPOMUC beam line was determined at the entrance of the interface. This was made with the help of the same MCP setup as used in the case of the NEPOMUC re-moderator. The intensity of the primary beam was during the measurements $3.9 \cdot 10^6 \frac{e^+}{s}$ and hence much less than at former measurement campaigns. This intensity drop was also confirmed at other instruments. The reason for the low intensity was a magnetized mu-metal shielding at the beam line which could not be replaced without extensive works at the NEPOMUC beam line including vacuum breaks. As shown in Fig. 4.43 the damage at the beam line lead to also to an elliptically deformed beam, with a length of the major axis of 9.8 mm (FWHM) and of the minor axis of 6.0 mm (FWHM) (see Fig. 4.44). Hence, not only the intensity was affected by the imperfect beam transport but also the phase space volume occupied by the beam was considerably perturbed. Nevertheless the data gained during this measurement campaign give the most comprehensive overview of the capabilities of the interface and are therefore presented here.

Transmission through the first column

Inside the first column are two constrictions with an open diameter of 7 mm. The first is the gap at the pre-buncher, which is used for the energy modulation, and the second one is the magnetic field termination. Since at both sites the beam is guided by the longitudinal magnetic field they limit the beam only in the real space. Behind the field termination the beam diverges and a further aperture eliminates now only those positrons which are at the boarder of the beam and which have additionally a high transversal momentum directed outwards. By regarding the original properties of the beam provided by the NEPOMUC re-moderator at the constrictions would be no positron loss and at the virtual aperture after the magnetic field termination only the positrons at the outermost regions of the occupied phase space volume would annihilate. Since the size of the beam actually used for the measurements was much larger and extended the open diameter of the constrictions considerably, the loses within the first first column were accordingly high leading to a total transmission of 25.0 %.

The transport within the re-moderation stage

The losses in the second section are dominated by the re-moderation process itself. In addition, there are also two constrictions by which the intensities of the incident and the re-moderated beam might be reduced. Both are located within the beam switch and in direct sight to the moderation crystal. Hence the radiation background at this positions is very high and a deeper analysis of the amount of positrons which annihilate at these points was not possible.

4 Positron beam preparation at NEPOMUC

To the sides the re-moderation crystal is surrounded by a hollow tungsten cylinder in order to keep the radiation exposure and the background for the measurements low. Only two small collinear channels were made additionally into this tungsten block which allow a direct sight onto the crystal from the sides. By observing the annihilation radiation of the positrons at the crystal the re-moderation efficiency can be calculated as follows: If the crystal and the electrodes in front of the crystal are set to a potential, that avoids the escape of re-emitted positrons the detected annihilation radiation C_{att} is proportional to the intensity of the incident beam. If the re-moderation crystal is set onto a slightly repulsive potential in order to guide the re-moderated positrons away as during routine operation, the detected radiation C_{rep} is proportional to the intensity of the incident beam subtracted by the intensity of the re-moderated beam. However, this estimation neglects the amount of reflected positrons which reduce the amount of the detected radiation in both cases. The fraction f of reflected positrons can reach up to 30 % of the incident beam in the case of heavy materials such as tungsten and at beam energies of 5 keV (see Fig. 2.1). Because it is unknown how many of these reflected positrons get actually out of the sight of the detector, only an upper and lower level of the efficiency can be given. The count rates in the detector are hence as follows:

$$\begin{aligned} C_{\text{att}} &\approx (1 - f)I_i \\ C_{\text{rep}} &\approx (1 - f)I_i - I_r \end{aligned} \quad (4.13)$$

By rearranging this equations it follows:

$$\epsilon = \frac{I_r}{I_i} = (1 - f) \frac{C_{\text{att}} - C_{\text{rep}}}{C_{\text{att}}} \quad (4.14)$$

With this equation, the efficiency of the re-moderation process calculates to 24.5 ± 4.5 %. Since the total efficiency of the second section was determined with 13.2 % there have to be some losses at the beam switch.

Positron loss due to the chopper installations

The transmission of the last section is determined by the space between the chopper plates and especially by the diameter of the chopper aperture. During the measurements an aperture with a diameter of 4 mm was used, and it turned out that this is mainly the limiting element for the transmission. If the voltage applied onto the drift tube was varied from 5250 eV to 5650 eV the transmission of the last section could be raised from 60.6 % to 87.9 %.

According to the rules of Gaussian optics the beam diameter over the whole transportation path and hence also after the re-moderations depends in first order linearly

on the diameter of the primary beam¹⁰. Hence if the primary beam gets smaller, e.g. at the level already attained, the transmission efficiency not only of the first column but also of the subsequent sections will raise. Therefore, by an enhancement of the primary beam the transmission of the complete assembly can be raised to a value limited by the re-moderation process and therefore at least to 20 %.

Phase space volume considerations

The phase space volume is reduced by the re-moderation and the resulting volume is determined by the re-emission process and the spot size at the re-moderation crystal. The latter one can be estimated in principle by the rules provided by Gaussian optics and the spot measured with the MCP setup, since the final diameter of this spot is determined mainly by the last lens. However, the beam is cropped at the chopper aperture, and hence not the original spot from the re-moderator is imaged but the aperture. Therefore, the spot size can be only estimated by comparing the experimental results with the simulations.

Because of the large primary beam and hence the large spot size at the re-moderator crystal the second beam transport scenario was used (cp. Fig. 4.36 on p. 106). According to the simulations¹¹, only those positrons, which stem from a spot size with a maximum radius of about 180 μm can be passed lossless through the chopper aperture, and hence the actual spot size has to be slightly larger than this.

The brightness enhancement can be estimated as follows: The maximum transversal energy after the re-moderation is about 0.1 eV, and before this process the maximum value is supposed to be in the same range as the maximum longitudinal energy spread and hence of about 5 eV. In order to regard the elliptical shape of the incident beam, for the calculation of the brightness enhancement the quotient of the maximum areas is used. Thus, the brightness enhancement calculates as follows:

$$\begin{aligned} \frac{B_{\text{rem}}}{B_{\text{inc}}} &= \frac{\pi ab \Delta E_{\perp \text{inc}}}{\pi r^2 \Delta E_{\perp \text{rem}}} \cdot \epsilon_1 \epsilon_2 \epsilon_3 \\ &= \frac{7.4 \text{ mm} \cdot 5.1 \text{ mm} \cdot 5 \text{ eV}}{(0.18 \text{ mm})^2 \cdot 0.1 \text{ eV}} \cdot 0.029 \approx 1680 \end{aligned} \quad (4.15)$$

Unlike as usual, in this equation the maximum dimensions and energy spreads instead of the FWHM values are used. This is necessary because only the maximum width of the spot at the re-moderation crystal can be gained from the simulations. The full transmission of the SPM interface is given by the product of the single efficiencies ϵ_i . If beside the transversal also the longitudinal energy spread is regarded the brightness

¹⁰The linearity is only given if the diameter of the primary beam is not reduced by apertures or constrictions in the first column.

¹¹The Fig. 4.36 shows the positron trajectories, with a 5 mm aperture being shown. This diameter equals the open diameter of the tungsten block, which is used to shield the annihilation radiation.

B^* is enhanced by a factor of roughly 85000.

4.2.4.3 Evaluation of the enhanced beam

The aim of the interface is to provide a beam that enables lifetime measurements at the SPM at least with the same lateral resolution as in the laboratory but within a shorter measurement time. If this aim is attained is not offhand evident by the brightness. For this purpose the intensities and the transversal phase space volumes of the beams provided by the beam preparation column in the laboratory and by the SPM interface have to be compared separately. A measure for the transversal phase space volume is the spot size, which can be attained with the beams at the re-moderator of the SPM (⊗ in Fig. 4.18). Operated with a new and strong 30 mCi ^{22}Na source the beam preparation column provides a beam with less than $5 \cdot 10^5 \frac{e^+}{s}$ and the minimal diameter which can be attained at the SPM re-moderator is about 20 μm .

In the case of the interface the transversal phase space volume can be calculated from the spot size d_1 which was attained with the lens at the exit of the chopper chamber. If aberrations are neglected this diameter calculates as follows:

$$d_1 = 2\sqrt{\frac{E_{\perp 1}}{E_{\parallel 1}} \frac{r_0}{\alpha_1}} \quad (4.16)$$

Where $r_0 = D_0/2$ is the radius of the imaged object, which is in this case the chopper aperture (2 mm), and α_1 is the image side aperture angle. $E_{\perp 1}$ and $E_{\parallel 1}$ are the transversal and longitudinal energies of the beam, respectively. Since the beam is approximately axially parallel in front of the electric lens the object diameter is equal to the lens aperture $D_0 \approx D_1$. This implicates also, that the image distance and focal length are approximately equal and that $\alpha_1 \approx D_1/(2f_1)$ where the focal length was about $f_1 = 70$ mm. By using this Eq. (4.16) can be written:

$$d_1 = 2\sqrt{\frac{E_{\perp 1}}{E_{\parallel 1}} \frac{D_1}{2\alpha_1}} = 2\sqrt{\frac{E_{\perp 1}}{E_{\parallel 1}}} f_1 \quad (4.17)$$

This equation can be rearranged in order to gain an expression for $\sqrt{E_{\perp 1}}$:

$$\sqrt{E_{\perp 1}} = \frac{d_1}{2f_1} \sqrt{E_{\parallel 1}} \quad (4.18)$$

The diameter d_2 of the minimal spot size, which can be attained at the SPM re-moderator, can be written in an analogue form as d_1 .

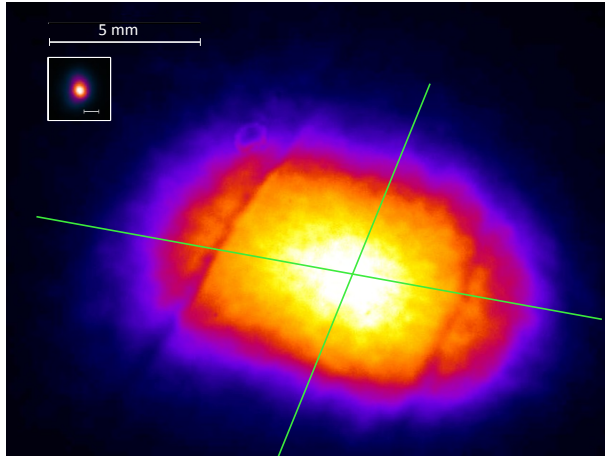


Figure 4.43: Intensity distribution of the primary beam recorded at the entrance of the SPM interface. Due to magnetized mu-metal shielding at the beam line the beam was considerably perturbed resulting in an elliptically deformed and enlarged intensity distribution. The lengths of the axes of the ellipse were determined by plotting the intensity profiles along the green lines (see Fig. 4.44). The two darker, nearly parallel lines at the borders of the distribution are imperfections in the MCP and not of interest. The insert shows the intensity distribution of the positron beam after being enhanced by the SPM interface at the same scale.

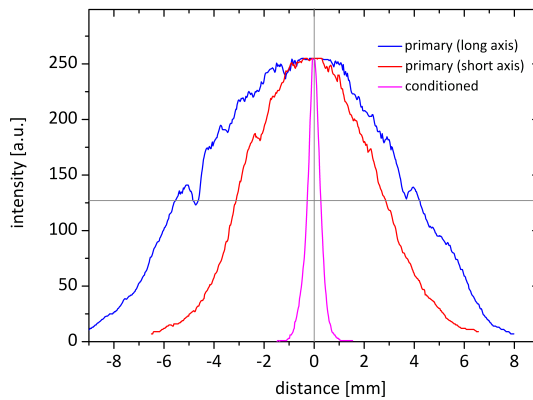


Figure 4.44: Intensity profiles of the positron beam recorded at the entrance of the interface and at the exit of the chopper chamber. The profiles of the primary beam have a width of to 9.8 mm and 6.0 mm (FWHM), respectively. The two fold re-moderated and focused beam has a diameter of about 540 μm (see Fig. 4.45).

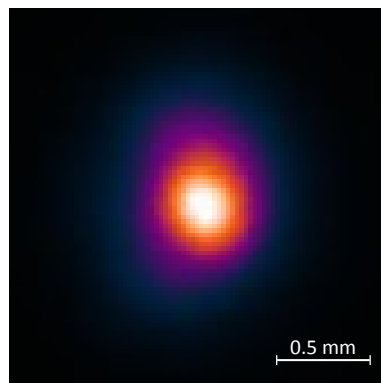


Figure 4.45: Intensity distribution of the conditioned beam recorded at the exit of the chopper chamber. The beam was focused with the help of the electrical lens at the end of the chopper chamber.

$$d_2 = 2\sqrt{\frac{E_{\perp 2}}{E_{\parallel 2}}} f_2 \quad (4.19)$$

The expressions $\sqrt{E_{\perp 1}}D_1$ and $\sqrt{E_{\perp 2}}D_2$, which occur in these equations, are the square roots of the phase space volume occupied by the beam and are thus constant and equal. This identity can be rearranged to $\sqrt{E_{\perp 2}} = \sqrt{E_{\perp 1}}\frac{D_1}{D_2}$ and together with Eq. (4.18) inserted in Eq. (4.19):

$$d_2 = 2\sqrt{\frac{E_{\perp 1}}{E_{\parallel 2}}\frac{D_1}{D_2}} f_2 = \sqrt{\frac{E_{\parallel 1}}{E_{\parallel 2}}\frac{D_1}{D_2}\frac{f_2}{f_1}} d_1 \quad (4.20)$$

With this equation the geometric diameter d_2 of the beam at the SPM re-moderator can be calculated in dependence of the lens aperture D_2 of the re-moderation lens, where the longitudinal energies are $E_{\parallel 1} = 800$ eV and $E_{\parallel 2} = 5$ keV, respectively. In order to calculate the total diameter the aberrations of the re-moderator lens have to be regarded. According to Eq. (3.37) and with the identity $\alpha_2 = D_2/(2f_2)$ the blur due to the spherical aberration can be written as follows:

$$d_s = 2r_s = \frac{1}{2}C_s \left(\frac{D_2}{2f_2}\right)^3 \quad (4.21)$$

From Eq. (3.38) and the same identity as above, it follows for the blur due to the chromatic aberration:

$$d_c = 2r_c = C_c \frac{\Delta E_{\parallel 2}}{E_{\parallel 2}} \frac{D_2}{f_2} \quad (4.22)$$

The focal length of the SPM re-moderator is $f_2 = 13.8$ mm and the aberration coefficient are $C_s = 2.77$ mm and $C_c = 6.16$ mm, respectively [15]. The longitudinal energy spread $\Delta E_{\parallel 2}$ depends on the time spread of the pulses in front of the second sine wave buncher because as larger the interval as higher has the modulating energy to be. Even by regarding a temporal spread of about 500 ps this would lead—according to Eq. (3.53)—to an energy spread of only about 15 eV. Since the aberrations are proportional and the geometric diameter inverse proportional to the lens aperture D_2 , there is an optimal value for the lens aperture of the re-moderator lens. In Fig. 4.46 the total diameter $d_{tot} = \sqrt{d_2^2 + d_s^2 + d_c^2}$ is plotted, and accordingly the spot size gets a value of about 27 μm at a lens aperture of 5.7 mm. Since it was neglected, that the recorded spot size d_1 at the end of the chopper chamber was enlarged due to aberrations, $E_{\perp 1}$ was overestimated and thus the calculated spot size is an upper limit. Nevertheless, by regarding the enormous dimensions of the primary beam at the entrance of the interface it was to expect that not the desired diameter of less than 20 μm can be attained.

If the high brightness of the re-moderated beam is conserved during the transport through the beam line to the interface the situation becomes very different. If the re-moderated beam is guided in such away, that its maximum diameter is 5 mm at the entrance of the SPM the geometrical diameter will decrease by a factor 5/7, since the incoming beam was trimmed to the open diameters of the pre-buncher gap and at the magnetic field termination, which are both 7 mm. Hence, the total diameter would be reduced to 19 μm (see Fig. 4.47). A further reduction can be attained if additionally the transversal energy spread is kept low by avoiding non-adiabatic beam transport. For instance, if the transversal energy spread is below a maximum of ± 1 eV the spot size at the re-moderator of the interface is roughly reduced by a factor of three (cp. Fig. 4.34). This entails that the geometrical diameter at the SPM re-moderator is reduced by this factor as well and that the total diameter becomes below 10 μm .

It can be concluded, that the SPM might attain the same resolution as in the laboratory even if operated with the heavily deformed beam. But it is obvious, that an enhanced transport of the primary beam is necessary and will lead to a higher resolution.

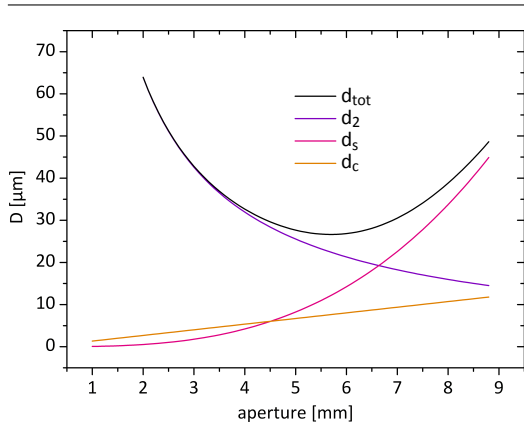


Figure 4.46: The total beam diameter d_{tot} as attainable at the crystal of the SPM re-moderator and the single contributions: the geometrical diameter d_2 , and the spherical and chromatic aberrations d_s and d_c .

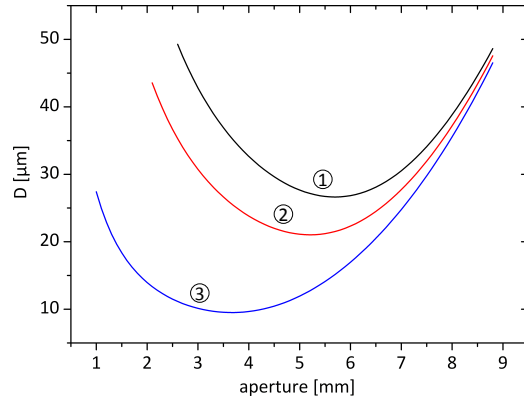


Figure 4.47: By an adiabatic beam transport, the attained spot size ① can be improve considerably. ②: Primary beam with a diameter of 5 mm and a transversal energy spread > 4 eV. ③: Primary beam with a diameter of 5 mm and a transversal energy spread ≤ 2 eV.

The re-moderator provide a beam with an intensity of up to $6.0 \cdot 10^7 \frac{e^+}{s}$ and at the beam port on which the interface is connected a beam intensity of $2 \cdot 10^7 \frac{e^+}{s}$ was already attained. With this intensities and the attained transmission of the interface the intensity of the conditioned beam would be between $6 \cdot 10^5 \frac{e^+}{s}$ and $1.8 \cdot 10^6$, and thus up to a factor of 3.6 more intense than the beam provided by the beam preparation section in the laboratory. The low transmission of the interface of about 3 % was caused by the perturbed beam and the fact that most of it annihilated already within

4 Positron beam preparation at NEPOMUC

the first column. Hence, the situation can be improved enormously by an accurate beam transport. Supposing that the losses within the first column can be reduced from 75 % to e.g. 10 % the intensity of the conditioned beam would raise by a factor of 3.6. As stated above, by a primary beam occupying a smaller phase space volume not only the transmission in the first column but also in the subsequent stages would be increased. Hence the transmission at the re-moderation stage is limited only by the re-moderation process itself to a value between the determined limits. By supposing a re-moderation efficiency of 24 % and a transmission of 95 % through the subsequent parts of the interface the total transmission will raise to about 20 %. Thus, the intensity of the conditioned beam will attain a value between $4 \cdot 10^6$ and $1.2 \cdot 10^7 \frac{e^+}{s}$. With this intensity a typical SPM measurement can be accomplished during one day instead of weeks.

5 First positron annihilation measurements at UMo

5.1 Overview and sample preparation

As a possible subject for measurements with the SPM an uranium molybdenum alloy embedded in an aluminum matrix has attracted attention. Today the nuclear fuel of the FRM II is a high-enriched uranium silicide and there are endeavors to replace this fuel by a medium enriched one. In order to do this and to keep up the concept of a single and compact core, which provides several advantages, the density of the fuel has to be increased. Since UMo has a high density it became a candidate to replace the uranium silicide not only at the FRM II. Because the new fuel has to be sealed within an aluminum cladding in the same way as the present fuel, UMo powder is dispersed in an aluminum matrix. The aluminum matrix ensures that the fuel and the cladding stick reliably together and heat transfer from the UMo particles to the surrounding during the operation in a reactor core. However, due to the irradiation during operation a large interdiffusion layer can be appear, which lead to an anomalous swelling and hence to the damage of the sealing [118]. In [118] it was shown, that this interdiffusion region can be generated not only by in-pile irradiation which leads also to a high activation of the uranium specimens but also by irradiating the sample with high energetic heavy ions provided by an accelerator. By this out-of-pile irradiation the heavy ions simulate the affect of the high energetic fission products. Since the specimens treated by this method are not activated it becomes possible to examine them by positron annihilation techniques.

In order to explore the potential of positrons as a tool to investigate the damage induced by this irradiation, preliminary measurements were made. For these very first experiments a pure UMo sample without the aluminum matrix was available¹. According to the distribution and energies of the nuclides generated by the fission of uranium the specimens were irradiated with ^{127}I with an energy of 70 MeV and a dose of $1 \cdot 10^{17}$ ions per cm^2 . Before the irradiation, the surface of the samples was ground and polished in order to remove the surface layer. After this procedure as well after the irradiation and the positron measurements the specimen was kept under vacuum conditions to avoid the formation of an oxide layer.

¹The specimen was kindly made available by Rainer Jungwirth who performed also the preparation and irradiation.

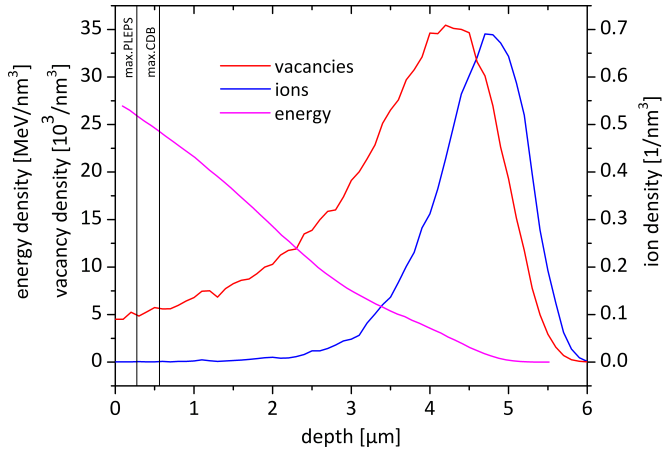


Figure 5.1: The distribution of the vacancies and the ^{127}I projectiles within the UMo target. Within the maximum depth which could be attained by the positron beam systems CDB and PLEPS the defect concentration is approximately constant and the concentration of iodine ions, which might perturb the positron annihilation measurements, is negligible. The third curve shows the energy input due to the irradiation. The implantation energy was 70 MeV and all distributions are normalized to a irradiation dose of $1 \cdot 10^{17}$ Ions per cm^2 .

Within the present work, the damage and the distribution of the projectiles in the UMo target were simulated with the help of the established TRIM-code². As shown in Fig. 5.1 the main damage and the peak of the stop distribution are much deeper than the maximum depth which can be examined with the positron beams provided by the CDB and PLEPS spectrometer³. For the first experiments this circumstance is of advantage, because hence it is ensured that the defect concentration is over the entire examination depth approximately constant and there is no iodine, which might perturb the positron measurements. According to the simulations even in low depths, where the positron measurements are performed, are by far as much vacancies, that a considerable amount of the positrons is trapped by these defects before they annihilate.

5.2 Positron annihilation measurements

The CDB-spectrometer at the NEPOMUC positron facility enables the lateral and depth resolved measurement of the S-parameter, whereby the implantation energy can be set variably up to a maximum of 30 keV. In order to determine the actual size and the homogeneity of the irradiated spot a spatially resolved measurement was performed first. As shown in Fig. 5.2 the irradiation gives a high contrast to the non-irradiated area of the specimen and a sub-structure within the irradiated area can be observed. The irradiated spot is elliptically shaped, has an extension of about 1.8 times 3 mm

²TRIM: transport of ions in matter

³There are no parameters for the mean stopping depth of positrons in uranium available. But since this depth is mainly dependent from the density, the fitting parameters of gold together with the density of the UMo sample were used in order to estimate the mean implantation depth in dependence of the implantation energy (see also Sec. 2.2).

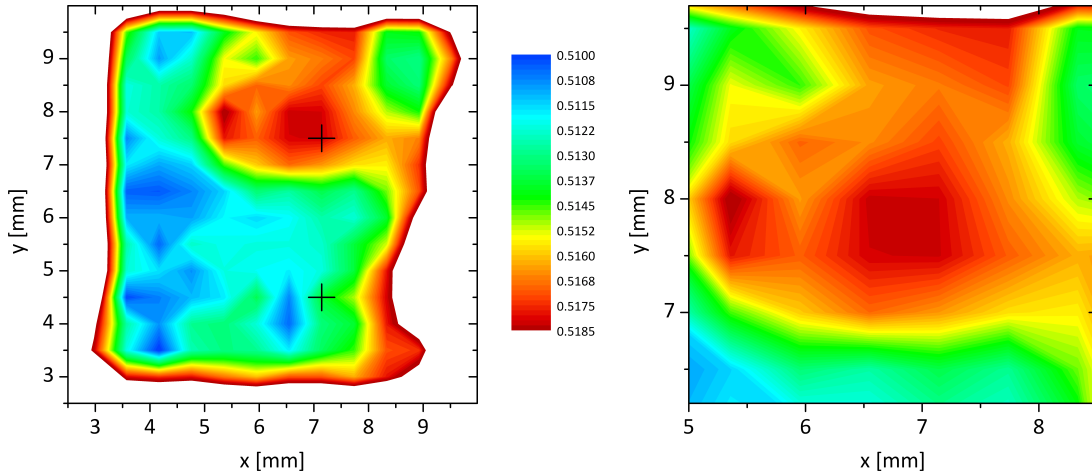


Figure 5.2: Two dimensional S-parameter scan over the irradiated UMo specimen at a positron energy of 25 keV. The irradiated spot (red) is clearly observable at the boarder of the specimen. It is elliptically shaped and shows a substructure. The two crosses indicate the positions at which the depth resolved S-parameter measurements were made.

and is located at the boarder of the specimen.

Since the irradiated and non-irradiated sites could be distinguished clearly, depth resolved measurements of the S-parameter at both sites were made. Such a measurement was also performed at a as-received specimen. This measurement was made for two reasons: First, knowing the S-parameter for the surface layer it can be proofed that there was no regrown layer at the polished specimen, and second it was contemplated to ascertain the thickness of this layer. As shown in Fig. 5.3 the S-parameter of the as-received sample keeps constant from 90 nm to the maximum depth of 561 nm and hence the surface layer has to be thicker than this maximum value. The drop at the lower energies indicates the back diffusion to the surface of the positrons. The lower the implantation energy and hence the closer the positrons are implanted to the surface the larger gets the amount of positrons diffusing back to the surface. Therefore, the S-parameter turns from the bulk value to the surface value continuously. Hence, from this curve the typical diffusion length in the surface layer can be derived to be about 90 nm.

The two other curves in Fig. 5.3 show the S-parameter in dependence of the implantation energy at an irradiated and a non-irradiated position at the polished specimen. A higher defect density causes a higher S-parameter. This is clearly observable especially at larger depths, when the measured S-parameter is not influenced by the surface or other layers. Starting at a depth of about 60 nm the S-parameter measured at the non-irradiated region gets higher toward the surface and the continuous trend indicates that there is no or at least a very thin surface layer. At the irradiated position

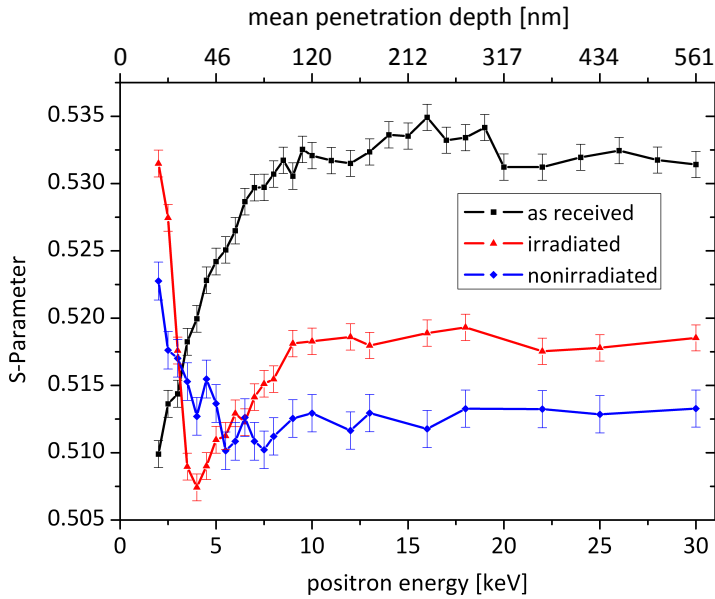


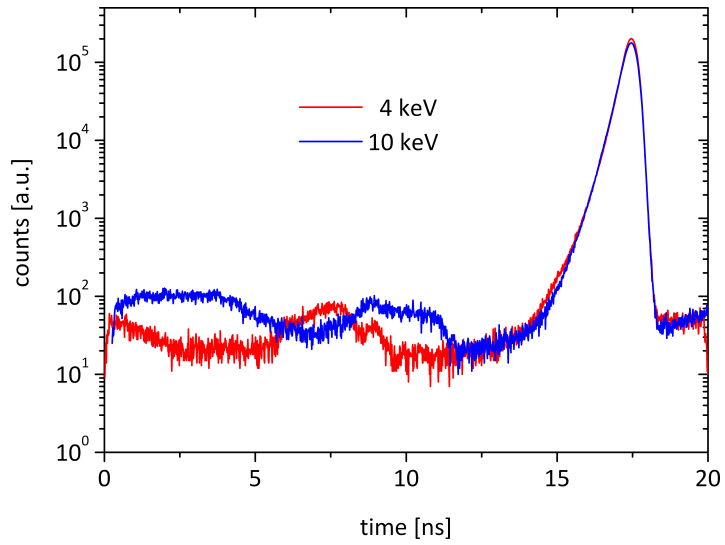
Figure 5.3: The S-parameter in dependence of the positron beam energy. Within the bulk the different specimens can be distinguished very clearly. The different characteristic of the irradiated and non-irradiated specimen at lower energies can be explained by an intermediate layer below the surface of the irradiated specimen.

the situation is different. Beginning at a depth of roughly 100 nm the S-parameter gets first lower and raises than toward the surface. A reasonable explanation for the drop of the S-parameter even below the value measured in the non-irradiated bulk is that the energy impact by the irradiation lead to an annealing or phase transition. Since the backside of the solid was cooled but the main energy loss of the ions occur at the front side such a local heating might be possible and lead to local annealing or phase transition (see Fig. 5.1). Such an intermediate layer would also explain the relatively flat rise between 4 and 9 keV. At the surface near region the slope of the irradiated curve is steeper than that of the non-irradiated curve. This might be explained by a longer diffusion length within the near surface region, what would support the assumption that there is a layer which was modified by the irradiation.

The S-parameter measurements provide information about the homogeneity and actual size of the irradiated area. Moreover, the depth resolved measurements of the S-parameter provide a *finger print* of the influence of the irradiation onto the positron in dependence of the implantation energy. Nevertheless, for a deeper understanding of the irradiation induced defect types, positron lifetime measurements are necessary.

In the case of the irradiated UMo, there are two challenges which have to be accomplished to gain meaningful lifetime measurements. The first arise by the high density and the high Z of the alloy. Both lead to a high amount of reflected positrons which create shadow peaks and also increase the continuous background in the lifetime spectra. The lifetime spectrometer PLEPS offers besides an excellent time resolution an outstanding high peak to background ratio of up to $1:10^4$. This performance is

Figure 5.4: Two exemplary positron lifetime spectra of UMo recorded at the PLEPS spectrometer with two different positron energies. Due to the reflected positrons the peak to background ratio gets lower whereby the position and intensity of the shadow peaks is dependent from the energy of the incident positrons. Nevertheless, in these spectra two different lifetimes can be identified with even by eye.



also achieved due to the high efforts to suppress the signal induced by the reflected positrons. Nevertheless, the UMo lifetime spectra show strong perturbations and hence the analyses of the measured spectra becomes more difficult and have to be made very thorough (see Fig. 5.4).

The second difficulty arises by the small and inhomogeneous irradiated spot. The position of the positron beam of the PLEPS at the specimen varies in dependence of the beam energy within an area with a diameter of about 4 mm⁴. Hence, it has to be checked if the PLEPS positron beam had really hit the irradiated region. If so, the energy dependence of the mean lifetime must have the same characteristic as the energy dependent S-parameter measurement at the irradiated site of the specimen (see Fig. 5.5). The comparison of the lifetime and the S-parameter shows a similar characteristic over a wide range. However, the lifetime curve is not as smooth as that one of the S-parameter especially at low energies, the valley which the S-parameter curve shows at 4 keV is shifted to 5 keV and the rise after this minimum is in the case of the lifetime curve much flatter. The greatest discrepancy, however, show the curves at energies above 14 keV. Since the distribution of the implantation depth becomes very broad at high energies and hence the lifetimes are averaged over a wide range such sudden changes are only explainable by a shift of the positron beam away from the irradiated spot. Energy dependent beam shifts might also elucidate the irregular distribution of the mean lifetime at the lower energies and the lower rise after the minimum. If the positron beam hits the irradiated area only partly the mean lifetime is averaged over the mean lifetimes of the irradiated and non-irradiated regions.

⁴The common specimen size used at PLEPS is about 8 × 8 mm

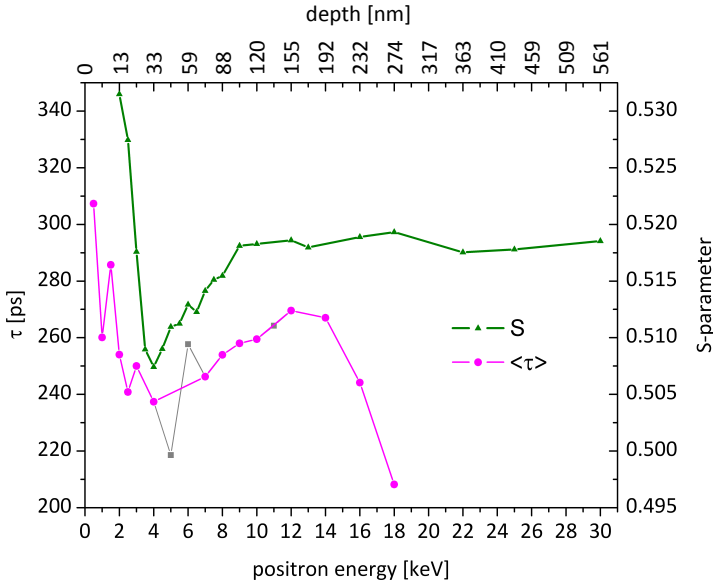
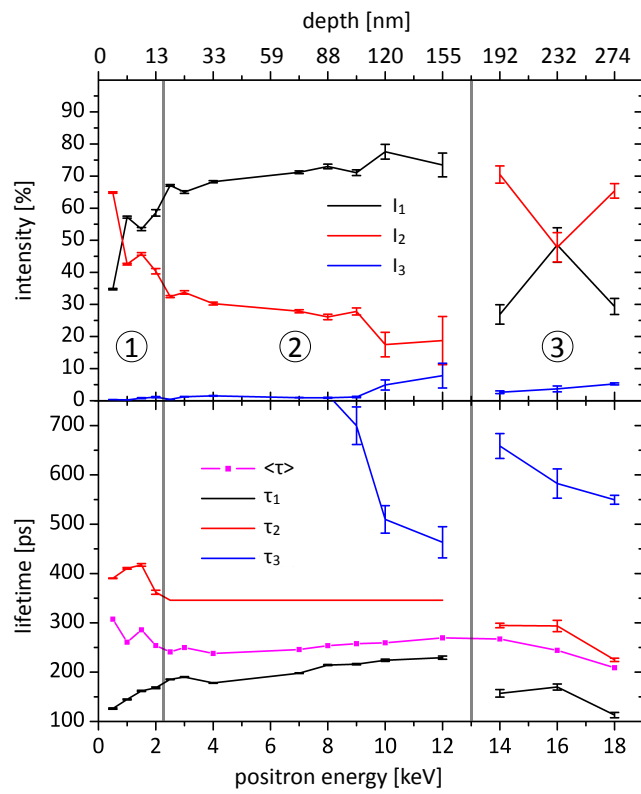


Figure 5.5: By comparing the energy dependence of the S-parameter and the mean lifetime it can be determined at which energies the beam of the PLEPS did not hit the irradiated region entirely. The curves show the same characteristics up to an energy of about 12 keV. Above this energy the curves diverge what is explained by a shift of the PLEPS beam away from the irradiated spot. The lifetime spectra at 5, 6 and 11 keV were decomposed into single lifetimes, since they do not follow the energy characteristic and/or a statistical correct decomposition was not possible.

The best decomposition of the mean lifetime was possible by separating the whole measured energy range into a surface region (0.5 – 2 keV), a region in which the damage from the irradiation gets more and more visible with higher positron energy (2.5 – 12 keV) and the energy range where the beam swept away from the irradiated spot (14 – 18 keV). The lifetime spectra at 5, 6 and 11 keV were not decomposed into single lifetimes, since they do not follow the energy characteristic and/or a statistical correct decomposition was not possible. Within all ranges the decomposition was made into three lifetimes and in the second range the constraint of an arbitrary but over the regarded energy range constant second lifetime was predefined (see Fig. 5.6).

The decomposed lifetimes in the third energy range are lower as in the second due to the averaging over irradiated and non-irradiated areas. Since the ratio of irradiated and non-irradiated area, observed with the positron beam changed with the implantation energy, there are considerably jumps in the lifetimes and intensities. Since these ratios are unknown, in the following only the first two energy regions are discussed. In the second energy range, the first lifetime τ_1 is between of 180 and 230 ps and the second τ_2 was fitted to 346 ps. Positron lifetimes in a pure uranium specimen in the γ -phase were in [119] measured. This lifetime spectra, were decomposed into two lifetimes τ_1^U and τ_2^U . The longer lifetime τ_2^U was in the range of 220 to 235 ps and was attributed to the annihilation in vacancies. Moreover, two more lifetimes τ_b^U and τ_{def}^U were calculated with the help of the trapping model. This lifetimes were attributed to the bulk lifetime and the lifetime of positrons trapped at grain boundaries, respectively. The first was in the range of 170 to 185 ps and the second was between 185 and 205 ps. The comparison of these lifetimes with the lifetimes measured in the present work,

Figure 5.6: The three positron lifetime components and their intensities gained from the fits of the measured lifetime spectra. To obtain reasonable fits over the whole energy range, it had to be separated in three parts.



5 First positron annihilation measurements at UMo

stimulates the assumption that τ_1 is a composition of the lifetimes of positrons trapped at grain boundaries and at vacancies. Since the second lifetime τ_2 is considerably longer as the lifetime assigned to positrons trapped in vacancies it has to be induced by larger open volume defects as i.e. small vacancy clusters. Due to the heavy radiation dose which was applied even larger defects might be possible and hence the third lifetime at the energy range from 9 to 12 keV might be assigned to such defects. The characteristic of the intensity I_3 would sustain this assumption but the large error bars of I_3 and I_2 as well as the rapid change of τ_3 suggests that this is an artifact of the decomposition. In the first energy range, the crossing of the intensities I_1 and I_2 is observable. This is typical and indicates the back diffusion of the positrons to the surface.

5.3 Summary and outlook for the UMo examinations

In the irradiated UMo sample single vacancies and vacancy clusters were observed with the help of positron lifetime measurements. Beside this very first results it is much more important to derive from these measurements the demands on further experiments allowing a more comprehensive understanding of the damage caused by the irradiation not only of the homogeneous UMo alloy but also of the dispersion within the aluminum matrix. Most important, the irradiation should provide a homogeneous and sufficient large spot with a diameter of about 6 mm at least. The small spot size of the available specimen was mainly caused by the request to attain the high dose, which is comparable to that one attained with an in-pile irradiation. Since for first positron measurements a much lower dose is sufficient a larger spot size should be feasible e.g. by wobbling the ion beam over the specimen. For the decomposition of a positron lifetime depth profile it is crucial to know the basic lifetimes e.g. the bulk lifetime, the surface lifetime, and/or the lifetime induced by single vacancies. Therefore, a series of samples which have been irradiated with different doses and a specimen which contains no defects are needed. In an advanced stadium of the examination specimens which were irradiated with the full dose are necessary. Because of the small spot size this samples have to be explored with the help of a focused positron beam e.g. provided by the SPM or the SPM interface. Moreover, a microbeam offers the possibility to enhance the depth resolution and the maximum attainable depth by scanning over a wedge cut. For all preparation processes before, during and after the irradiation it has to be ensured that the samples are not modified in an unintended way. This can be made by varying the preparation methods e.g. by using different dose rates during the irradiation and using different polishing methods. In addition, however, the properties of the specimen have to be checked also by contrary measurement methods. E.g. the phase of the different treated specimens can be determined by X-ray diffraction and the surface can be examined e.g. by Auger electron spectroscopy.

Lifetime measurements with the PLEPS and the SPM at such a series of well prepared specimens would give information about the defect types induced by a specific irra-

5.3 Summary and outlook for the UMo examinations

diation dose and are the basis for further lifetime examinations of e.g. samples with different ratios of the alloying constituents or for lateral resolved measurements with the SPM at UMo dispersions within an aluminum matrix. In addition, the CDB spectrometer can be used for a deeper examination of the chemical vicinity of the defects created in the UMo specimens.

6 Conclusion and outlook

Both, the NEPOMUC re-moderator and the SPM interface were set into operation successfully, and their excellent performance was demonstrated in the experiments and by supplementary trajectory simulations. In addition, first positron annihilation measurements of an ion irradiated UMo alloy were accomplished. The irradiation with ^{127}I created open volume defects and led therefore, to a change in the S-parameter. Thus, the irradiated spot could be clearly identified by spatially resolved Doppler broadening measurements and a substructure became observable. Furthermore, two different defect types were observed by measuring the positron lifetime at the newly implemented PLEPS. The short positron lifetime τ_1 was ascribed to single vacancies and the longer lifetime τ_2 to small vacancy clusters.

The NEPOMUC re-moderator provides a beam with a diameter of less than 2 mm (FWHM), a longitudinal as well as transversal energy spread of less than 2.5 eV (FWHM) and an intensity of up to $6 \cdot 10^7 \frac{e^+}{s}$. The kinetic energy of the re-moderated beam is 20 eV during routine operation. However, beams with higher energies of up to 200 eV can be created with similar beam characteristics, as well. The primary beam of NEPOMUC has a diameter of more than 7 mm (FWHM), an energy spread of 50 eV (FWHM) and an intensity of $9 \cdot 10^8 \frac{e^+}{s}$. The NEPOMUC re-moderator enhances the brightness of the primary beam by a factor of more than 16. This enhancement mainly stems from the reduction of the broad transversal momentum distribution. Although this broad energy distribution makes the reduction of the diameter very challenging, a factor of nearly 4 was attained. Considering also the longitudinal energy spreads of the incident and re-moderated beam, the phase space density is enhanced by a factor of more than 300. Due to the combination of the long focal electric transport lens at the entrance of the re-moderation stage, and the short focal magnetic probe forming lens at the re-moderation crystal, the total efficiency of the re-moderation setup reaches $6.55 \pm 0.25 \%$, which is the highest value attained at a high intense positron source world wide. Due to this improved beam quality it was not only possible to enhance the performance of the existing spectrometers PAES and CDB, but it allowed also the implementation of the PLEPS and the SPM interface at NEPOMUC.

The newly installed buncher devices of the SPM interface convert the continuous beam of the NEPOMUC re-moderator into a pulsed positron beam with a high performance. The pre-buncher and the first sine wave buncher are able to compress 56 % of the continuous beam into a time frame of 2 ns with an repetition rate of 50 MHz. This duration is short enough to be compressed basically aberration-free to sharp time

6 Conclusion and outlook

pulses by the second sine wave buncher. To enable the aberration free bunching, a re-moderation stage is placed between the first and second buncher. The efficiency of the re-moderation process at this stage amounts to 24.5 ± 4.5 %. It was demonstrated, that with the beam provided by this re-moderator, it will be feasible to perform high resolved lifetime measurements at the SPM with a lateral resolution in the micrometer range.

However, to attain a spatial resolution below $1 \mu\text{m}$, the transport of the beam from the NEPOMUC re-moderator to the SPM interface has to be improved. Shortly behind the NEPOMUC re-moderator the diameter of the beam is less than 5 mm (FWTM) but it was heavily perturbed during the transport to the SPM interface, resulting in an elliptically shaped beam with an extension of $14.8 \times 10.2 \text{ mm}^2$. Furthermore, a certain amount of the longitudinal energy spread of 5 eV is also induced by the imperfect beam transport. It was shown, by conserving the diameter of the re-moderated beam during the beam transport, the attainable resolution will be better as at the laboratory. The trajectory simulations of the incident beam revealed, if an entirely adiabatic beam transport is ensured and hence the maximal transversal energy spread of the incident beam is reduced to 2 eV a resolution well below $1 \mu\text{m}$ can be attained. A new beam line, which is carefully designed with respect of an adiabatic beam transport, is already under construction and will provide the full performance of the beam created by the NEPOMUC re-moderator at the entrance of the SPM interface.

In addition, the enhanced beam transport will ensure the high counting rates at the SPM, which were the decisive reasons for the implementation of the SPM at NEPOMUC. It was shown that a reduction of the measurement time by a factor of at least 24 is possible. By this intensity, the timescale for a comprehensive examination of three-dimensional defect structures will no longer be month but days. Thus the microscopic resolved positron lifetime measurement will become a standard tool for a wide range of defect studies.

Acknowledgment

This work would not be existent and probably I would not even be engaged in positron physics without Dr. Christoph Hugenschmidt, who attracted my attention to positrons. As head of the positron group he provides a working atmosphere, which is not only characterized by a high scientific demand but is also pleasant and motivating.

I have to thank Dr. Gottfried Kögel, whose continual striving for an even more enhanced positron lifetime spectrometer peaked in the SPM and thus in the design ideas of the SPM interface, as well. His enormous experience and his support especially during the exhausting measurement campaigns helped me to implement the NEPOMUC re-moderator and the SPM interface successfully.

I wish to thank Prof. Dr. Klaus Schreckenbach for a lot of valuable remarks and his support especially at the last steps of this work. Also Prof. Dr. Günther Dollinger provided me support and financed the project. Special thanks go to him for the few little pushes he gave me to bring me on. I have to thank Prof. Dr. Winfried Petry, who saw the potential of the SPM and gave me financial support during the whole time.

Accomplishing a work successfully *and* with pleasure needs the right colleagues. During the whole time I enjoyed being a part of the positron group at the FRM II and thus I have to thank all former, actual and *nearly* members of the group: Thomas Brunner, Katrin Buchner, Hubert Ceeh, Karin Hain, Stefan Legl, Benjamin Löwe, Jakob Mayer, Philip Pikart, Florin and Reinhard Repper, Markus Reiner, Dr. Martin Stadlbauer, Christian Steyer and Alexander Wolf. Thank you all for the countless interesting discussions and for the funny moments we had!

During the first two years, the people of the LRT 2 at the university of the federal armed forces in Munich provided me an enjoyable place to work. I thank Christoph Greubel and Volker Hable for sharing the office with a positron guy as well as Dr. Andreas Bergmaier, Dr. Patrick Reichart, and Dr. Peter Sperr for sharing not only their scientific experience with me. A special thank goes to Dr. Werner Egger, who introduced me into the scientific world as well as the *Beschaffungswesen* of the UniBw and who always had the time for an interesting talk about physics in a broader sense.

It would not have been possible to assemble neither the NEPOMUC re-moderator nor the SPM interface, if there have not been the extensive support of several workshops on the campus. Representative for all the *invisible hands*, who participated in the machining of the numerous parts, I thank the supervisors of the workshops: Mr. Christian

6 Conclusion and outlook

Herzog (FRM II workshop), Mr. Manfred Pfaller (central workshop of the department of physics) and Mr. Uli Ebner (workshop of the department of medical engineering). Also for machining and technical support I wish to thank Mr. Wolfgang Engl and Mr. Peter Wiczorek at the LRT 2.

A very special thank goes to my parents, who gave me the opportunity to study physics and finally to accomplish this work. Thank you for your manifold support not only for this work.

The greatest thank I owe to my beloved wife Alexandra, who gave and still gives me so much encouragement! Thank you, that you gave me the enormous latitude for this work, that you have been there when I needed you and that you gave our wonderful children Marlene and Jakob their lives.

Bibliography

- [1] R. N. West. Positron studies of condensed matter. *Adv. Phys.*, 22(3):263–383, 1973.
- [2] Peter J. Schultz and K. G. Lynn. Interaction of positron beams with surfaces, thin films, and interfaces. *Rev. Mod. Phys.*, 60(3):701–779, Jul 1988.
- [3] M. J. Puska and R. M. Nieminen. Theory of positrons in solids and on solid surfaces. *Rev. Mod. Phys.*, 66(3):841–897, Jul 1994.
- [4] Paul Coleman, editor. *Positron Beams and their applications*. World Scientific Publishing Co. Pte. Ltd., 2000.
- [5] R. Krause-Rehberg and H. S. Leipner. *Positron annihilation in semiconductors: defect studies*. Springer, Berlin, Heidelberg, New York, 1999.
- [6] A. David, G. Kögel, P. Sperr, and W. Triftshäuser. Lifetime measurements with a scanning positron microscope. *Phys. Rev. Lett.*, 87(6):067402, Jul 2001.
- [7] W. Triftshäuser, G. Kögel, P. Sperr, D. T. Britton, K. Uhlmann, and P. Willutzki. A scanning positron microscope for defect analysis in materials science. *Nucl. Instr. Meth. B*, 130(1-4):264–269, July 1997.
- [8] K. Uhlmann, W. Triftshäuser, G. Kögel, P. Sperr, D. T. Britton, A. Zecca, R. S. Brusa, and G. Karwasz. A concept of a scanning positron microscope. *Fresenius J. Anal. Chem.*, 353(5):594–597, January 1995.
- [9] W. Egger, G. Kögel, P. Sperr, W. Triftshäuser, S. Rödling, J. Bär, and H. J. Gudladt. Vacancy clusters close to a fatigue crack observed with the München scanning positron microscope. *Appl. Surf. Sci.*, 194(1-4):214–217, June 2002.
- [10] W. Egger, G. Kögel, P. Sperr, W. Triftshäuser, J. Bär, S. Rödling, and H. J. Gudladt. Measurements of defect structures of a cyclically deformed Al-Mg-Si alloy by positron annihilation techniques. *Mater. Sci. Eng. A*, 387-389:317–320, December 2004.
- [11] R. Krause-Rehberg, F. Börner, F. Redmann, W. Egger, G. Kögel, P. Sperr, and W. Triftshäuser. Improved defect profiling with slow positrons. *Appl. Surf. Sci.*, 194(1-4):210–213, June 2002.

Bibliography

- [12] C. Hugenschmidt, B. Löwe, J. Mayer, C. Piochacz, P. Pikart, R. Repper, M. Stadlbauer, and K. Schreckenbach. Unprecedented intensity of a low-energy positron beam. *Nucl. Instr. Meth. A*, 593(3):616 – 618, 2008.
- [13] A. P. Mills. Brightness enhancement of slow positron beams. *Appl. Phys.*, 23:189–191, October 1980.
- [14] W. E. Frieze, D. W. Gidley, and K. G. Lynn. Positron-beam-brightness enhancement: Low-energy positron diffraction and other applications. *Phys. Rev. B*, 31(9):5628–5633, May 1985.
- [15] D. T. Britton, K. Uhlmann, and G. Kögel. Magnetic positron optics. *Appl. Surf. Sci.*, 85:158 – 164, 1995.
- [16] Nagayasu Oshima, Ryoichi Suzuki, Toshiyuki Ohdaira, Atsushi Kinomura, Takamitsu Narumi, Akira Uedono, and Masanori Fujinami. Brightness enhancement method for a high-intensity positron beam produced by an electron accelerator. *J. Appl. Phys.*, 103(9):094916, 2008.
- [17] D. Schödlbauer, P. Sperr, G. Kögel, and W. Triftshäuser. A pulsing system for low energy positrons. *Nucl. Instr. Meth. B*, 34(2):258 – 268, 1988.
- [18] P Willutzki, J Störmer, G Kögel, P Sperr, D T Britton, R Steindl, and W Triftshäuser. An improved pulsed low-energy positron system. *Meas. Sci. Technol.*, 5(5):548–554, 1994.
- [19] P. Sperr, G. Kögel, P. Willutzki, and W. Triftshäuser. Pulsing of low energy positron beams. *Appl. Surf. Sci.*, 116:78 – 81, 1997.
- [20] P. A. M. Dirac. A theory of electrons and protons. *Proceedings of the Royal Society of London. Series A, Containing Papers of a Mathematical and Physical Character*, 126(801):360–365, 1930.
- [21] Carl D. Anderson. Energies of cosmic-ray particles. *Phys. Rev.*, 41(4):405–421, Aug 1932.
- [22] Carl D. Anderson. Cosmic-ray positive and negative electrons. *Phys. Rev.*, 44(5):406–416, Sep 1933.
- [23] A. Ore and J. L. Powell. Three-photon annihilation of an electron-positron pair. *Phys. Rev.*, 75(11):1696–1699, Jun 1949.
- [24] Peter J. Mohr, Barry N. Taylor, and David B. Newell. CODATA recommended values of the fundamental physical constants: 2006. *Rev. Mod. Phys.*, 80(2):633, 2008.

- [25] J Mäkinen, S Palko, J Martikainen, and P Hautojarvi. Positron backscattering probabilities from solid surfaces at 2 – 30 keV. *J. Phys.: Condens. Matter*, 4(36):L503–L508, 1992.
- [26] A. Perkins and J. P. Carbotte. Effect of the positron-phonon interaction on positron motion. *Phys. Rev. B*, 1(1):101–107, Jan 1970.
- [27] J. Oliva. Inelastic positron scattering in an electron gas. *Phys. Rev. B*, 21(11):4909–4917, Jun 1980.
- [28] K. A. Ritley, K. G. Lynn, V. J. Ghosh, D. O. Welch, and M. McKeown. Low-energy contributions to positron implantation. *J. Appl. Phys.*, 74(5):3479–3496, 1993.
- [29] A. F. Makhov. *Sov. Phys. Solid State*, 2, 1961.
- [30] E. Soininen, J. Mäkinen, D. Beyer, and P. Hautojärvi. High-temperature positron diffusion in Si, GaAs, and Ge. *Phys. Rev. B*, 46(20):13104–13118, Nov 1992.
- [31] M Bertolaccini, A Bisi, G Gambarini, and L Zappa. Positron states in ionic media. *J. Phys. C: Solid St. Phys*, 4(6):734–745, 1971.
- [32] Werner Brandt. Positron dynamics in solids. *Appl. Phys.*, 5(1):1–23, October 1974.
- [33] M. Stadlbauer, C. Hugenschmidt, K. Schreckenbach, and P. Boni. Investigation of the chemical vicinity of crystal defects in ion-irradiated Mg and a Mg-Al-Zn alloy with coincident Doppler broadening spectroscopy. *Phys. Rev. B*, 76(17):174104, 2007.
- [34] R. N. West, J. Mayers, and P. A. Walters. A high-efficiency two-dimensional angular correlation spectrometer for positron studies. *J. Phys. E. Sci. Instrum.*, 14(4):478–488, 1981.
- [35] H. Haghighi, J. H. Kaiser, S. Rayner, R. N. West, J. Z. Liu, R. Shelton, R. H. Howell, F. Solal, and M. J. Fluss. Direct observation of Fermi surface in $YBa_2Cu_3O_{7-\delta}$. *Phys. Rev. Lett.*, 67(3):382–385, Jul 1991.
- [36] Paul Coleman. *Positron Beams and their applications*, chapter The generation and transport of positron beams, pages 11–40. World Scientific Publishing Co. Pte. Ltd., 2000.
- [37] B. Strasser, C. Hugenschmidt, and K. Schreckenbach. Set-up of a slow positron beam for Auger spectroscopy. *Mat. Sci. Forum*, 363-365:686–688, 2001.
- [38] K. G. Lynn, B. Nielsen, and J. H. Quateman. Development and use of a thin-film transmission positron moderator. *Appl. Phys. Lett.*, 47(3):239–240, 1985.

Bibliography

- [39] C. E. Mellish and J. A. Payne. Production of carrier-free cobalt-58 by pile irradiation of nickel. *Nature*, 178(4527):275–276, August 1956.
- [40] Benjamin L. Brown. A cobalt 58 ‘slow positron generator’. *Appl. Surf. Sci.*, 116:104 – 107, 1997.
- [41] Decay data search - nudat database: <http://nucleardata.nuclear.lu.se/database/nudat/>.
- [42] D. T. Britton, M. Härting, M. R. B. Teemane, S. Mills, F. M. Nortier, and T. N. Van der Walt. A southern african positron beam. *Appl. Surf. Sci.*, 116:53 – 58, 1997.
- [43] F. Reurings, A. Laakso, K. Rytsölä, A. Pelli, and K. Saarinen. Compact positron beam for measurement of transmission moderator efficiencies and positron yields of encapsulated sources. *Appl. Surf. Sci.*, 252(9):3154 – 3158, 2006.
- [44] Groden R. Gilmore. *Practical gamma-ray spectrometry*. Hoboken, N.J. : Wiley ; Chichester : John Wiley [distributor], 2nd edition, 2008.
- [45] Photon cross section data for a single element, compound, or mixture. National Institute of Standards and Technology: <http://physics.nist.gov/PhysRefData/Xcom/html/xcom1.html>, 2009.
- [46] R. H. Howell, R. A. Alvarez, and M. Stanek. Production of slow positrons with a 100-MeV electron linac. *Appl. Phys. Lett.*, 40(8):751–752, 1982.
- [47] T. Akahane, T. Chiba, N. Shiotani, S. Tanigawa, T. Mikado, R. Suzuki, M. Chiwaki, T. Yamazaki, and T. Tomimasu. Stretching of slow positron pulses generated with an electron linac. *Appl. Phys. A*, 51(2):146–150, August 1990.
- [48] T. Kurihara, Y. Nagashima, T. Shidara, H. Nakajima, S. Ohsawa, M. Ikeda, T. Oogoe, K. Kakihara, Y. Ogawa, A. Shirakawa, K. Furukawa, T. Sanami, and A. Enomoto. Present status of the slow positron facility at KEK. *Meas. Sci. Technol.*, 445-446:486–488, 2004.
- [49] H. Schut, A. van Veen, C.V. Falub, J. de Roode, and F. Labohm. Performance of an intense nuclear-reactor based positron beam. *Mat. Sci. Forum*, 363-365:430–432, 2001.
- [50] B. Krusche and K. Schreckenbach. Intense positron sources by pair creation with neutron capture γ -rays. *Nucl. Instr. Meth. A*, 295(1-2):155 – 171, 1990.
- [51] R. G. Greaves and C. M. Surko. Positron trapping and the creation of high-quality trap-based positron beams. *Nucl. Instr. Meth. B*, 192(1-2):90 – 96, 2002.

- [52] J. P. Marler and C. M. Surko. Positron-impact ionization, positronium formation, and electronic excitation cross sections for diatomic molecules. *Phys. Rev. A*, 72(6):062713, Dec 2005.
- [53] J. P. Sullivan, A. Jones, P. Caradonna, C. Makochekanwa, and S. J. Buckman. A positron trap and beam apparatus for atomic and molecular scattering experiments. *Rev. Sci. Instrum.*, 79(11):113105, 2008.
- [54] S. J. Gilbert, C. Kurz, R. G. Greaves, and C. M. Surko. Creation of a monoenergetic pulsed positron beam. *Appl. Phys. Lett.*, 70(15):1944–1946, 1997.
- [55] R. G. Greaves, M. D. Tinkle, and C. M. Surko. Creation and uses of positron plasmas. *Phys. Plasmas*, 1(5):1439–1446, 1994.
- [56] C M Surko, G F Gribakin, and S J Buckman. Low-energy positron interactions with atoms and molecules. *J. Phys. B: At., Mol. Opt. Phys.*, 38(6):R57–R126, 2005.
- [57] Leon Madansky and Franco Rasetti. An attempt to detect thermal energy positrons. *Phys. Rev.*, 79(2):397, Jul 1950.
- [58] W. Cherry. PhD thesis, Princeton University Press, 1958. available from University Microfilms.
- [59] John M. J. Madey. Evidence for the emission of slow positrons from polyethylene. *Phys. Rev. Lett.*, 22(15):784–787, Apr 1969.
- [60] D. G. Costello, D. E. Groce, D. F. Herring, and J. Wm. McGowan. Evidence for the negative work function associated with positrons in gold. *Phys. Rev. B*, 5(4):1433–1436, Feb 1972.
- [61] K F Canter, P G Coleman, T C Griffith, and G R Heyland. Measurement of total cross sections for low energy positron-helium collisions. (positron backscattering from metal surface). *J. Phys. B: At. Mol. Phys.*, 5(8):L167–L169, 1972.
- [62] P. G. Coleman, T. C. Griffith, and G. R. Heyland. A time of flight method of investigating the emission of low energy positrons from metal surfaces. *Proceedings of the Royal Society of London. Series A, Mathematical and Physical Sciences (1934-1990)*, 331(1587):561–569, January 1973.
- [63] Allen P. Mills, Jr. Efficient generation of low-energy positrons. *Appl. Phys. Lett.*, 35(5):427–429, 1979.
- [64] D. A. Fischer, K. G. Lynn, and D. W. Gidley. High-resolution angle-resolved positron reemission spectra from metal surfaces. *Phys. Rev. B*, 33(7):4479–4492, Apr 1986.

Bibliography

- [65] Cherry A. Murray and Allen P. Mills. Narrow beam emission of slow positrons from negative affinity surfaces. *Solid State Commun.*, 34(10):789 – 794, 1980.
- [66] A Goodyear, A P Knights, and P G Coleman. Energy spectroscopy of positrons re-emitted from polycrystalline tungsten. *J. Phys.: Condens. Matter*, 6(45):9601–9611, 1994.
- [67] E. M. Gullikson, A. P. Mills, and C. A. Murray. Dependence of the positron reemission probability on the positron work function of a metal surface. *Phys. Rev. B*, 38(3):1705–1708, Jul 1988.
- [68] G. Amarendra, K. F. Canter, and D. C. Schoepf. Study of positron yield of W(100) single crystalline foil with in situ surface characterization. *J. Appl. Phys.*, 80(8):4660–4664, 1996.
- [69] G. Amarendra, R. Rajaraman, S. Rajagopalan, R. Suzuki, and T. Ohdaira. Influence of defect-impurity complexes on slow positron yield of a tungsten moderator: Positron annihilation, Auger, and SIMS study. *Phys. Rev. B*, 69(9):094105, Mar 2004.
- [70] A. Vehanen, K. G. Lynn, Peter J. Schultz, and M. Eldrup. Improved slow-positron yield using a single crystal tungsten moderator. *Appl. Phys. A*, 32(3):163–167, November 1983.
- [71] R. J. Wilson and A. P. Mills. Positron and positronium emission from tungsten (111). *Phys. Rev. B*, 27(7):3949–3954, Apr 1983.
- [72] F. M. Jacobsen, M. Charlton, J. Chevallier, B. I. Deutch, G. Laricchia, and M. R. Poulsen. The effect of laser annealing of thin W(100) films on positron transmission reemission properties. *J. Appl. Phys.*, 67(1):575–577, 1990.
- [73] Peter J. Schultz, K. G. Lynn, W. E. Frieze, and A. Vehanen. Observation of defects associated with the Cu/W(110) interface as studied with variable-energy positrons. *Phys. Rev. B*, 27(11):6626–6634, Jun 1983.
- [74] P. J. Schultz, E. M. Gullikson, and A. P. Mills. Transmitted positron reemission from a thin single-crystal Ni(100) foil. *Phys. Rev. B*, 34(1):442–444, Jul 1986.
- [75] A. Zecca, R. S. Brusa, M. Bettonte, E. Rajch, S. Mariazzi, and G. P. Karwasz. A novel set-up for positron scattering in gases. *Rad. Phys. Chem*, 68(1-2):319 – 322, 2003.
- [76] Masanori Fujinami, Satoshi Jinnō, Masafumi Fukuzumi, Takumi Kawaguchi, Koichi Oguma, and Takashi Akahane. Production of a positron microprobe using a transmission remoderator. *Anal. Sci.*, 24(1):73–79, 2008.

- [77] Christian Piochacz. Entwicklung und Aufbau eines Transmissionsremoderators für Positronen. Diploma thesis, Lehrstuhl für Experimentalphysik E21, Technische Universität München, 2005.
- [78] A. Goodyear and P. G. Coleman. Development of a reflection geometry positron reemission microscope. *Appl. Surf. Sci.*, 85:98 – 105, 1995.
- [79] K. G. Lynn, E. Gramsch, S. G. Usmar, and P. Sferlazzo. Development of a cone-geometry positron moderator. *Appl. Phys. Lett.*, 55(1):87–89, 1989.
- [80] E. M. Gullikson and A. P. Mills. Positron dynamics in rare-gas solids. *Phys. Rev. Lett.*, 57(3):376–379, Jul 1986.
- [81] A. P. Mills, Jr. and E. M. Gullikson. Solid neon moderator for producing slow positrons. *Appl. Phys. Lett.*, 49(17):1121–1123, 1986.
- [82] D. Vasumathi, G. Amarendra, K. F. Canter, and A. P. Mills. Installation of a Kr moderator in the high-brightness beam at Brandeis. *Appl. Surf. Sci.*, 85:154 – 157, 1995.
- [83] H. Busch. Berechnung der Bahn von Kathodenstrahlen im axialsymmetrischen elektromagnetischen Felde. *Annalen der Physik*, 386(25):974–993, 1926.
- [84] Martin Reiser. *Theory and Design of Charged Particle Beams*. WILEY-VCH Verlag GmbH & Co. KGaA, Weinheim, 2008.
- [85] Peter W. Hawkes and E. Kasper, editors. *Principles of Electron Optics*. Academic Press, 1996.
- [86] P. Grivet. *Electron Optics*. Pergamon Press, Oxford and New York, 1972.
- [87] John David Jackson. *Classical electrodynamics*. John Wiley & Sons, Inc, New York [et al.], 3 edition, 1999.
- [88] D. E. Groce, D. G. Costello, J. W. McGowan, and D. F. Herring. Time-of-flight observation of low-energy positrons. *Bull. Am. Phys. Soc.*, 13:1397, 1968.
- [89] Lew A. Artsimowitsch and Roald S. Sagdejew. *Plasmaphysik für Physiker*. Teuner, Stuttgart, 1983.
- [90] D. Gerola, W. B. Waeber, M. Shi, and S. J. Wang. Quasidivergency-free extraction of a slow positron beam from high magnetic fields. *Rev. Sci. Instrum.*, 66(7):3819–3825, 1995.
- [91] W. Stoeffl, P. Asoka-Kumar, and R. Howell. The positron microprobe at lnl. *Appl. Surf. Sci.*, 149(1-4):1–6, August 1999.
- [92] E. Harting and F.H. Read. *Electrostatic Lenses*. Elsevier, Amsterdam and Oxford and New York, 1976.

Bibliography

- [93] Alfredo Dupasquier and Allen P. Mills, editors. *Positron Spectroscopy of Solids*, chapter Slow-Positron Optic, pages 361–383. IOS Press, 1995.
- [94] G. R. Brandes, K. F. Canter, T. N. Horsky, P. H. Lippel, and Jr. A. P. Mills. Scanning positron microbeam. *Rev. Sci. Instrum.*, 59(2):228–232, 1988.
- [95] David L. Webster. Cathode-ray bunching. *J. Appl. Phys.*, 10(7):501–508, July 1939.
- [96] W. T. Milner. Double-drift beam bunching systems. *IEEE Trans. Nucl. Sci.*, 26(1):1445–1449, 1979.
- [97] Paul Willutzki. *Verbesserung und Erweiterung des gepulsten Positronenstrahlsystems für temperaturabhängige Lebensdauer-messungen von Positronen in Festkörpern*. PhD thesis, Universität der Bundeswehr München, Fakultät für Luft und Raumfahrttechnik, Insitut für Nukleare Festkörperphysik, 1994.
- [98] Werner Bauer-Kugelmann. *Technische Weiterentwicklungen am gepulsten Positronenstrahlsystem PLEPS*. PhD thesis, Universität der Bundeswehr München, Fakultät für Luft und Raumfahrttechnik, Insitut für Nukleare Festkörperphysik, 2000.
- [99] Armin David. *Messungen mit dem weltweit ersten Rasterpositronenmikroskop*. PhD thesis, Universität der Bundeswehr München, Fakultät für Luft und Raumfahrttechnik, Insitut für Nukleare Festkörperphysik, 2000.
- [100] Samuel Y. Liao. *Microwave Devices and Circuits*, chapter Microwave Linear-Beam Tubes, pages 335–424. Prentice Hall, Englewood Cliffs, NJ, 3 edition, 1990.
- [101] Dieter Schödlbauer. *Aufbau und Inbetriebnahme einer gepulsten Positronenquelle für Lebensdauer-messungen*. PhD thesis, Universität der Bundeswehr München, Fakultät für Luft und Raumfahrttechnik, Insitut für Nukleare Festkörperphysik, 1987.
- [102] T.K. Fowler and W.M. Good. A theory on obtaining short bursts of ions from a beam of ions. *Nuclear Instruments and Methods*, 7(3):245–252, June 1960.
- [103] K. Fallström and T. Laine. Construction of the Helsinki University of Technology (HUT) pulsed positron beam. *Appl. Surf. Sci.*, 149(1-4):44–48, August 1999.
- [104] C. Hugenschmidt, K. Schreckenbach, M. Stadlbauer, and B. Straßer. Low-energy positrons of high intensity at the new positron beam facility NEPOMUC. *Nucl. Instr. Meth. A*, 554(1-3):384 – 391, 2005.
- [105] C. Hugenschmidt, B. Straßer, and K. Schreckenbach. Investigation of positron work function and moderation efficiency of Ni, Ta, Pt and W(100). *Appl. Surf. Sci.*, 194(1-4):283 – 286, 2002.

- [106] C. Hugenschmidt, G. Kögel, R. Repper, K. Schreckenbach, P. Sperr, B. Straßer, and W. Triftshäuser. Monoenergetic positron beam at the reactor based positron source at FRM-II. *Nucl. Instr. Meth. B*, 192(1-2):97 – 101, 2002.
- [107] Germar Triftshäuser. *Neutroneninduzierte Positronenquelle am Forschungsreaktor München FRM*. PhD thesis, Technische Universität München, Institut für Kernphysik und Nukleare Festkörperphysik, Lehrstuhl für Experimentalphysik E21, 1996.
- [108] Martin Simon Springer. *Optimierung einer neutroneninduzierten Positronenquelle am QR-Neutronenleiter des FRM*. PhD thesis, Technische Universität München, Institut für Kernphysik und Nukleare Festkörperphysik, Lehrstuhl für Experimentalphysik E21, 1998.
- [109] Axel Pichlmaier. Entwicklung einer Remoderationsstufe für Positronen. Master's thesis, Technische Universität München, Fakultät für Physik, Insitut E 21, 1995.
- [110] Benno Straßer. Aufbau eines remoderierten Positronenstrahls. Master's thesis, Technische Universität München, Fakultät für Physik, Insitut E 21, 1996.
- [111] Ben Ehrhardt. Magnetische Strahlweiche für das Münchner Rasterpositronenmikroskop. Master's thesis, Institut für angewandte Physik und Messtechnik, Fakultät für Luft- und Raumfahrttechnik, Universität der Bundeswehr München, 2005.
- [112] J. Mayer, C. Hugenschmidt, and K. Schreckenbach. Study of the surface contamination of copper with the improved positron annihilation-induced Auger electron spectrometer at NEPOMUC. *Appl. Surf. Sci.*, 255(1):220–222, October 2008.
- [113] Jakob Mayer. personal communication, 2009.
- [114] Christian Piochacz, Gottfried Kögel, Werner Egger, Christoph Hugenschmidt, Jakob Mayer, Klaus Schreckenbach, Peter Sperr, Martin Stadlbauer, and Günther Dollinger. A positron remoderator for the high intensity positron source NEPOMUC. *Appl. Surf. Sci.*, 255(1):98–100, October 2008.
- [115] Martin Stadlbauer. personal communication, 2007.
- [116] P. Sperr, P. Willutzki, and M.R. Maier. On the electronic design and the performance of a ramp generator for a pulsed low energy positron beam. *Mat. Sci. Forum*, 175 - 178:993–996, 1995.
- [117] Daniel Passbach. Konstruktion und Aufbau eines 50 MHz-Bunchers für PLEPS III. Master's thesis, Institut für Nukleare Festkörperphysik, Fakultät für Luft- und Raumfahrttechnik, Universität der Bundeswehr München, 1997.

Bibliography

- [118] Nico Wieschalla. *Out-of-pile examination of the high density U-Mo/Al dispersion fuel*. PhD thesis, Institut für Experimentalphysik E21, Physik Department, Technische Universität München, 2006.
- [119] G. Kögel, P. Sperr, W. Triftshäuser, and S.J. Rothman. Positron lifetime and Doppler-broadening studies of vacancy formation and phase transformation in uranium. *J. Nucl. Mater.*, 131(2-3):148–157, April 1985.

List of publications

- C. Piochacz, W. Egger, C. Hugenschmidt, G. Kögel, K. Schreckenbach, P. Sperr, and G. Dollinger. Implementation of the Munich scanning positron microscope at the positron source NEPOMUC. *phys. stat. sol. (c)*, 4(10):4028–4031, 2007.
- Christian Piochacz, Gottfried Kögel, Werner Egger, Christoph Hugenschmidt, Jakob Mayer, Klaus Schreckenbach, Peter Sperr, Martin Stadlbauer, and Günther Dollinger. A positron remoderator for the high intensity positron source NEPOMUC. *Appl. Surf. Sci.*, 255(1):98–100, October 2008.
- C. Hugenschmidt, T. Brunner, S. Legl, J. Mayer, C. Piochacz, M. Stadlbauer, and K. Schreckenbach. Positron experiments at the new positron beam facility NEPOMUC at FRM II. *phys. stat. sol. (c)*, 4(10):3947–3952, 2007.
- C. Hugenschmidt, G. Dollinger, W. Egger, G. Kögel, B. Löwe, J. Mayer, P. Pikart, C. Piochacz, R. Repper, K. Schreckenbach, P. Sperr, and M. Stadlbauer. Surface and bulk investigations at the high intensity positron beam facility NEPOMUC. *Appl. Surf. Sci.*, 255(1):29 – 32, 2008.
- C. Hugenschmidt, T. Brunner, J. Mayer, C. Piochacz, K. Schreckenbach, and M. Stadlbauer. Determination of positron beam parameters by various diagnostic techniques. *Appl. Surf. Sci.*, 255(1):50 – 53, 2008.
- C. Hugenschmidt, B. Löwe, J. Mayer, C. Piochacz, P. Pikart, R. Repper, M. Stadlbauer, and K. Schreckenbach. Unprecedented intensity of a low-energy positron beam. *Nucl. Instr. Meth. A*, 593(3):616 – 618, 2008.
- P. Sperr, W. Egger, G. Kögel, G. Dollinger, C. Hugenschmidt, R. Repper, and C. Piochacz. Status of the pulsed low energy positron beam system (PLEPS) at the Munich Research Reactor FRM-II. *Appl. Surf. Sci.*, 255(1):35 – 38, 2008.
- M. Stadlbauer, C. Hugenschmidt, C. Piochacz, B. Straßer, and K. Schreckenbach. Spatially resolved investigation of thermally treated brass with a coincidence Doppler spectrometer. *Appl. Surf. Sci.*, 252(9):3269 – 3273, 2006.
- K. Schreckenbach, C. Hugenschmidt, B. Lowe, J. Maier, P. Pikart, C. Piochacz, and M. Stadlbauer. Performance of the (n,γ) -based positron beam facility NEPOMUC. In Jan Jolie, Andreas Zilges, Nigel Warr, and Andrey Blazhev, editors, *AIP Conf. Proc.*, volume 1090, pages 549–553. AIP, 2009.